MODELLING OF GALACTIC AND JOVIAN ELECTRONS IN THE HELIOSPHERE

DANIEL M. MOEKETSI Hons. B.Sc.

Thesis accepted in partial fulfilment of the requirements for the degree Magister Scientiae in Physics at the North-West University (Potchefstroom Campus)

Supervisor: Prof. M. S. Potgieter
Assistant Supervisor: Dr. S. E. S. Ferreira

July 2004
Potchefstroom
South Africa

Abstract

A three-dimensional (3D) steady-state electron modulation model based on Parker (1965) transport equation is applied to study the modelling of ~ 7 MeV galactic and Jovian electrons in the inner heliosphere. The latter is produced within Jupiter's magnetosphere which is situated at ~ 5 AU in the ecliptic plane. The heliospheric propagation of these particles is mainly described by the heliospheric diffusion tensor. Some elements of the tensor, such as the diffusion coefficient in the azimuthal direction, which were neglected in the previous two-dimensional modulation studies are investigated to account for the three-dimensional transport of Jovian electrons. Different anisotropic solar wind speed profiles that could represent solar minimum conditions were modelled and their effects were illustrated by computing the distribution of 7 MeV Jovian electrons in the equatorial regions. In particular, the electron intensity time-profile along the Ulysses spacecraft trajectory was calculated for these speed profiles and compared to the 3–10 MeV electron flux observed by the Kiel Electron Telescope (KET) on board the Ulysses spacecraft from launch (1990) up to end of its first out–of–ecliptic orbit (2000). It was found that the model solution computed with the solar wind profile previously assumed for typical solar minimum conditions produced good compatibility with observations up to 1998. After 1998 all model solutions deviated completely from the observations. In this study, as a further attempt to model KET observations more realistically, a new relation is established between the latitudinal dependence of the solar wind speed and the perpendicular polar diffusion. Based on this relation, a transition of an average solar wind speed from solar minimum conditions to intermediate solar activity and to solar maximum conditions was modelled based on the assumption of the time-evolution of large polar coronal holes and were correlated to different scenarios of the enhancement of perpendicular polar diffusion. Effects of these scenarios were illustrated, as a series of steady-state solutions, on the computed 7 MeV Jovian and galactic electrons in comparison with the 3–10 MeV electron observed by the KET instrument from the period 1998 up to the end of 2003. Subsequent effects of these scenarios were also shown on electron modulation in general. It was found that this approach improved modelling of the post-1998 discrepancy between the model and KET observations but it also suggested the need for a time-dependent 3D electron modulation model to describe modulation during moderate to extreme solar maximum conditions.

Keywords: cosmic rays, heliosphere, solar wind speed, polar coronal holes, Jovian electrons, galactic electrons

Nomenclature

AU	Astronomical Unit = 1.49×10^{8} km
ADI	Alternating Direction Implicit
CIRs	Corotating Interaction Regions
CME	Coronal Mass Ejection
COSPIN	Cosmic and Solar Particle Investigation
CRs	Cosmic Rays
DCs	Diffusion Coefficients
EPHIN	Electron – Proton Helium Instrument
ESA	European Space Agency
HD	Hydrodynamic
HCS	Heliospheric Current Sheet
HMF	Heliospheric Magnetic Field
KET	Kiel Electron Telescope
LIS	Local Interstellar Spectra
NASA	National Aeronautic and Space Administration
NLGC	Nonlinear Quiding Center theory
SEPs	Solar Energetic Particles
SOHO	Solar and Heliopheric Observatory
SWOOPS	Solar Wind Observations Over the Polar region of the Sun
TPE	Transport Equation
TS	Termination Shock
2D	Two – Dimensional
3D	Three – Dimensional

Contents

Chapter 1

Introduction

Galactic cosmic rays (GCRs) originate from astrophysical sources in the Galaxy enter almost isotropically the region of interstellar space influenced by the Sun known as the heliosphere. In the heliosphere, they interact with the turbulent magnetised plasma so that their intensity is reduced below the level of their interstellar spectra, a phenomenon called the heliospheric modulation of cosmic rays. Besides GCRs, there is another population of charged particles of importance to this study which originate within the heliosphere known as "Jovian electrons" which also experience a similar process. The latter is produced by the Jovian magnetosphere located at ~ 5 AU in the ecliptic plane (e.g., Teegarden, 1974). This study focuses mainly on modelling the modulation of these low-energy electrons in the inner heliosphere (≤ 10 AU).

Significant progress has been made over the past few decades in modelling modulation of cosmic rays in the heliosphere. Among these is the recent application of an advanced steady-state three-dimensional (3D) electron modulation model (Ferreira, 2002) which describes the relevant physics of the heliospheric transport and modulation of low-energy (< 30 MeV) Jovian and galactic electrons. This model, also used for this study, has successfully produced a good compatibility with the 3 - 10 MeV electron flux observed by the Kiel Electron Telescope (KET) instrument (e.g., Heber et al., 2003a,b) aboard the Ulysses spacecraft during solar minimum to moderate conditions (1994-1998). After this period, the model predictions deviate completely from the observations. This deviation will be further investigated.

In previous modulation studies (e.g., Hattingh, 1998; Ferreira, 1998; Minnie, 2002; Ferreira, 2002; Langner, 2004), the only realistic profile of the solar wind speed assumed was the one with

highly latitude dependent speed, that is changing from a slow solar wind in the equatorial region with an average speed of 400 km s^{-1} to a fast speed of 800 km s^{-1} in the solar polar regions. This profile is *only* consistent with Ulysses spacecraft observations during solar minimum conditions. In this study, other solar wind speed profiles are modelled which could represent solar conditions after solar minimum. Effects of their variability are illustrated on the computed 7 MeV electron intensities and compared to the electron flux observed along the Ulysses trajectory for the first out-of-ecliptic orbit.

The main aim of this thesis is to study and establish a relation between two essential parameters of the modulation model, that is the latitudinal dependence of the solar wind speed and the heliospheric perpendicular diffusion. Further, it is to enable improved modelling these parameters with varying heliospheric conditions and to illustrate, in general, their subsequent effects on low energy ($\sim$ 7 MeV) Jovian and galactic electron modulation, in particular the post-1998 discrepancy between the model solutions and the 3 -10 MeV KET observations.

An introduction to cosmic rays and the heliosphere is given in **Chapter 2** along with all the related major concepts and definitions used in this study. The Ulysses mission is also discussed with the KET and the SWOOPS instruments which provide electron and solar wind speed data in this study.

A concise overview of the heliospheric transport and modulation of low energy (3 - 30 MeV) electrons, in particular Jovian electrons, is given in **Chapter 3**. It begins with a brief background on observations of these electrons since the early 1970's to date with various space probes and further gives an overview of the development and advancement of the Jovian propagation models used to explain these observations. Finally, a short discussion is given on the modulation and source spectrum of Jovian electrons.

Chapter 4 gives a brief summary of the steady-state 3D electron modulation model (Ferreira, 2002) used in this study.

Aspects of the heliospheric diffusion tensor constructed by Ferreira et al. (2002) to establish compatibility with Ulysses spacecraft observations (Heber et al., 2001) of a few MeV Jovian and galactic electrons in the heliosphere are investigated in **Chapter 5**. These include the spatial and rigidity dependence of elements of the tensor which are important for electron modulation. The other elements of the tensor which were neglected in previous modulation studies because

of the limitations imposed by 2D modulation models, become of particular interest in this Chapter in order to understand the 3D transport and modulation of low-energy electrons in the inner heliosphere, in particular, the prominent azimuthal distribution of electrons produced by the Jovian magnetosphere in the equatorial region.

In **Chapter 6**, the different profiles of solar wind speed applicable to solar minimum conditions are modelled and their effects on the computed low energy ($\sim$ 7 MeV) Jovian and galactic electron intensity are illustrated in comparison to the electron flux observed along the Ulysses trajectory.

A new relation is established between the latitudinal dependence of the solar wind speed and the heliospheric polar diffusion in **Chapter 7**. Using this relation, a transition of average solar wind speed from solar minimum to intermediate solar activity and to solar maximum conditions correlated with different scenarios of heliospheric polar diffusion is modelled based on the assumption of the time evolution of polar coronal holes. Effects of these different scenarios assumed to correspond to different solar conditions are illustrated as a series of steady-state solutions on the post-1998 electron observations along Ulysses trajectory. Subsequent effects of these different heliospheric polar diffusion scenarios are illustrated on the low-energy electron modulation.

In **Chapter 8**, a summary and the conclusions of this study are given.

Extracts from this thesis were published in accredited scientific journals by Ferreira et al. (2003a) and Ferreira et al. (2003b).

Aspects of this work were personally presented during the International Cosmic Ray Workshop in Potchefstroom (March, 2002) and Bochum, Germany (March, 2003) and also during the South African Institute of Physics (SAIP) Conference in Potchefstroom (September, 2002) and in Stellenbosch (June, 2003).

Aspects of this work also formed part of poster presentations at the following conferences:

- The 34th Scientific Assembly of COSPAR/World Space Congress 2002, Houston, USA by Ferreira et al., 2002).
- The International Symposium on "Plasma in the laboratory and the Universe", Como, Italy, September, 2003 (recently published by Heber et al., 2004).

- The 35th Scientific Assembly of COSPAR 2004, Paris, France by Henize et al., 2004).

Chapter 2

Cosmic rays, the Sun and the heliosphere

2.1 Introduction

This Chapter gives an introduction to the study of cosmic rays and the heliosphere. It starts with a brief discussion on the origin of cosmic rays and further discusses the Sun and the solar wind plasma, the heliosphere, heliospheric magnetic field and current sheet, and solar cycle variations. The Ulysses space mission is also discussed as related to the Kiel Electron Telescope instrument which provides a wide range of electron and other data, and the Solar Wind Observations Over the Polar region of the Sun (SWOOPS) instrument which provides solar wind speed data used in this study (Chapters 6 and 7).

2.2 Origin of cosmic rays, cosmic radiation

Cosmic rays (CRs), which are wrongly called rays, are energetic charged particles with kinetic energy, $E \gtrsim 1$ MeV, originating from astrophysical sources and are accelerated to high velocities to become cosmic radiation which propagate throughout the galaxy. These particles were discovered in 1912 by Victor Hess during the historic balloon flights and their origins were identified as extraterrestial (e.g., Simpson, 1992; Simpson, 1997). CRs detected at Earth consist of $\sim$ 97% protons, $\sim$ 2% electrons and positrons and $\sim$ 1% heavier nuclei (e.g., Longair, 1990;

Simpson, 1992). CRs can be categorised in different populations as follows:

(1) Galactic CRs originating from far outside the solar system. It is believed that the energy transfer processes during supernova explosions in the galaxy are major sources of these particles (see a detailed review by Jones and Ellison, 1991). Experimental evidence of this was found by e.g. Koyama et al. (1995) and confirmed by Tanimori et al. (1998).

(2) Solar energetic particles (SEPs) originating from the Sun and produced mainly during solar flares (e.g., Forbush, 1946; Smith et al., 2003).

(3) The anomalous component of CRs are formed due to the ionization of interstellar neutral atoms relatively close to the Sun and are then transported to and accelerated at the solar wind termination shock (e.g., Garcia-Munoz et al., 1973; Fisk et al., 1974, Fichtner, 2001a).

(4) Electrons originating from the Jovian magnetosphere (e.g., Simpson et al., 1974; Teegarden et al., 1974; Chennete et al., 1974; Heber et al., 2003).

The low-energy Jovian and galactic electrons are considered for the purpose of this study.

2.3 The Sun and solar wind

Our nearest star, the Sun located at an average distance of 1 AU from the planet Earth is a middle aged, main sequence star. Its surface is not solid but a spherical plasmatic gas with radius of about $r_{\odot} \sim 0.005$ AU and it has a differential rotation period which increases in latitude from an average value of ~ 25 days at the equator to ~ 32 days near the polar regions. The Sun is mainly composed of hydrogen ($\sim 90\%$) and helium ($\sim 10\%$) with some signatures of other heavy elements.

The light of the Sun comes from the photosphere, at about 5800 K (Kelvin). Around this lies a region of hot gas, the chromosphere, visible during solar eclipses, and it extends $\sim 10^3$ km from the photosphere. Above that there is a more tenuous and even hotter layer, the corona which extends out into space to $\sim 10^6$ km from the chromosphere.

The visible dark areas of irregular shape on the photosphere that are cooler than the entire solar surface are called sunspots. Detailed records of the sunspot number, which is a direct indication of the level of solar activity, have been kept since 1749 and are shown in Figure 2-1 up to the end of 2003. From these monthly averaged values, it is evident that the Sun has a

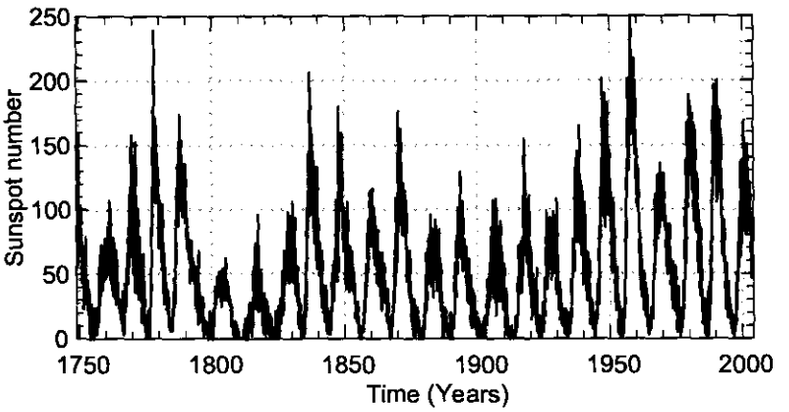

Figure 2-1: Monthly averaged sunspot number from the year 1749 up to the end of 2003 (data from http://www.spaceweather.com).

quasi-periodic $\sim$ 11 year activity cycle. Every $\sim$11 years the Sun moves through a period of fewer and smaller sunspots which is called 'solar minimum' followed by a period of larger and more sunspots which is called 'solar maximum' (e.g., Smith and Marsden, 2003).

The plasmatic atmosphere of the Sun constantly blows away from its surface to maintain equilibrium (Parker, 1958, 1961, 1963). This is possible because temperatures in the corona are so high that the solar material is not gravitationally bound to the Sun. The escaping hot coronal plasma from the Sun is called the solar wind. The solar wind carries the solar magnetic field into interplanetary space, forming the heliospheric magnetic field (HMF) which is mostly responsible for the modulation of CRs in the heliosphere.

The solar wind (originally called "solar corpuscular radiation") was first proposed by Biermann (1951, 1961) to account for the behaviour of comet tails that always pointed directly away from the Sun regardless of the position of the comet. Biermann has found that the pressure of the solar radiation alone cannot explain his observation and has suggested that the solar wind always exists and effects the formation of comet tails. Biermann's estimates of the solar wind speed, V, ranged between 400 - 1000 km s^{-1} which were remarkably accurate. However, the name 'solar wind' was first introduced by Parker (1958). This was confirmed in 1959 by the Soviet Luna 3 Spacecraft and has been the object of study ever since

(http://sohoww.nascomgo/explore/swvelocity). For a review see Marsch et al. (2003).

Observations made over many years showed that V is not uniform over all latitudes and can be divided into the fast solar wind and the slow solar wind. The basic reason is that the Sun's magnetic field dominates the original outflow of the solar wind (e.g., Smith, 2000). If the solar magnetic field is perpendicular to the radial outflow of the solar wind it can prevent the outflow. This is usually the case at low solar latitudes where the near Sun magnetic field lines are parallel to the Sun's surface. These field lines are in the form of loops which begin and end on the solar surface and stretch around the Sun to form the streamer belts as shown in Figure 2-2. These streamers belts are regarded as the most plausible sources of the slow solar wind speed which has typical average velocities of up to V= 400 km s^{-1} (e.g., Schwenn, 1983; Marsch, 1991; Phillips et al., 1995; McComas, 1998; McComas, 2002a). Other indications are that the slow solar wind speed may arise from the edges of large coronal holes or from smaller coronal holes (e.g., Hundhausen, 1977; McComas et al., 2000; McComas et al., 2002a).

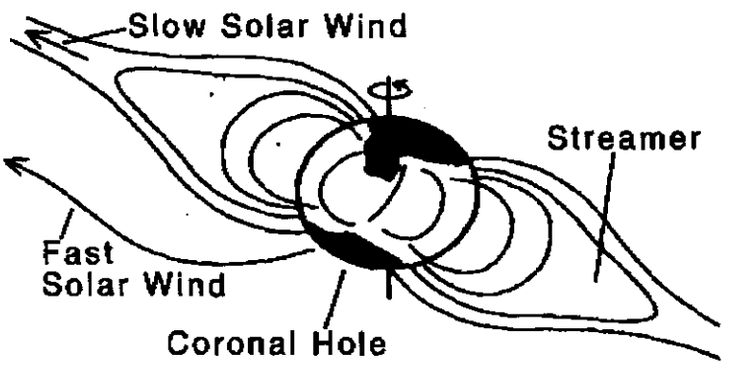

Figure 2-2: The solar magnetic field during declining phase of solar cycle illustrating polar coronal holes (shaded regions) and streamers as sources of fast and slow solar wind speed (from Suess et al., 1998).

The fast solar wind speed with a characteristic average speed of up to V = 800 km s^{-1} emanates from the polar coronal holes which are located at the higher heliographic latitudes (e.g., Krieger et al., 1973; Nolte et al., 1976; Zirker, 1977; McComas et al., 2000; McComas et al., 2002b; Neugebauer et al., 2002, 2003; Hu et al., 2003) illustrated in Figure 2-2. In these regions the magnetic field lines are open and frozen into the solar wind plasma and carried into interplanetary space. The faster solar wind plasma from the polar regions can extend close

to the solar equator and overtake the earlier emitted slow stream, resulting in a "corotating interaction region" (CIR), for a review see Odstrcil (2003). The effect on CR modulation of these relatively short-term features are not studied in this work. For the purpose of modelling the realistic changes in the solar wind speed with varying solar activity in this study, it is important to relate it with the time evolution of the large polar coronal holes which is done in Chapter 7.

The latitudinal dependence of V during solar minimum activity has been confirmed by Ulysses observations (e.g., Phillips et al., 1994; 1995) and is shown in Figure 2-3 as six hour averages during the fast pole-to-pole transit of the Ulysses spacecraft. Ulysses is the first spacecraft to explore both equator and the polar regions of the Sun and its mission is discussed in Section 2.8. Evident from Figure 2-3 are significant variations of V with heliolatitude where Ulysses has observed a high solar wind speed, 700 - 800 km s^{-1}, at $\geq 20^0$ S. In the $\sim 20^0$ S to the $\sim 20^0$ N band it observed medium to slow speeds, to increase again to a speed between 700 - 800 km s^{-1} at $\sim 20^0$ N thus confirming the existence of the fast and slow solar wind streams during solar minimum. For solar maximum activity no well-defined high speed solar wind is observed (e.g., Richardson et al., 2001).

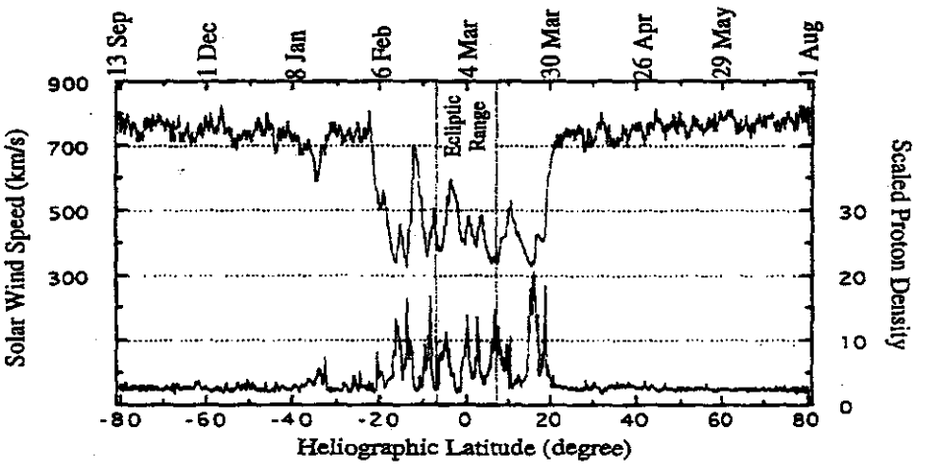

Figure 2-3: Six-hour average solar wind speed for the pole-to-pole transit of Ulysses from peak southerly latitude of -80.2^0 on 12 September 1994 to the corresponding northerly latitude on 31 July 1995 (adapted from Phillips et al., 1995).

The radial dependence of V between 0.1 AU and 1.0 AU was studied by e.g., Kojima et al. (1991) and Sheeley et al. (1997). They have found that both the low and high speed winds accelerate within 0.1 AU of the Sun and become a steady flow at 0.3 AU. Using measurements from Pioneer 10 and 11 and Voyagers 1 and 2, Gazis et al. (1994) and Richardson et al. (2001) have found that the slow averaged solar wind speed does not vary with distance up to 50 AU. However, it does show a solar cycle dependence with values about 20% higher during solar minimum than during solar maximum. At solar maximum there is a mixture of high speed and low speed winds in the region of the equator (Gazis et al., 1991; McComas et al., 2002a).

The average solar wind velocity $\mathbf{V}$ in the modulation models is modelled as

$$\mathbf{V}(r,\theta) = V(r,\theta)\,\mathbf{e}_r = V(r)\,V(\theta)\,\mathbf{e}_r, \tag{2.1}$$

where r is the radial distance, θ the polar angle and $\mathbf{e}_r$ the unit vector component in the radial direction. The radial dependence $V(r)$ of the solar wind plasma (e.g., Hattingh, 1998) is given as

$$V(r) = V_0 \left\{ 1 - \exp\left[\frac{40}{3} \left(\frac{r_\odot - r}{r_0} \right) \right] \right\}, \tag{2.2}$$

with $V_0 = 400$ km s^{-1}, $r_\odot$ the solar radius, $r_0 = 1$ AU and r given in AU. The latitude dependence $V(\theta)$ of the solar wind speed during solar minimum conditions (Hattingh, 1998) is given as

$$V(\theta) = 1.5 \mp 0.5 \tanh\left[\frac{2\pi}{45^0} \left(\theta - 90^0 \pm \varphi \right) \right], \tag{2.3}$$

in the northern and southern hemisphere respectively with $\varphi = 35^0$. This latitudinal dependence of the V produces compatibility with the observations (e.g., Phillips et al., 1995; McComas et al., 2002b; Ferreira, 2002; Ferreira et al., 2003a, Langner, 2004) and is illustrated in Chapter 6. A significant progress is made in Chapter 6 and 7 to improve modelling of Equation (2.1) for varying heliospheric conditions.

2.4 The heliosphere

The region of interstellar space occupied by magnetised plasma originating from the Sun is called the heliosphere. A simplistic understanding of the heliosphere is that the solar wind flows radially outward from the Sun and therefore blows a spherical bubble that continually expands. However, the interstellar space is not empty and contains matter in the form of the local interstellar medium (LISM). The LISM is known to consist of some combination of dust, neutral gas, ionized plasma, magnetic fields and galactic cosmic rays (e.g. Smith, 2001). The best known interstellar component is neutral gal (H, He) which enters the heliosphere more or less directly because it does not interact with the solar wind. The heliosphere can be viewed as a huge laboratory where we can directly observe and measure physical parameters that cannot be scaled down to terrestrial laboratories. See the review by Fichtner (2000a).

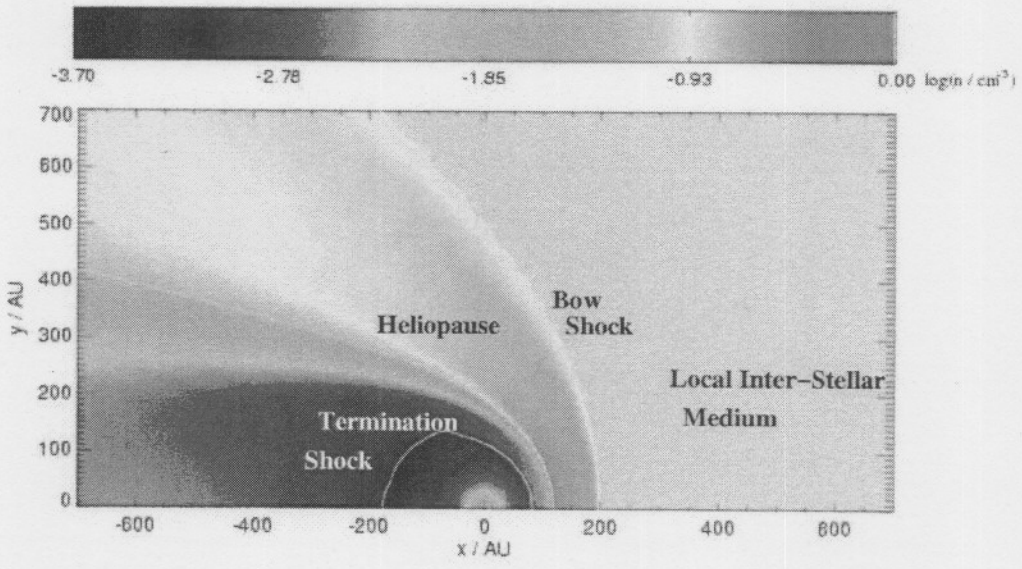

Figure 2-4: The structure of the heliosphere resulting from an axisymmetric hydrodynamic (HD) model (Fahr, 2000). The proton number density that is seen in the rest frame of the Sun equals the neutral gas number density in the local interstellar medium ($n_p = n_H = 0.1$ cm^{-3}, Scherer et al., 2001).

Figure 2-4 illustrates the geometrical structure of the heliosphere resulting from an axisymmetric HD model (e.g., Fahr, 2000). The interaction of the supersonic solar wind plasma with

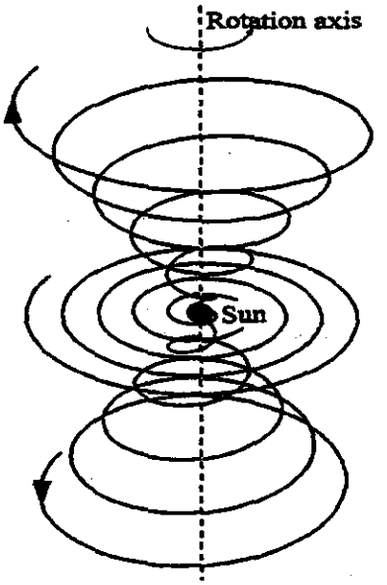

Figure 2-5: A 3D representation of the Parker HMF spiral structure with the Sun at the origin. Spirals rotate around the the polar axis for $\theta = 45^0, \theta = 90^0$ and $\theta = 135^0$ (from Hattingh, 1998).

the LISM leads to a transition from supersonic to subsonic speeds at the termination shock (TS). Such a transition might also occur for the interstellar wind at the heliospheric bow shock. The estimates for the location of the TS range between $\sim$ 70 AU and $\sim$ 100 AU (e.g., Stone et al., 1996; Whang and Burlaga, 2000), but the present consensus is that the TS should be near $\sim$ 90 AU in the upwind direction (e.g., Stone and Cummings, 2001). Recent observations indicate that Voyager 1 is in the vicinity of the TS (e.g., Stone and Cummings, 2003) or may have even crossed it (Krimigis et al., 2003). In this study, the TS is disregarded because focus is on modulation of low-energy electrons in the inner heliosphere ($<$ 10 AU). The heliopause is the boundary layer between the interstellar medium and the solar wind plasma. Its position is uncertain, probably at least 30 - 50 AU beyond the TS, certainly more in the down-wind direction. In this study the outer boundary is specified to be at 120 AU (see also Chapter 4).

2.5 Heliospheric magnetic field

In 1958, Parker put forth a model for the HMF that has been the accepted standard for decades. In this model, Parker (1958) assumed that the footpoints of the HMF remain rooted with respect to the Sun at the solar wind source surface, where the solar wind flow becomes radial. Due to the combined effect of radial outward convection of the solar wind plasma and the rotation of the Sun, the field lines form Archimedean spirals that lies on the cones of constant heliographic latitude, as shown in Figure 2-5.

Parker (1958) derived an equation for the spiral HMF (also known as the Parker field) given by

$$\mathbf{B} = \frac{B_0 r_0^2}{r^2} \left(\mathbf{e}_r - \tan\psi \mathbf{e}_\phi \right), \tag{2.4}$$

where $\mathbf{B}$ is the HMF vector with components in the radial $\mathbf{e}_r$ and azimuthal $\mathbf{e}_\phi$ directions respectively, B_0 is the magnitude of the HMF which averages $\sim$5 nT at Earth, $r_0 = 1$ AU, and ψ the spiral angle, that is defined as the angle between the outward radial direction and the direction of the HMF lines at a certain position. It is mathematically expressed as

$$\psi = \arctan\left[\frac{\Omega\left(r - r_\odot\right)}{V}\right], \tag{2.5}$$

with Ω the angular velocity of the Sun about its rotation axis, $r_\odot$ the solar radius, and V the solar wind speed. The spiral angle indicates how tightly wound is the spiral structure of the HMF lines. At high latitudes the spiral angle is less tightly wound and the field lines are nearly radial. Substituting Equation (2.5) into (2.4) yields

$$B = \frac{B_0 r_0^2}{r^2} \sqrt{1 + \left[\frac{\Omega\left(r - r_\odot\right)\sin\theta}{V}\right]^2}, \tag{2.6}$$

for the magnitude of the Parker HMF throughout the heliosphere. The polar angle θ is measured from 0^0 at the polar axis of the Sun with $\theta = 90^0$ the equatorial plane.

However, at high latitude the geometry of HMF is not just an ordinary Parker spiral as argued by Jokipii and Kóta (1989). The solar surface, where the "feet" of the field lines occur, is not a smooth surface, but a granular turbulent surface that keeps changing with time,

especially in the polar regions. This turbulence may cause the "footpoints" of the polar field lines to wander randomly, creating transverse components in the field, thus causing temporal deviations from the smooth Parker geometry. The effect of the more turbulent magnetic field in these regions is to increase the mean magnetic field strength. However, Jokipii and Kóta (1989) suggested a modification to Equation (2.6) so that

$$B = \frac{B_0 r_0^2}{r^2}\sqrt{1 + \left[\frac{\Omega\,(r - r_\odot)\sin\theta}{V}\right]^2 + \left(\frac{r\delta_m}{r_\odot}\right)}. \tag{2.7}$$

For $\delta_m = 0$ in Equation (2.7) there is no modification so that the standard Parker geometry is obtained. In this work it is assumed that $\delta_m = 0.002$ (Haasbroek, 1993). This modification causes the HMF to vary as $\frac{1}{r}$ throughout most of the heliosphere while retaining the same direction as the Parker field. Qualitatively, this modification is supported by measurements made of HMF in the polar regions of the heliosphere by Ulysses (e.g., Balogh et al., 1995). This equation is used in most modulation models (e.g., Ferreira, 2002; Langner, 2004).

The purpose of this modification is to alter the drift patterns that CRs experience by reducing them in the heliospheric polar regions. This study focus on modelling of Jovian and galactic electrons in the inner heliosphere at low energies (< 30 MeV), where effects of drifts are negligibly small, so that this modification does not have a significant influence. (e.g., Ferreira, 2002; see also Chapter 7).

Another modification was proposed by Smith and Bieber (1991) who based their modification on magnetic field data. This modification also changes the geometry of the magnetic field and affects the field strength over the poles. For an implementation of this modification in a numerical model see Haasbroek (1997). An alternative model for HMF has been proposed by Fisk (1996) based on the argument that the Sun does not rotate rigidly, but rather differentially with solar poles rotating $\sim 20\%$ slower than the solar equator (e.g., Snodgrass, 1983). Because of the complexity of this field, it is not incorporated in the numerical modulation model used in this study. For more information from cosmic ray point of view about this field the reader is referred to Kóta and Jokipii (1997), Kóta and Jokipii (1999), Van Niekerk (2000), Burger and Hattingh (2001).

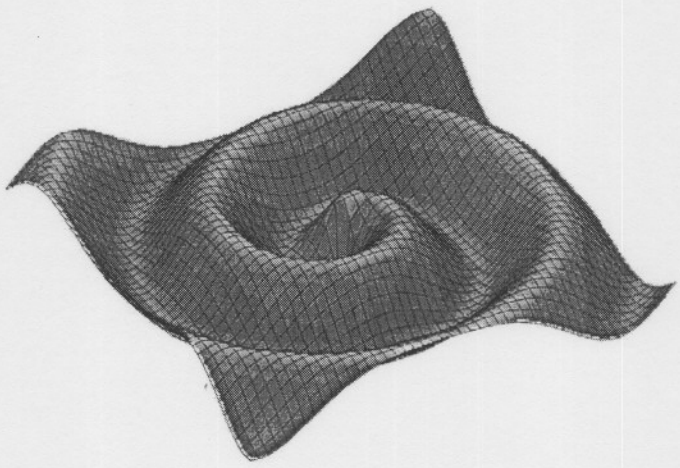

Figure 2-6: A schematic 3D idealization of the HCS configuration for the first 10 AU when $\alpha = 25^0$. The Sun is in the middle (adapted from Ferreira, 2002).

2.6 Heliospheric current sheet

The existence of a heliospheric current sheet (HCS), earlier called an interplanetary sector boundary, has been known since it was first identified by Wilcox and Ness (1965). The HCS separates regions of the solar wind where the magnetic field points towards or away from the Sun. Because the magnetic and rotational axis of the Sun are not aligned, the rotation of the Sun causes the HCS to have a warped or "wavy" structure. Since the Sun has typically an 11 - year activity cycle, the waviness of HCS correlates with solar activity. This implies that during the solar maximum the angle between the Sun's magnetic and rotational axis, known as the tilt angle α, increases to more than 70^0 although difficult to observe. During the period of lower solar activity the rotation and magnetic axis of the Sun become nearly aligned, causing the relatively small neutral sheet waviness ($5^0 - 10^0$). The wavy structure of the solar wind is carried out radially by the constant solar wind plasma as shown in Figure 2-6. This figure illustrates a 3D idealization of the HCS configuration for the first 10 AU when $\alpha = 25^0$. (For review , see Smith, 2001)

For a constant and radial solar wind speed, the position and wavy structure of the HCS is (e.g., Jokipii and Thomas, 1981) given by

$$\theta' = \frac{\pi}{2} + \sin^{-1}\left\{\sin\alpha \sin\left[\phi + \frac{\Omega\left(r - r_{\odot}\right)}{V}\right]\right\}, \tag{2.8}$$

which for a small value of α can be approximated by

$$\theta' = \frac{\pi}{2} + \alpha \sin\left[\phi + \frac{\Omega\left(r - r_{\odot}\right)}{V}\right]. \tag{2.9}$$

To include the polarity of the magnetic field, Equation (2.4) is modified so that

$$\mathbf{B} = A_c B_0 \left(\frac{r_0}{r}\right)^2 \left(\mathbf{e}_r - \tan\psi \mathbf{e}_r\right)\left[1 - 2H\left(\theta - \theta'\right)\right] \tag{2.10}$$

with θ' the polar angle of the HCS and $A_c = \pm 1$ a constant determining the polarity of the HMF which alternates every 11 years in value. Periods when the magnetic field lines are directed outward in the northern hemisphere and inwards in the southern hemisphere are called $A > 0$ polarity epochs with $A_c = +1$. For $A < 0$ periods, $A_c = -1$ and the direction of HMF reverses. The Heaviside step function in Equation (2.10) is given by

$$H\left(\theta - \theta'\right) = \begin{cases} 0 \text{ when } \theta < \theta' \\ 1 \text{ when } \theta > \theta' \end{cases}. \tag{2.11}$$

This function causes the HMF to change polarities across the HCS. If this function is used directly in the numerical modulation model, the discontinuity causes severe numerical problems. To overcome this problem the Heaviside function is approximated (Hattingh, 1998, Langner, 2004) by

$$H'\left(\theta - \theta'\right) \approx \tanh\left[2.75\left(\theta - \theta'\right)\right]. \tag{2.12}$$

2.7 Solar cycle variations

It well known in the field of heliospheric physics that the measurements of the sunspot numbers (shown in Figure 2-1) indicate that the Sun has a quasi-periodic $\sim$ 11 year cycle called a solar activity cycle. Every 11 years the Sun moves through a period of fewer and smaller sunspots, a period called "solar minimum" and a period of larger and more sunspots called

"solar maximum" conditions.

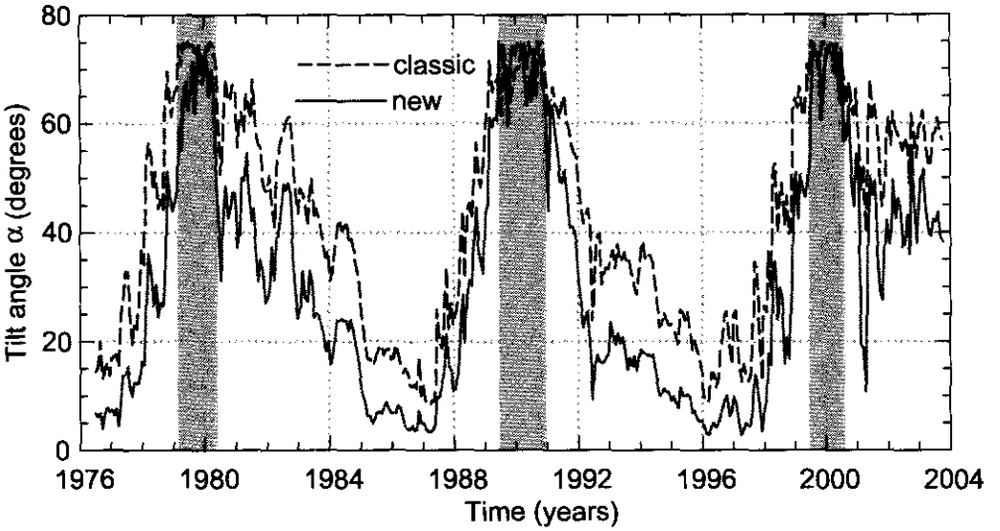

Figure 2-7: The tilt angle α from the first value recorded in 1976 until recently. Two different models for tilt angles are shown namely "classic" (dashed line) and "new" (solid line). The "classic" model uses a line-of-sight boundary condition and newer model uses a radial boundary condition at the photosphere. (Wilcox Solar observatory: http://quake.standford.edu; see also Hoeksema, 1992).

The effects of solar cycle variations in the Sun's magnetic dipole angle have considerable effects on the structure of the HCS with the tilt angle α following the changes in magnetic dipole angle of the Sun which is nearly aligned with the Sun's rotation axis near solar minimum and almost equatorial at solar maximum (Hoeksema, 1992). Figure 2-7 shows α from the first value recorded in 1976 until recently. Two different models for α are shown namely the "classic" and "new" model (Wilcox Solar Observatory: http://quake.stanford.edu). It is evident that α varies from small to a larger value between solar minimum and solar maximum (shaded-band) tracing out an 11 year solar cycle. For the discussions of the modulation effects on the differences between the two approaches, see Ferreira and Potgieter (2004). Of particular interest from this Figure is that one can deduce the duration of extreme solar maximum period (shaded regions), e.g. around the year 2000, the duration was about 1.2 years. The solar cycle changes of α has no significant direct effect on low-energy electron modulation. (Chapter 7).

It is also evident from measurements of the magnitude of the HMF at Earth (not shown) that

the time-dependent magnetic field $B(t)$ varies with solar activity and shows a good correlation with α. In fact there is a factor ~ 2 increase in $B(t)$ from solar minimum to solar maximum for a particular solar cycle (see Ferreira, 2002; Ferreira and Potgieter, 2004). This aspect is not utilized in this study.

In modulation modelling α and $B(t)$ have more relevance to the long-term modulation of CRs than sunspot numbers. In this thesis emphasis will be on the solar cycle dependence of the solar wind speed.

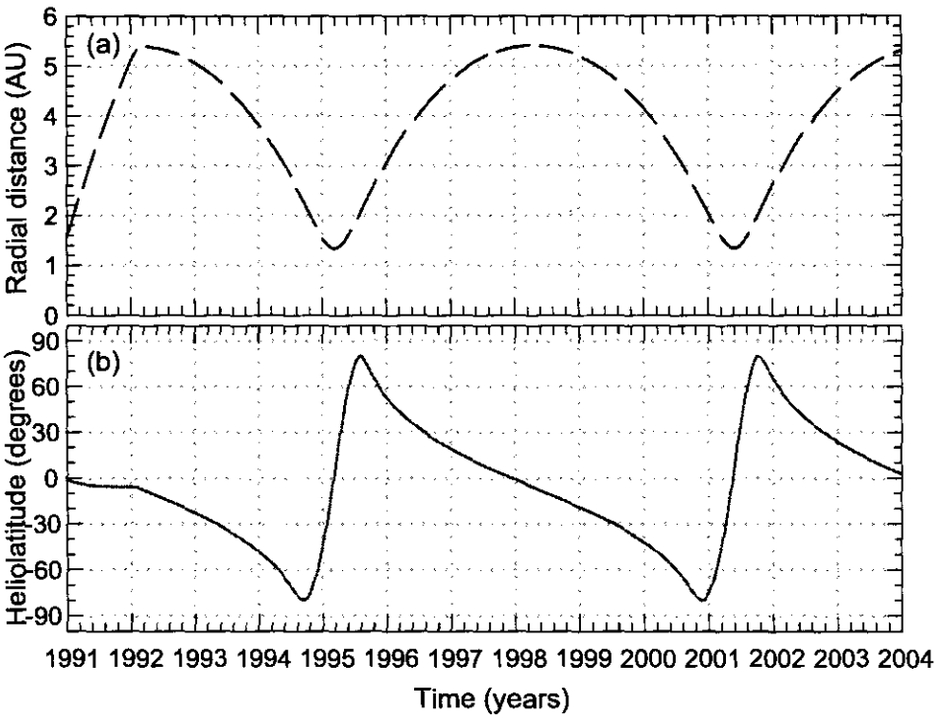

Figure 2-8: Trajectory of the Ulysses spacecraft in (a) radial and (b) heliographic coordinates from launch in 1990 up to the end of 2003. (Data from http: /SWOOPS.lanl.gov/recentvu.html).

2.8 Ulysses mission

A joint European Space Agency (ESA) and National Aeronautic and Space Administration (NASA) mission, Ulysses, named after the hero of Greek legend, is one of the most important

missions to study several aspects of the heliosphere and in particular CR modulation (e.g., Rastoin, 1995; Heber, 2002). This is the first spacecraft to undertake measurements far from the ecliptic and over the polar regions of the Sun, thus obtaining first-hand knowledge concerning the high latitudes of the inner heliosphere. The Ulysses mission, together with the KET which is part of the Ulysses COsmic and Solar Particle Investigation (COSPIN), has been described by Simpson et al. (1992a, 1992b), Marsden (1993), Wenzel (1993), Ferrando et al. (1996) and Heber et al. (1997). (See also the Ulysses home page: http://helio.estec.esa.nl/ulysses/).

The trajectory of the Ulysses spacecraft is shown in Figure 2-8 in terms of (a) radial distance and (b) the heliographic latitudes. After its launch on 6 October 1990, the spacecraft moved close to the ecliptic plane to Jupiter (at $\sim$ 5 AU), and from where it started, to move to higher latitudes south of the ecliptic plane. In mid-1994, the highest southern latitude with $\theta \approx 80^0$ was reached. From there, Ulysses moved to the northern polar region which was reached in mid-1995 and returned to the ecliptic plane again in 1998. After $\sim$1998 Ulysses started the second out-of-ecliptic orbit moving into the southern heliospheric polar regions. It reached $\theta \approx 80^0$ at the end of 2000 and crossed the equatorial plane in May 2001. On 5 February 2004, the spacecraft was again close to the giant planet, Jupiter. Unlike the 1992 fly-by, however, this was a distant 'encounter' (closest approach was 1990 Jovian radii from the planet's centre, compared with 6 Jovian radii in 1992). Another interesting difference between the two fly-bys is that this time the spacecraft approached the planet from high southern heliolatitudes. This difference had already become apparent in the radio data from the Unified Radio and Plasma Wave (URAP) experiment on board Ulysses, which in February and March 2003 detected intense radio emission from Jupiter at levels well above those seen in 1993 when Ulysses was at a comparable distance from the planet (approximately 2.8 AU). Details of the trajectory of the Ulysses spacecraft can be found on the Ulysses homepage: http://helio.estec.esa.nl/ulysses/.

Onboard Ulysses are nine scientific instruments of which the KET provides a wide range of e.g. electron fluxes from about 2.5 MeV to 6 GeV. In this study the 3 - 10 MeV ($\sim$ 7 MeV) electrons (e.g., Heber et al., 2001a,b; Heber et al., 2003a,b) from launch up to the end of 2003 are used in Chapter 6 and 7 respectively. Also used in this study is the solar wind speed data from the SWOOPS instrument (e.g., McComas, 2000; McComas, 2002b). This experiment on board Ulysses is actually made up of two instruments, the ion spectrometer and

the electron spectrometer. The ion spectrometer measures the positive ions within the solar wind plasma and the electron spectrometer measures the free electrons with in the solar wind plasma. In this way, the solar wind plasma speed can be measured simultaneously. (See also http://sci.esa.int/jump.cfm).

The Ulysses mission is highly successful and has contributed significantly to the current knowledge regarding the inner heliosphere. The mission has already been in progress for 13 years and has been recently extended to continue until March 2008. This latest extension, the third in the history of the joint ESA - NASA mission, will enable Ulysses to add an important chapter to its survey of the high latitude heliosphere. See the following publications for a review: Marsden (1995; 2001), Balogh et al. (2001), Smith et al., (2003).

2.9 Summary

In this Chapter a brief introduction was given of the concepts used in the heliospheric modulation of cosmic rays which will be used in this study. These include the origin of cosmic rays, the Sun and solar wind, the heliosphere, heliospheric magnetic field, heliospheric current sheet, the tilt angle and solar cycle variations. The Ulysses mission was briefly discussed as related to the KET and SWOOPS instruments.

In the next Chapter, a discussion is given about low-energy electrons in the inner heliosphere.

Chapter 3

Low-energy electrons in the inner heliosphere

3.1 Introduction

This Chapter serves as a concise discussion of the propagation and modulation of low-energy (3 - 30 MeV) electrons, in particular Jovian electrons in the inner helisophere. It begins with a brief background on observations of these electrons since the early 1970's to date with various space probes, and further it gives an overview of the development and advancement of the Jovian propagation models used to explain these observations. Finally, a short discussion is given on the modulation and source spectrum of Jovian electrons.

3.2 Sources of few MeV cosmic ray electrons in the inner heliosphere

The cosmic ray electron component is one of the rarer species constituting only about $\sim 1\%$ of the total cosmic radiation. They are $\sim 10^4$ times less massive and are oppositely charged than the dominant cosmic ray species making it more difficult to measure their intensities. They undergo modulation during propagation in the heliosphere, resulting in considerable modification of their energy spectra. In order to study their mode of propagation and modulation in the heliosphere, we need to know their origin which is briefly discussed next. There are different

main sources contributing to few-MeV electron 's intensities in the inner heliosphere ($\leq$ 10 AU).

3.2.1 Astrophysical sources

It is believed that astrophysical phenomena such as supernova explosions are the main sources of cosmic rays electrons in our galaxy. This electron population, known as galactic electrons is accelerated by these supernova blast waves (e.g., Jones and Ellison 1991; Koyama et al., 1995; Tanimori et al., 1998) and penetrates the heliosphere isotropically to be modulated by different physical process in the heliosphere (Discussed in Chapter 4). They are the most dominant electron population near the heliospheric polar regions and at distances beyond 10 AU in the equatorial plane (e.g., Ferreira et al. 2001b). They form an essential part of this study, but will not be given much attention in this Chapter.

3.2.2 Solar flares and shocks

Solar flares are regarded as the main source of solar electrons with energies up to a few hundred MeV which can be observed on Earth for short periods only (e.g., Forbush, 1946; del Peral et al., 2003). Transients such as coronal mass ejections and shocks in the interplanetary medium, can also produce these electrons. Contribution of this electron population is not considered within the scope of this study because the focus is based on modelling of Jovian and galactic electrons in the inner heliosphere.

3.2.3 Jovian magnetosphere

It was discovered in 1973 during the Jupiter fly-by of the Pionner 10 spacecraft that the Jovian magnetosphere at $\sim$ 5 AU in the ecliptic plane is a relatively strong source of electrons with energies up to $\sim$ 30 MeV (e.g., Teegarden et al., 1974; Chennette et al., 1974; and Simpson et al., 1974; Simpson et al., 1978). Teegarden et al. (1974) further identified Jupiter as the source of "quit time" electrons observed at 1 AU (e.g., McDonald et al., 1972; and L'Heureux and Meyer, 1976). These electrons, called Jovian electrons were also measured along the trajectory of Pioneer 11 up to 16^0 heliographic latitude and resulted in a strong evidence for diffusive transport of electrons perpendicular to the mean heliospheric magnetic field (Chennete et al., 1974; Hamilton and Simpson, 1979). Studying their intensity-time profile for the period 1978-

1984, as observed by the University of Chicago electron spectrometer on board the ISSE3 (ICE) spacecraft, Moses (1987) found that the Jovian electron intensity demonstrates little or no solar cycle variation.

The most recent measurements of these low energy electrons in the inner heliosphere (e.g., Ferrando et al., 1993a,b, Heber et al., 2003a,b, 2004) have been made with the KET (e.g., Simpson et al., 1992a,b) as discussed in Chapter 2. The propagation and modulation of these electrons in the inner heliosphere form (up to 10 AU) the most important component of this study. Observations from the Electron-Proton Helium instrument (EPHIN) onboard the SOHO spacecraft are also available but have not been used in this study.

An overview of earlier developments and recent advancement of Jovian propagation models is given in the following section.

3.3 A brief overview of Jovian electron propagation models and their results

3.3.1 The Conlon and Chenette diffusion model

To explain the Pioneer 10 and 11 interplanetary Jovian electron observations, Conlon (1978) developed the first Jovian propagation model based on the convection-diffusion equation:

$$\frac{\partial U}{\partial t} = \nabla \cdot (\mathbf{K} \cdot \nabla U - \mathbf{V}U) = 0 \tag{3.1}$$

where U represents the number density of Jovian electrons, $\mathbf{K}$ the diffusion tensor, and $\mathbf{V}$ the solar wind velocity. This model was modified and described by Rastoin (1995). The diffusion coeficients used (e.g., Rastoin, 1995; and Ferrando, 1997) were derived from previous spacecraft observations. Because of their assumptions of Cartesian geometry, the constant solar wind speed of 450 km s^{-1} and the Parker geometry of the HMF lines, the model solutions (solid lines) were only compatible with KET observations (black data curve) in the region close to the Jovian point source as shown in Figure 3-1. They were also inconsistent in accounting for the modulation of galactic electrons.

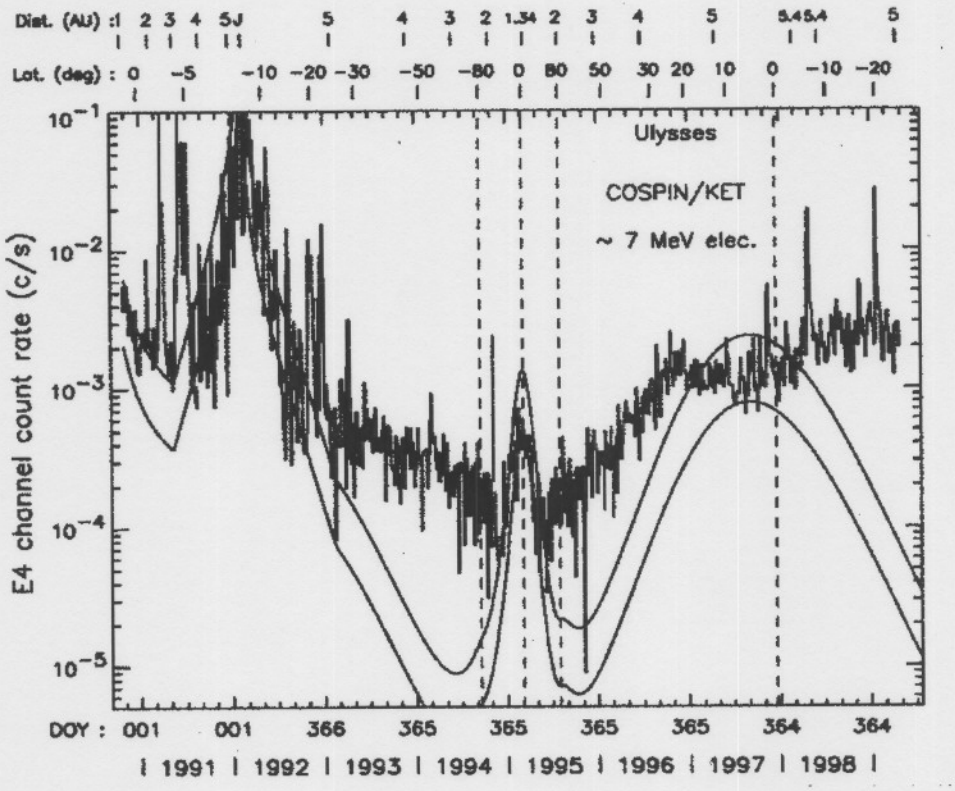

Figure 3-1: Count rate of the 3-10 MeV KET electron channel (four day averages). The smooth solid lines are the prediction an of earlier Jovian electron propagation model (e.g., Conlon and Chennete,1977; Rastoin, 1995); nominal (upper solid line) and scaled by one third (lower solid line). (From Ferrando et al., 1999).

3.3.2 The 2D shock acceleration models

An axisymmetric (2D) shock acceleration models were developed (e.g., Jokipii and Kotá 1991; Moraal et al., 1991; Haasbroek, 1997; Haasbroek et al., 1997a,b) for propagation of Jovian electrons in the outer heliosphere and their acceleration at the heliospheric termination shock (TS). Moraal et al. (1991) suggested that these electrons may be reaccelerated to cosmic ray energies at the termination shock and to subsequently alter electron fluxes observed at Earth, but Potgieter and Ferreira (2002) illustrated that these Jovian electrons are not significantly influenced by the presence of the solar wind termination shock. The 2D shock acceleration models are not applied in this study because of their limitations due to the implicit assumption

of a ring source and, therefore, cannot account for the three dimensional transport of Jovian electrons in the inner heliosphere as studied in this work.

3.3.3 The 3D modulation models

Observations made along the unique Ulysses trajectory revealed the effects of the third dimension of the inner heliosphere and imposed a challenge to the modulation modelers to construct realistic models to account for the 3D heliospheric transport of Jovian and galactic electrons. Fichtner et al. (2000b) developed a 3D steady-state, non-drift model and a more recent time-dependent version (e.g., Fichtner et al., 2001b; Kissmann et al., 2004) based on the Parker (1965) transport equation and are most suitable to simulate the modulation of Jovian and galactic electrons in the inner heliosphere. The latter is still being further developed and will therefore not be applied in this study.

3.3.4 The 3D Jovian electron model

Besides the Fichtner et al. (2000b) model, Ferreira et al. (2001a,b), by using a different numerical approach, developed an advanced 3D steady-state Jovian electron modulation model based on the Parker transport equation including gradient, curvature, and current sheet drifts. The details of this numerical model will be discussed in the following Chapter. This model and the Fichtner et al. (2000b) model yield similar solutions when the same set of transport parameters is assumed. Figure 3-2 shows the features of the three-dimensional distribution of 7 MeV Jovian electrons within 10 AU of the heliosphere computed with this model. Here, the Jovian source is located at 5 AU in the equatorial plane.

Using this 3D Jovian electron model, Ferreira et al. (2001a) studied the latitudinal transport of both 7 MeV Jovian and galactic electrons by illustrating how the electron intensities are affected at different latitudes by the enhancement of perpendicular diffusion in the polar direction. In particular, the electron intensity-time profiles along the Ulysses trajectory were calculated for different assumptions for heliospheric polar diffusion and compared to the 3-10 MeV electron flux observed by Ulysses from launch up to the end of the first out-of-ecliptic orbit. Comparison of the model computations and observations gave an indication as to the magnitude of heliospheric polar diffusion. This has improved our understanding of the role

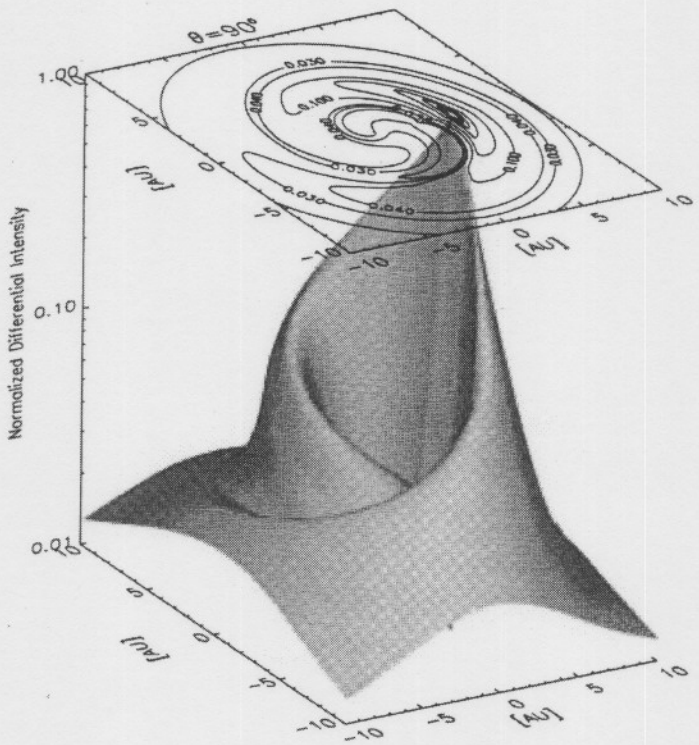

Figure 3-2: Computed distribution of 7 MeV Jovian electrons for the inner 10 AU of the heliosphere. The source is at 5 AU. (From Ferreira 2002).

that perpendicular diffusion plays to transport low energy electrons to high-latitudes. The relative contributions of the Jovian and galactic electrons to the total electron intensity were also successfully computed along the Ulysses trajectory.. These aspects will be revisited in this work.

Ferreira et al. (2001b) further studied the radial transport of $\sim$ 16 MeV Jovian and galactic electrons by comparing model computations with the electron intensities (e.g., Eraker et al., 1982; Lopate, 1991) observed by the University of Chicago experiment on board the Pioneer 10 spacecraft up to $\sim$70 AU. It was shown that the computed electron intensities are sensitive to the radial dependence of the diffusion coefficients in the inner heliosphere and that the compatibility between the model and observations gives an indication as to the radial dependence of the diffusion coefficients. The relative contributions of Jovian and galactic electrons to the total

electron intensity were also computed along the Pioneer 10 trajectory. It was illustrated that the Jovian electrons dominate the total electron intensity in the inner equatorial regions only up to $\sim$ 9 AU. From 15 AU outward, the Jovian contribution becomes insignificant, decreasing rapidly as a function of increasing distance.

Ferreira (2002) also produced a model solutions compatible with the 3 - 10 MeV KET observations of Ulysses first out of ecliptic orbit (up to $\sim$ 1998). These results indicated that no time-dependence changes in the transport parameters were required to compute realistic electron modulation during solar minimum conditions. But, when this model was applied to solar maximum conditions, the period after 1998 by assuming the same set of transport parameters as during solar minimum periods, the computed intensities were significantly lower than the observed 3 - 10 MeV electrons (Heber et al., 2003a,b; Ferreira et al., 2003a,b). These observed low-energy electron intensities stayed almost unchanged, in contrast to higher energies where observed intensities decreased as solar activity picked up. Heber (2002) argued that these low-energy observations could neither be explained by solar particles nor by locally accelerated electrons and should therefore be of galactic and Jovian origin.

To improve modelling of the compatibility between the model computations and the 3 - 10 MeV observations after 1998, a study of effects of changing only the solar wind speed in the model with changing heliospheric conditions has been conducted in Chapter 6 and some of the results thereof were published in Ferreira et al., (2003a,b). An overview of Jovian electron modulation in general is given in the next section.

3.4 Modulation of Jovian electrons

Electron data collected on Earth by IMP8 showed unexpected increases in the measured flux levels during quiet times (e.g., McDonald et al., 1972). The discovery of Jovian electrons by Pioneer 10 led to the recognition of this quiet time electron increase as being of Jovian origin (Teegarden et al., 1974; Mewaldt et al., 1976). Observations of these electrons at 1 AU showed a strong modulation with a period of 13 months (Mewaldt et al., 1976), which is associated with the Jovian synodic period. Every 13 months, the heliospheric magnetic field lines connect more effectively between the Earth and Jupiter so that electrons transported along the field

lines can easily reach the Earth. At other times, these electrons also have to diffuse across the field lines toward the Earth, and normal to heliospheric equatorial region to high latitude (e.g., Hamilton, 1979).

When Ulysses was within 1 AU of Jupiter during the first encounter, it observed short and sharp increases and decreases of low-energy electron fluxes which are called Jovian jets (bursts). These jets are characterised by a spectrum identical to the electron spectrum within the Jovian magnetosphere and a strong anisotropy (e.g., Chenete et al., 1974; Ferrando et al., 1993a). A similar feature has also recently been observed (Heber et al., 2004). The causes of these short-time variations in the Jovian electron flux are not yet well described and is a topic for future studies.

By using the 3D Jovian electron modulation model and assuming the relative position of the Sun and Jupiter as the only time-varying factor, Ferreira (2002) could compute the 13-month periodicity of Jovian electrons observed at 1AU with the IMP satellite as shown in Figure 3-3.

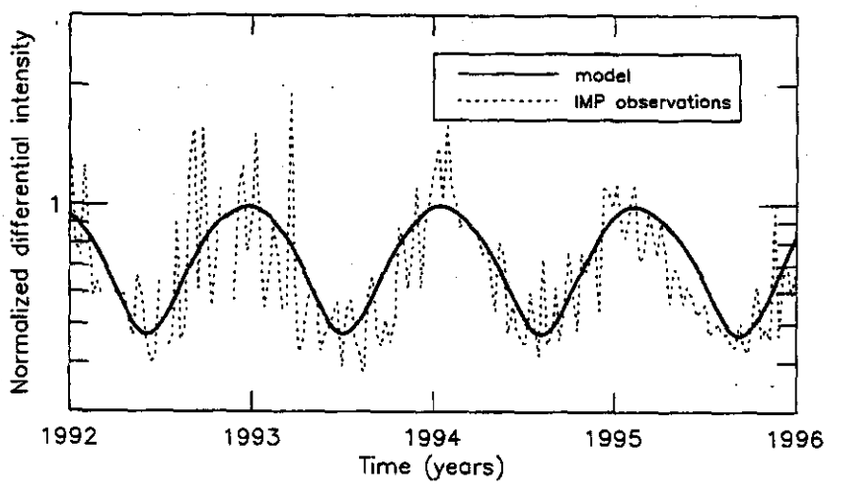

Figure 3-3: Normalised computed 7 MeV electron intensities at Earth in units of particles $m^{-2}s^{-1}sr^{-1}MeV^{-1}$ for the period 1992 -1996 (dark solid line), in comparison with averaged 2 - 12 MeV electron data from IMP. (From Ferreira, 2002).

Jovian electrons observed at 1 AU also experience $\sim$ 27-day modulation due to corotating interaction regions perturbing interplanetary propagations (e.g., Conlon and Simpson, 1977).

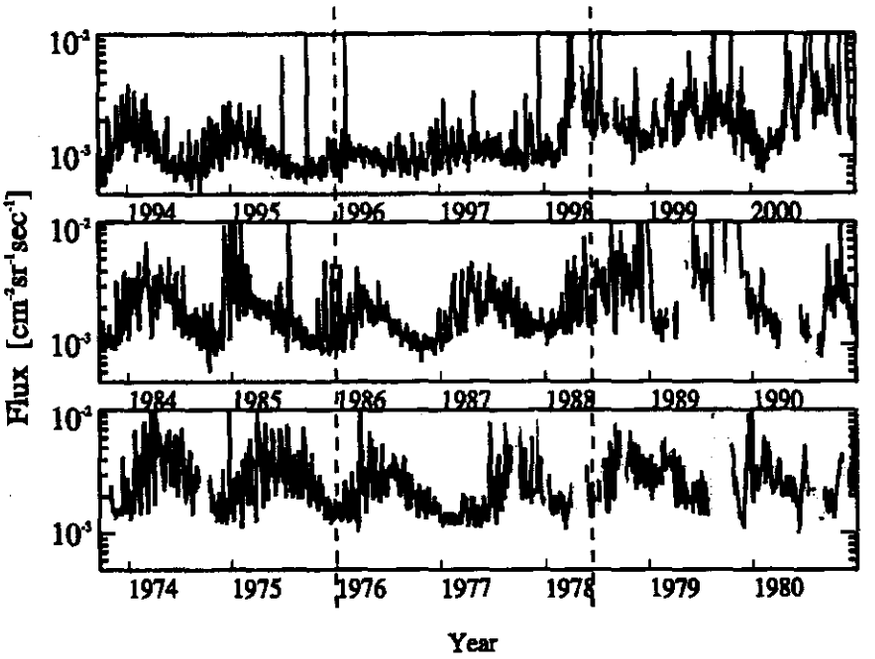

Figure 3-4: Daily averaged electron fluxes in the 2- 12 MeV energy range at Earth measured by the IMP8/CRNC intrument (Kanekal et al., 2003). The top, middle and bottom panels show electron fluxes for years 1993 to 2001, 1984 to 1991 and 1974 to 1981 respectively. Dashed vertical lines denote a two year period around solar cycle minima. (From Kanekal et al., 2003).

A different study of the effects of CIRs on the shorter-term modulation of low-energy electrons in the inner heliosphere has been done recently by Kissmann et al., (2004). These effects were not taken into account for this study.

It was suggested by Morioka and Tsuchiya (1997) that Jovian electrons are also modulated by solar wind variations at Jupiter. By scrutinizing Pioneer 11 electron data collected during 1974, they found that the Jovian electron intensity was inversely correlated with solar wind dynamic pressure. Tsuchiya et al. (1999) also suggested that the polarity of the heliospheric magnetic field at the vicinity of Jupiter may control the release rate of Jovian electrons into the interplanetary space.

More recently, Kanekal et al. (2003), by analysis of electron data observed at Earth during the time period 1992 to 2002 with instruments on board SAMPEX and IMP8, discovered a puzzling non-transient decrease in Jovian fluxes near solar cycle minimum (from 1996-1998) as

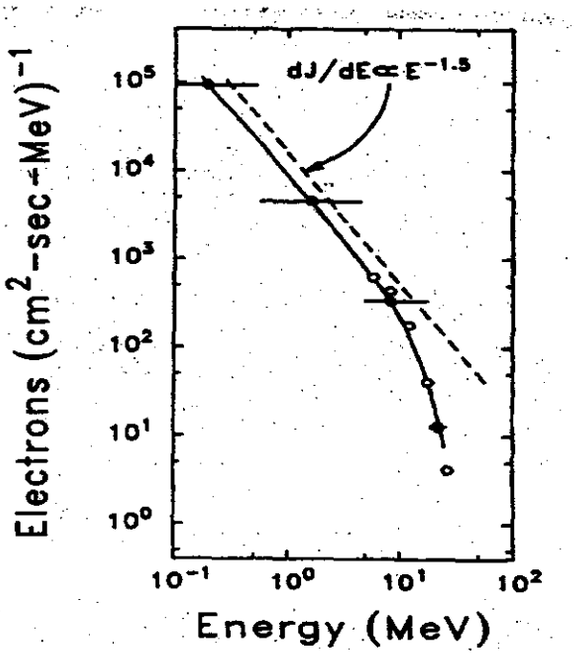

Figure 3-5: Comparison of the Pioneer 10 electron spectrum (filled circles) within the Jovian magnetosphere during the time of maximum flux (Baker and Van Allen, 1976) and ISEE 3 spectrum (open circles). The intensity normalization of the ISEE 3 data is arbitrary. (From Moses, 1987).

shown in the top panel of Figure 3-4. The Jovian electron flux diminished significantly from early 1996 to the end of 1997, then recovered subsequently and was observed until the end of 2001. In an attempt to explain these observations, they suggested either a change in the Jovian source function strength and/or a softening of the Jovian electron spectrum may account for these apparent anomalous observations.

3.5 The Jovian electron source spectrum

Moses (1987) showed that the Jovian electron spectrum between 5 and 30 MeV, measured by the University of Chigago instrument on board ISEE 3, during a period of best magnetic connection between Jupiter and Earth, and Pioneer 10 electron spectrometer obtained within Jovian magnetosphere (e.g., Baker and Van Allen, 1976) as shown in Figure 3-5, can be fitted

by a simple power-law

$$j \propto E^{-\gamma} \tag{3.2}$$

with γ the spectral index and j the differential intensity. A power-law representation of the observed electron spectrum at 1 AU requires the spectral index to be a function of energy, which increases from $\gamma \approx 1.5$ at low energies to $\gamma \lesssim 6$ at high energies. Moses (1987) also found agreement with electron spectra of other authors in overlapping regions of energy (e.g.,Teegarden et al., 1974; Eraker, 1982; Eraker and Simpson, 1979). How the Jovian source function is constructed to simulate Jovian electron modulation will be discussed in the next Chapter.

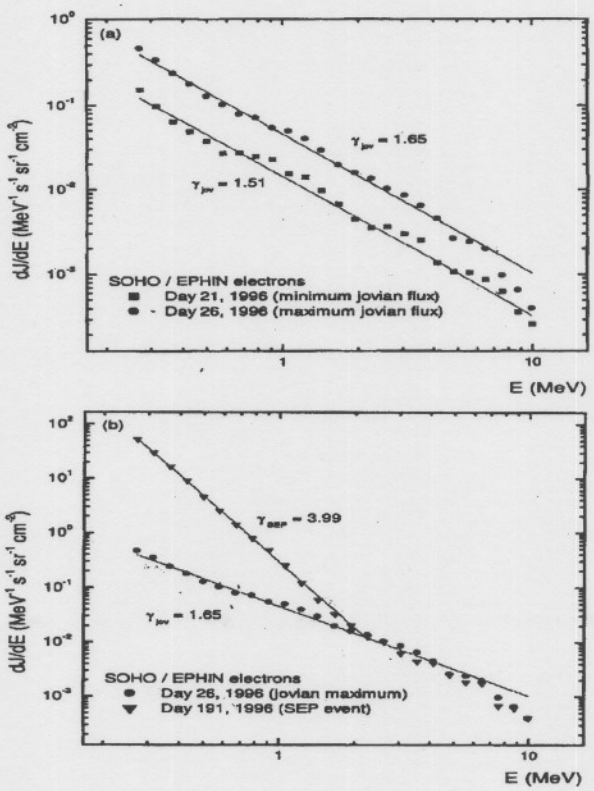

Figure 3-6: (a) Fits of the electron fluxes to an energy power-law during a day of minimum and maximum Jovian flux observed by the SOHO/EPHIN sensor. (b) Comparison between the Jovian electron flux and the electron flux of a solar energetic particle event . (From del Peral et al., 2003).

Most recently, del Peral et al. (2003) showed measurements of the Jovian electron spectra at 0.99 AU from the SOHO/EPHIN sensor observed during a day (day 21, 1996) of minimum flux and a day (day 26, 1996) of maximum flux fitted by Equation (3.2) with spectral index $\gamma = \gamma_{jov} = 1.51$ and $\gamma_{jov} = 1.65$ respectively as shown in Figure 3-6(a). These values of the spectral indices are in good agreement with the values expected from the Jovian magnetosphere. The other electron population observed shows a spectral index of $\gamma_{SEP} > 2$, shown in Figure 3-6(b) as $\gamma_{SEP} = 3.99$, which indicates that it is of solar origin associated with a solar energetic particle (SEP) event.

3.6 Summary

In this Chapter a short overview of the propagation and modulation of low energy electrons (3 - 10 MeV) in the inner heliosphere were given, with main emphasis on Jovian electrons. These include the sources contributing to the few MeV electron intensities in the inner heliosphere, an overview of Jovian electron propagation and modulation models, and a brief discussion on the observed modulation and spectra of Jovian electrons.

In the next Chapter, the 3D Jovian electron modulation model will be discussed in more detail including the Jovian source function.

Chapter 4

The electron modulation model

4.1 Introduction

This Chapter is devoted to giving a brief summary of the steady-state cosmic ray electron modulation model (Ferreira, 2002) which is based on Parker's transport equation and is used in this study. It begins with a short discussion of the cosmic ray transport equation and the modulation processes incorporated therein. A further discussion on the 3D Jovian modulation model including the Jovian source function and the electron local interstellar spectrum (LIS) is given.

4.2 The transport equation and modulation processes

The intensity changes of cosmic rays in the heliosphere with time as a function of energy and position is called the modulation of cosmic rays. The equation describing these modulation mechanisms was developed by Parker (1965) and is known to date as the transport equation (TPE). This equation was rederived (Gleeson and Axford, 1967) and refined by others (Gleeson and Axford, 1968; Jokipi and Parker, 1970) and is given by

$$\frac{\partial f}{\partial t} = \boldsymbol{\nabla} \cdot (\mathbf{K} \cdot \boldsymbol{\nabla} f - \mathbf{V} f) + \frac{1}{3} (\boldsymbol{\nabla} . \mathbf{V}) \frac{\partial f}{\partial \ln P} + Q, \tag{4.1}$$

where $f(\mathbf{r}, P, t)$ is the omni-directional cosmic ray (CR) distribution function dependent on position $\mathbf{r}$, rigidity P, and time t. The rigidity is defined to be $P = pc/q$ with p the particle

momentum, q the charge and c the speed of light. Since pc has units of energy, and q has the unit of charge, it is easy to show that P has the unit of volts. The useful unit for practical purpose is normally gigavolts (GV). It is also easy to show that for electrons with energies of interest to this study that $P \approx E$,where E is kinetic energy of the particles (See also Ferreira, 2002). The relationship between the differential CR intensity j and the distribution function f is given by $j \propto P^2 f$. The solar wind velocity is denoted by $\mathbf{V}$, and $\mathbf{K}$ designates the diffusion tensor and will be discussed in Chapter 5. The terms in the TPE include the following processes:

(1) The term on the left describes the changes in the CR distribution with time.

(2) The first term on the right describes spatial diffusion parallel and perpendicular to average heliospheric magnetic field as well as particle drifts in the background magnetic field.

(3) The second term describes the outward particle convection due to the radial solar wind.

(4) The third term includes adiabatic energy changes caused by the solar wind and HMF.

(5) The final term describes possible sources of CRs inside the heliosphere.

Understanding these processes and their consequences is one of the most important areas of CR modulation studies.

4.3 The 3D Jovian electron modulation model

Ferreira et al. (2001a,b) developed an advanced steady-state, 3D Jovian electron modulation model which is based on Equation (4.1) and describes the relevant physics of heliospheric transport of low energy (< 30 MeV) Jovian and galactic electrons (see also section 3.4). The numerical implementation of this model is briefly discussed in this section.

To solve Equation (4.1) numerically, it is rewritten in a coordinate system corotating with the Sun and the heliospheric current sheet is assumed to be static in this system. The transport equation takes the form (e.g., Kóta and Jokipii, 1983; Hattingh, 1998):

$$0 = \boldsymbol{\nabla} \cdot (\mathbf{K} \cdot \boldsymbol{\nabla} f - \mathbf{V}^* f) + \frac{1}{3} (\boldsymbol{\nabla} \cdot \mathbf{V}^*) \frac{\partial f}{\partial \ln P} + Q, \tag{4.2}$$

with $\mathbf{V}^* = \mathbf{V} - \boldsymbol{\Omega} \times \mathbf{r}$ with $\boldsymbol{\Omega}$ the rotational velocity of the Sun. Then in a spherical

coordinate system (r, θ, ϕ) and assuming a steady-state, Equation (4.2) takes the form:

$$\left[\frac{1}{r^2}\frac{\partial}{\partial r}\left(r^2 K_{rr}\right) + \frac{1}{r\sin\theta}\frac{\partial K_{\phi r}}{\partial \phi}\right]\frac{\partial f}{\partial r} + \left[\frac{1}{r^2\sin\theta}\frac{\partial}{\partial \theta}\left(K_{\theta\theta}\sin\theta\right)\right]\frac{\partial f}{\partial \theta}$$

$$+\left[\frac{1}{r^2\sin\theta}\frac{\partial}{\partial r}\left(rK_{r\phi}\right) + \frac{1}{r^2\sin^2\theta}\frac{\partial K_{\phi\phi}}{\partial \phi} + \Omega\right]\frac{\partial f}{\partial \phi}$$

$$+K_{rr}\frac{\partial^2 f}{\partial r^2} + \frac{K_{\theta\theta}}{r^2}\frac{\partial^2 f}{\partial \theta^2} + \frac{K_{\phi\phi}}{r^2\sin^2\theta}\frac{\partial^2 f}{\partial \phi^2} + \frac{2K_{r\phi}}{r\sin\theta}\frac{\partial^2 f}{\partial r\partial \phi}$$

$$+\left[-\left\langle \mathbf{v}_d\right\rangle_r\right]\frac{\partial f}{\partial r} + \left[-\frac{1}{r}\left\langle \mathbf{v}_d\right\rangle_\theta\right]\frac{\partial f}{\partial \theta} + \left[-\frac{1}{r\sin\theta}\left\langle \mathbf{v}_d\right\rangle_\phi\right]\frac{\partial f}{\partial \phi}$$

$$-V\frac{\partial f}{\partial r} + \frac{1}{3r^2}\frac{\partial}{\partial r}\left(r^2 V\right)\frac{\partial f}{\partial \ln p} = -Q, \tag{4.3}$$

where $K_{rr}, K_{r\theta}, K_{r\phi}, K_{\theta r}, K_{\theta\theta}, K_{\theta\phi}, K_{\phi r}, K_{\phi\theta}$ and $K_{\phi\phi}$ are the elements of the tensor $\mathbf{K}$ in Equation (4.2) and will be formally discussed in Chapter 5. The components of the drift velocity are given as:

$$\left\langle \mathbf{v}_d\right\rangle_r = -\frac{sign(Bq)}{r\sin\theta}\frac{\partial}{\partial \theta}\left(\sin\theta K_{\theta r}\right), \tag{4.4}$$

$$\left\langle \mathbf{v}_d\right\rangle_\theta = -\frac{sign(Bq)}{r}\left[\frac{1}{\sin\theta}\frac{\partial}{\partial \phi}\left(K_{\phi\theta}\right) + \frac{\partial}{\partial r}(rK_{r\theta})\right],$$

$$\left\langle \mathbf{v}_d\right\rangle_\phi = -\frac{sign(Bq)}{r}\frac{\partial}{\partial \theta}\left(K_{\theta\phi}\right),$$

or alternatively

$$\mathbf{v}_d = \boldsymbol{\nabla} \times K_A \mathbf{e}_B$$

$$= \boldsymbol{\nabla} \times \left(K_A \mathbf{e}_B\right)\left[1 - 2H\left(\theta - \theta'\right)\right] + 2\delta_D\left(\theta - \theta'\right)K_A \mathbf{e}_B \times \boldsymbol{\nabla}\left(\theta - \theta'\right), \tag{4.5}$$

with $\mathbf{e}_B = \mathbf{B}_m/B$, H the heaviside function given by Equation (2.11), K_A the drift coefficient and δ_D the Dirac-function, given by Hattingh (1998). The first term in Equation (4.5) describes the gradient and curvature drift caused by HMF, and the second term describes the drift caused by the heliospheric current sheet (HCS). The term Q on the right side of Equation (4.3) describes for this work the Jovian source function and will be discussed in detail in Section 4.5.

4.4 Solution of the TPE

Equation (4.3) is solved numerically using the following boundary conditions:

(1) The heliosphere is assumed to be spherical with an outer boundary at $r_b = 120$ AU where the LIS is used as an input spectrum (discussed later in Section 4.6).

(2) The inner boundary is specified at $r = r_\odot$ and assumes that the radial gradient of the distribution function just outside the boundary is equal to the gradient just inside. For two-dimensional models, a reflecting Sun was assumed as an inner boundary condition (e.g., Potgieter, 1984; Hattingh, 1993).

This implies that no particles enter or leave the Sun:

$$\left.\frac{\partial f}{\partial r}\right|_{r=r_\odot} = 0. \tag{4.6}$$

Recently Siluszyk and Alania (2001) showed that

$$\left.\frac{\partial f}{\partial r}\right|_{r=r_\odot} \neq 0, \tag{4.7}$$

could be a more appropriate boundary condition implying an absorbing Sun. However, this only effects CR intensities within 1 AU.

(3) At the heliospheric poles it is assumed that:

$$\left.\frac{\partial f}{\partial \theta}\right|_{\theta=0} = 0. \tag{4.8}$$

Equation (4.3) is a parabolic differential equation and is solved by applying the Alternating Direction Implicit (ADI) method, which is a modification of Cranck-Nicholson finite difference method. Douglas (1955) had initially developed this method to solve parabolic differential equations in terms of two spatial coordinates and a time coordinate (see also Douglas, 1962; Potgieter, 1984). A solution is calculated in the following way using this numerical scheme (Hattingh, 1998; Ferreira, 2002):

(1) A first solution, using the LIS as an initial condition, is determined at a third of a momentum step forward by solving the differential equation implicitly in the direction of the first spatial coordinate, the radial distance r.

(2) A second solution is determined at another third of a momentum (or rigidity or energy) step forward, in terms of the first solution by solving the differential equation implicit in the direction of the second spatial coordinate, the polar angle θ.

(3) This whole process is then repeated for the last spatial coordinate, the azimuthal angle ϕ, to determine a solution at the last third of momentum step forward in terms of the previous two solutions.

(4) The result is a system of linear equations which can be solved using the Thomas algorithm (e.g., Lapidus and Pinder, 1982).

The numerical scheme of solving the TPE in three space coordinates and a rigidity coordinate was first done in the local research group by Williams (1990) for a flat heliospheric current sheet and later by Hattingh (1998) for a wavy heliospheric current sheet. The technical details used in solving the TPE numerically were fully described recently by Hattingh (1998) and Ferreira (2002) and will not be repeated here.

4.5 The Jovian electron source function

Rastoin (1995) and Ferrando et al. (1991) used the basic source function given by Equation (3.2) with $\gamma = 2.5$ at all energies to simulate Jovian electrons spectra measured by the University of Chigago instrument on ISEE 3 (ICE) (Moses, 1987) during a period of best magnetic connection between Jupiter and Earth as well as Pioneer 10 electron spectra (e.g., Eraker, 1982; Lopate, 1991; Lopate, 2001) as shown in Figure 4.1. Later, Haasbroek (1997) used a source function which was originally derived by Baker and Van Allen (1976) with a roll-over in the spectral index from $\gamma = 1.5$ to $\gamma = 3.5$ at 5 MeV and is expressed in terms of the differential intensity as a function of kinetic energy E as:

$$j_{source}(E) = C_c \left(\frac{E}{E_0}\right)^{-1.5} \left(1 + \frac{E}{h_c}\right)^{-n_c} \tag{4.9}$$

with $C_c = 4 \times 10^8$ particles $\mathrm{m^{-2}s^{-1}sr^{-1}MeV^{-1}}$, $n_c = 3.5$, $h_c = 5$ MeV and $E_0 = 1$ MeV. This source function is shown in Figure 4-1(a). More recently, Ferreira et al. (2002) indicated that the spectrum given by Equation (3.2) does fit the lowest energy Pioneer 10 data, but then decreases as a function of increasing energy much faster than indicated by the data because the

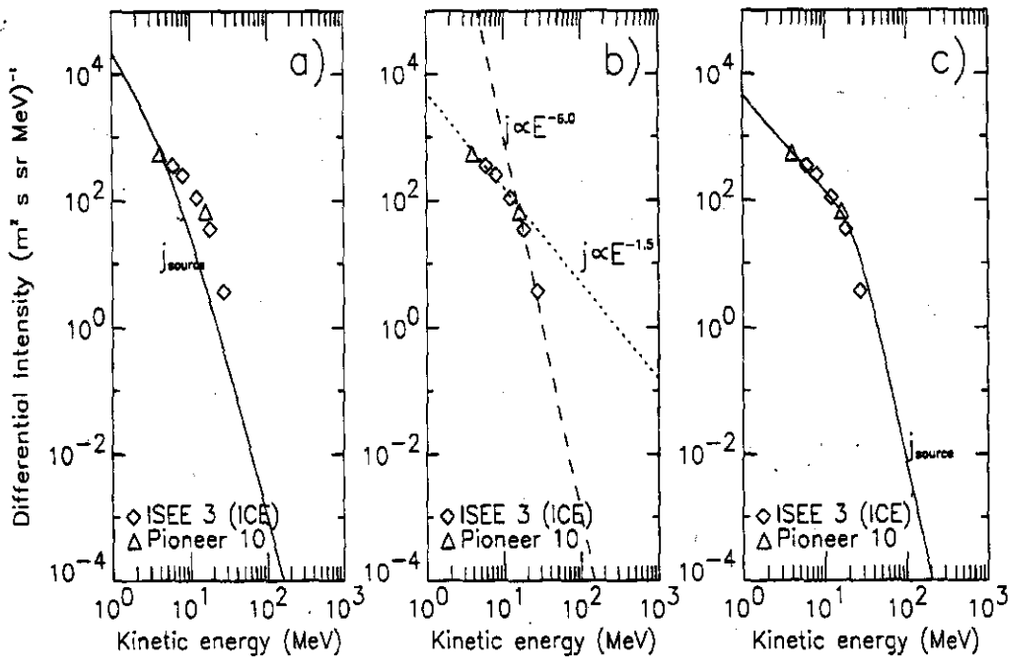

Figure 4-1: (a) The source function as used by Haasbroek (1997) given by Equation (4.9). Also shown are low-energy Jovian electron data from ISEE 3 ICE (e.g., Moses, 1987) and Pioneer 10 (e.g., Eraker, 1982; Lopate, 1991). (b) Spectra where $j(E) \propto E^{-1.5}$ (dotted line) and $j(E) \propto E^{-6.0}$ (dashed line). (c) The source function which is given by Equation (4.10) in comparison with observations. (From Ferreira, 2002).

roll-over from $\gamma = 1.5$ to $\gamma = 3.5$ occurs at a very low energy. By simulating the spectra where $j(E) \propto E^{-1.5}$(dotted line) and $j(E) \propto E^{-6.0}$(dashed line) as shown in Figure 4-1(b), Ferreira et al. (2001a) could produce compatibility with the observed roll-over for the Jovian spectrum from $\gamma = 1.5$ to $\gamma = 6.0$ at ~ 20 MeV.

To construct the Jovian source function Q in Equation (4.3), Ferreira et al. (2001a) invoked the superposition of the spectra $j(E) \propto E^{-1.5}$ and $j(E) \propto E^{-6.0}$ and obtained:

$$Q = j_{source}(E) = 1.5 \left(\frac{c_k j_{1.5} d_k j_{6.0}}{c_k j_{1.5} + d_k j_{6.0}} \right), \tag{4.10}$$

with

$$j_{1.5} = 5.0 \times 10^3 \left(\frac{E}{E_o} \right)^{-1.5}, \tag{4.11}$$

$$j_{6.0} = 10^9 \left(\frac{E}{E_o}\right)^{-6.0},$$

$$c_k = 0.6,$$

$$d_k = 5.0,$$

with j_{source} in units of particles $m^{-2}s^{-1}sr^{-1}MeV^{-1}$. This function is shown in Figure 4-1(c) and has also been used in modulation studies by Ferreira et al. (2001a; 2001b), Ferreira and Potgieter (2002), Ferreira (2002) and Langner (2004) to describe a source spectrum of low-energy electrons at Jupiter and is also used in this study.

4.6 The electron local interstellar spectrum

The LIS for electrons is defined as an unmodulated spectrum of cosmic ray electrons before entering the heliosphere and is specified as an initial condition at the outer modulation boundary and then modulated throughout the heliosphere according to TPE. In this study the electron LIS of Langner et al. (2001a,b,c) is used and is shown later in Chapter 8 (see also langner 2000). The parameterisation of this LIS is given by:

$$j_{LIS} = \frac{214.32 + 3.32\ln(P)}{1 + 0.26\ln(P) + 0.02(\ln(P))^2} \tag{4.12}$$

when $P \leq 0.0026$ GV,

$$j_{LIS} = 1.7\left(\frac{52.55 + 23.01P}{1 + 148.62P}\right)^2$$

when $0.0026 < P \leq 0.1$ GV,

$$j_{LIS} = \frac{1555.89 + 17.36P - 3.4 \times 10^{-3}P^2 + 5.13 \times 10^{-7}P^3}{(1 - 11.22P + 7532.93P^2 + 2405.01P^3 + 103.87P^4)}$$

when $0.1 < P \leq 10$ GV,

$$j_{LIS} = 1.7\exp\left(-0.89 - 3.22\ln\left(R\right)\right)$$

when $P > 10$ GV, with j_{LIS} the differential intensity in units of particles $\mathrm{m}^{-2}\mathrm{s}^{-1}\mathrm{sr}^{-1}\mathrm{MeV}^{-1}$. (See also Langner, 2004).

4.7 Summary

A brief discussion was given on the well known transport equation and the transport processes applicable to the modulation of cosmic rays. The 3D Jovian electron modulation model and the numerical implementation thereof were discussed including the Jovian source function, and the galactic electron LIS.

The heliospheric diffusion tensor for low energy electrons is the main topic of study in the next Chapter.

Chapter 5

Aspects of the heliospheric diffusion tensor

5.1 Introduction

The general purpose of this Chapter is to give a theoretical background on certain aspects of the heliospheric diffusion tensor incorporated in the TPE (Equation 4.2) discussed in Chapter 4. A particular purpose is to investigate the spatial and rigidity dependence of various elements of the tensor constructed by Ferreira et al. (2001a,b) from the work of Burger et al. (2000). This was to establish compatibility with Ulysses spacecraft observations (Heber et al., 2001) of a few-MeV Jovian and galactic electrons in the heliosphere during solar minimum conditions. Some elements of the tensor which were mostly neglected in previous modulation studies become of interest in this work in order to understand the 3D transport and modulation of low-energy electrons in the inner heliosphere, in particular the azimuthal distribution of electrons produced by the Jovian magnetosphere in the heliospheric equatorial region.

5.2 The diffusion tensor

The transport of charged particles in the heliosphere can be described by a heliospheric diffusion tensor. This tensor in Equation 4.2 is given by

$$\mathbf{K} = \begin{bmatrix} K_{\parallel} & 0 & 0 \\ 0 & K_{\perp\theta} & K_A \\ 0 & -K_A & K_{\perp r} \end{bmatrix}, \tag{5.1}$$

where $K_{\parallel}$ is the diffusion coefficient parallel to the mean HMF, $K_{\perp\theta}$ and $K_{\perp r}$ denote the diffusion coefficients (DCs) perpendicular to the mean HMF (dashed lines) in the polar and radial direction respectively, as illustrated schematically in Figure 5-1.

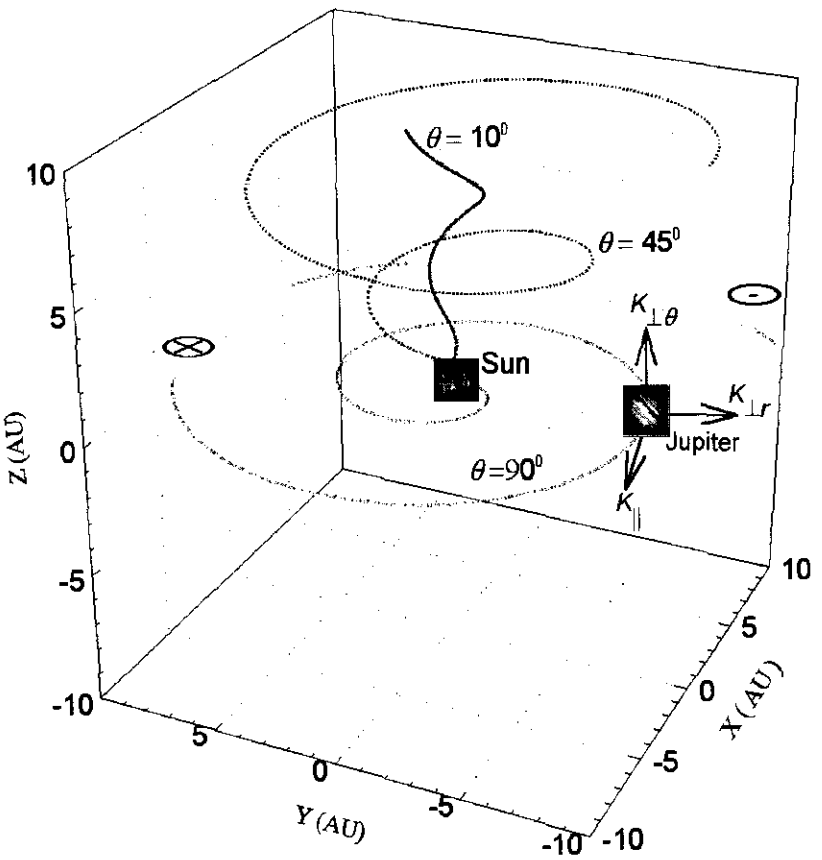

Figure 5-1: A 3D idealization of diffusive propagation of low energy electrons, produced by the magnetosphere of Jupiter at 5 AU, with the Sun at the center. The HMF spiral lines are shown at $\theta = 10^0$, $\theta = 45^0$, and $\theta = 90^0$ respectively. The elements $K_{\parallel}$, $K_{\perp\theta}$ and $K_{\perp r}$ of the tensor given by Equation (5.1) are illustrated.

Representative HMF spiral lines are shown at $\theta = 10^0$, $\theta = 45^0$ and $\theta = 90^0$ respectively,

with the Sun at the center. The symbol $\otimes$ denotes the magnetic field directed into the page while $\odot$ denotes the opposite. Jupiter is also shown at 5 AU in the equatorial plane as the main source of low energy electrons in the inner heliosphere.

The anti-symmetric elements K_A, describe particle drifts which include gradient, curvature and heliospheric current sheet drift in the large scale HMF. The tensor given by Equation (5.1) emerges naturally in the development of the TPE using the Boltzman equation, or by using physical arguments as Jokipii and Parker (1970).

The elements of the diffusion tensor with respect to heliocentric spherical coordinates are obtained by using the transformation matrix

$$\mathbf{T} = \begin{bmatrix} \cos\psi & 0 & \sin\psi \\ 0 & 1 & 0 \\ -\sin\psi & 0 & \cos\psi \end{bmatrix}, \tag{5.2}$$

where ψ is the spiral angle of the HMF given by Equation (2.5). That is:

$$\begin{bmatrix} K_{rr} & K_{r\theta} & K_{r\phi} \\ K_{\theta r} & K_{\theta\theta} & K_{\theta\phi} \\ K_{\phi r} & K_{\phi\theta} & K_{\phi\phi} \end{bmatrix} = \mathbf{TKT}^T, \tag{5.3}$$

$$= \begin{bmatrix} \cos\psi & 0 & \sin\psi \\ 0 & 1 & 0 \\ -\sin\psi & 0 & \cos\psi \end{bmatrix} \begin{bmatrix} K_\parallel & 0 & 0 \\ 0 & K_{\perp\theta} & K_A \\ 0 & -K_A & K_{\perp r} \end{bmatrix} \begin{bmatrix} \cos\psi & 0 & -\sin\psi \\ 0 & 1 & 0 \\ \sin\psi & 0 & \cos\psi \end{bmatrix}, \tag{5.4}$$

$$= \begin{bmatrix} K_\parallel \cos^2\psi + K_{\perp r}\sin^2\psi & -K_A\sin\psi & (K_{\perp r} - K_\parallel)\cos\psi\sin\psi \\ K_A\sin\psi & K_{\perp\theta} & K_A\cos\psi \\ (K_{\perp r} - K_\parallel)\sin\psi\cos\psi & -K_A\cos\psi & K_{\perp r}\cos^2\psi + K_\parallel\sin^2\psi \end{bmatrix}, \tag{5.5}$$

where the superscript T in Equation (5.3) denotes the transpose.

In previous modulation studies much interest was based on the diffusion coefficients:

$$K_{rr} = K_\parallel \cos^2\psi + K_{\perp r}\sin^2\psi, \tag{5.6}$$

and

$$K_{\theta\theta} = K_{\perp\theta}, \tag{5.7}$$

because of the nature of the 2D modulation models used, where K_{rr} describes the effective diffusion coefficient in the radial direction and $K_{\theta\theta}$ the effective diffusion in the heliospheric polar direction. However, in this study the steady-state 3D Jovian electron modulation model of Ferreira (2002) described in Chapter 4 is used and it requires a particular consideration of the other diffusion coefficients to fully understand the azimuthal distribution of electrons produced by the Jovian magnetosphere in the three dimensional heliosphere. This azimuthal dependence will be illustrated in Chapter 6.

Hence, the diffusion coefficients:

$$K_{\phi\phi} = K_{\perp r}\cos^2\psi + K_{\parallel}\sin^2\psi, \tag{5.8}$$

and

$$K_{\phi r} = \left(K_{\perp r} - K_{\parallel}\right)\sin\psi\cos\psi = K_{r\phi}, \tag{5.9}$$

also become of special interest in this work where $K_{\phi\phi}$ describes the effective diffusion coefficient in the azimuthal direction and $K_{\phi r}$ is the diffusion coefficient in the ϕr direction and can be regarded as a "correction" term which marginally reduces the radial and azimuthal gradients of CRs in Equation (4.3). The expressions for $K_{\parallel}$, $K_{\perp r}$ and $K_{\perp\theta}$ assumed in this study are the same as in the study of Ferreira (2002) and will be further discussed in the next sections.

Shown in Figure 5-2 are $\cos^2\psi$ (dash-dot-dash lines), $\sin^2\psi$ (dashed lines) and $\sin\psi.\cos\psi$ (dotted lines) as a function of radial distance r in the polar regions ($\theta = 10^0$) and at the heliospheric equatorial plane ($\theta = 90^0$), respectively. Evidently, $\cos^2\psi$ near the poles decreases as function of increasing radial distance, even more significantly in the equatorial plane, while $\sin^2\psi$ increases rapidly in the inner heliosphere to become almost constant in the outer heliosphere for both polar and equatorial regions. Furthermore, the product $\sin\psi.\cos\psi$ near the poles increases rapidly as a function of increasing radial distance in the inner heliosphere but

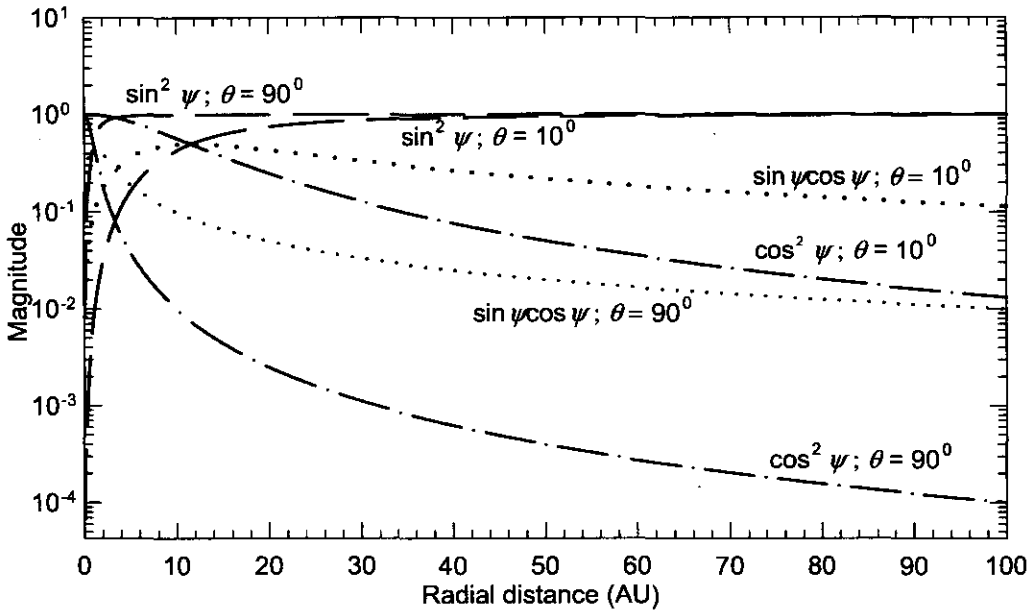

Figure 5-2: An illustration of the terms $\cos^2\psi$ (dash-dot-dash lines), $\sin^2\psi$ (dashed lines) and $\sin\psi\cos\psi$ (dotted lines) in Equation (5.8) and (5.9), as a function of radial distance r for the polar regions ($\theta = 10^0$) and equatorial plane ($\theta = 90^0$).

then decreases. The implications of the radial and latitudinal dependence of these terms in the heliospheric diffusion tensor will be discussed in the following sections.

5.3 The parallel diffusion coefficient

The parallel mean free path is related to the parallel diffusion coefficient by

$$\lambda_{\parallel} = K_{\parallel}\frac{3}{v}, \tag{5.10}$$

with v the speed of particles. Bieber et al. (1994) calculated $\lambda_{\parallel}$ shown in Figure 5-3 by using two models for dynamical turbulence, namely the damping model and the random sweeping model. The left panels show the prediction for slab geometry, while the right panels show the predictions for slab and 2D geometry. Of particular interest from this Figure is that

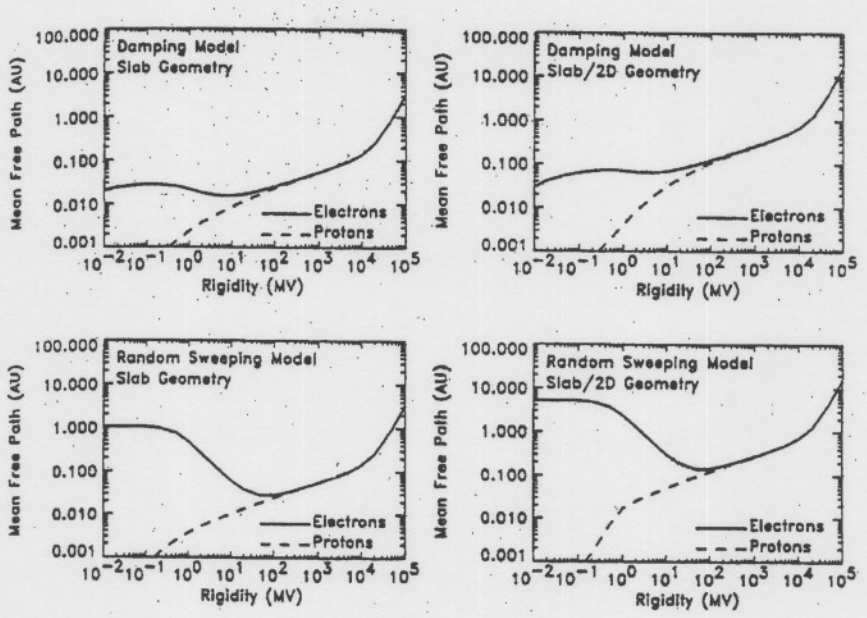

Figure 5-3: The parallel mean free path at Earth as predicted by two models for dynamical turbulence (Bierber et al., 1994). The two top panels correspond to damping model and two bottom panels to the random sweeping model. The left panels show the predictions only for slab geometry and the two right panels for the composite slab geometries. (From Dröge, 2000).

$\lambda_{\parallel}$ for protons (dashed line) and electrons (solid line) is fundamentally different at low and intermediate rigidities (< 50 MV) due to an explicit speed dependence of $\lambda_{\parallel}$.

Ferreira (2002) used the damping model for dynamic turbulence and complicated properties of $\lambda_{\parallel}$ as described by Burger et al. (2000) for higher rigidities, assuming a rigidity independent $\lambda_{\parallel}$ for $P \leq 200$ MV as required by observations to construct a $K_{\parallel}$ for electrons applicable to the whole heliosphere given by:

$$K_{\parallel} = K_0 \beta f_1 (r, P) \tag{5.11}$$

where

$$f_1 (r, P) = 0.2 g (P) c (r) h (r, P) , \tag{5.12}$$

with

$$h(r,P) = 0.02\left(\frac{P}{P_0}\right)^2\left(\frac{r}{r_0}\right)^{1.7} + 0.02\left(\frac{P}{P_0}\right)\left(\frac{r}{r_0}\right)^{2.2} + 0.2\left(\frac{P}{P_0}\right)^{1/3}\left(\frac{r}{r_0}\right) + 7.0e(r)\,, \quad (5.13)$$

$$c(r) = \begin{cases} 1 \text{ if } r > r_c \\ m(r) \text{ if } r \leq r_c \end{cases}, \quad (5.14)$$

$$m(r) = \frac{r_0}{r_c}\xi\left(\frac{r}{r_0}\right)^{\xi}, \quad (5.15)$$

and

$$g(P) = \left(\frac{P_0}{P_s}\right)^{0.4}, \quad (5.16)$$

where $\xi = \left(\frac{r}{r_c}\right)^x$, $x = \left(\frac{0.016}{P/P_0}\right)^{0.2}$, $r_c = \frac{r_0}{0.1+(P_s/P_0)^{1.4}}$ and

$$e(r) = \begin{cases} (10r_0/r)^k \text{ if } r > 10 \text{ AU} \\ 1 \text{ if } r \leq 10 \text{ AU} \end{cases}, \quad (5.17)$$

with $k = 125 \times 10^{-4}(r/r_0)^2$. Here β is the ratio of the speed of cosmic ray particles v to the speed of light c, $K_0 = 4.5 \times 10^{22}\text{cm}^2\ \text{s}^{-1}$, $P_0 = 1$ GV, $r_0 = 1$ AU and $P_s = P$ when $P < 1$ GV and $P_s = 1$ GV when $P \geq 1$ GV. Equation (5.11) results in a $K_{\|}$ which is a superposition of terms each dominating for different rigidity values and radial distances. For a complete discussion see Ferreira (2002). This rigidity and spatial dependence will be studied in the next sections.

Teufel and Schlickeiser (2002, 2003), for example, calculated analytically new general formulas for the parallel mean free path at Earth of CR particles for two particular turbulence models, slab-like dynamical and random sweeping turbulence, by assuming a turbulence power spectrum with vanishing power below a minimum wavenumber. Using some of these results, Schalchi and Schlickeiser (2004) have calculated $\lambda_{\|}$ successfully for composite slab/2D geometry.

Most recently, a promising theory for perpendicular diffusion known as the Nonlinear Guiding Center (NLGC) theory has been proposed by Matthaeus et al. (2003a,b). This theory

provides an integral equation for perpendicular mean free path (see also Schalchi et al., 2004). For other very recent developments see Bieber et al. (2004), Minnie et al. (2003) and Zank et al. (2004).

These new approaches for CR proton mean free paths are not applied in this work because the focus is based on the diffusion coefficients computed by Ferreira et al. (2001a,b) that simulate realistic modulation of low energy Jovian and galactic electrons in the inner heliosphere during solar minimum activity.

5.3.1 The rigidity dependence

Shown in Figure 5-4 (a) is the computed rigidity dependence of $K_{\|}$ (Ferreira et al., 2001a,b) at 1 AU (solid line) and 5 AU (dashed line) in the equatorial plane. The rigidity dependence of $K_{\|}$ is determined by the four terms in $h(r, P)$ given by Equation (5.13). It is evident from the Figure 5-4 (a) that $K_{\|}$ at Earth is changing slowly for $P \leq 0.1$ GV but is increasing significantly for $P > 0.1$ GV up to $P \sim 1.0$ GV. At these rigidities, low energy electrons data are fitted well (Ferreira, 2002). For higher rigidities, $P > 1.0$ GV, $K_{\|} \propto P^3$. At these rigidities $K_{\|}$ is suitable for energetic cosmic ray protons (Burger et al., 2000). At 5 AU, $K_{\|}$ has a similar rigidity dependence as at 1 AU. The kink at about 1 GV is an artificial effect attributed to the superposition of terms in Equation (5.13) with different rigidity dependence. Its effect on electron modulation was not investigated in the studies of Ferreira (2002) because the focus was based on low-energy electrons. At higher rigidities, drifts dominate and the effect of this kink is negligibly small on electron modulation (see Chapter 8). For the studies of higher energy electrons, this kink in the rigidity dependence of $K_{\|}$ may require a further inspection.

From Equation (5.10) follows that $\lambda_{\|}$ has the same rigidity dependence as $K_{\|}$ down to rather low energies (which is not the case for protons). It has also became evident in the work of Ferreira (2002) that $\lambda_{\|}$ has the following dependences as a function of decreasing rigidity: $\lambda_{\|} \propto P^2$, changing to $\lambda_{\|} \propto P$, then to $\lambda_{\|} \propto P^{1/3}$ and finally is almost independent of P for $P \leq 200$ MV.

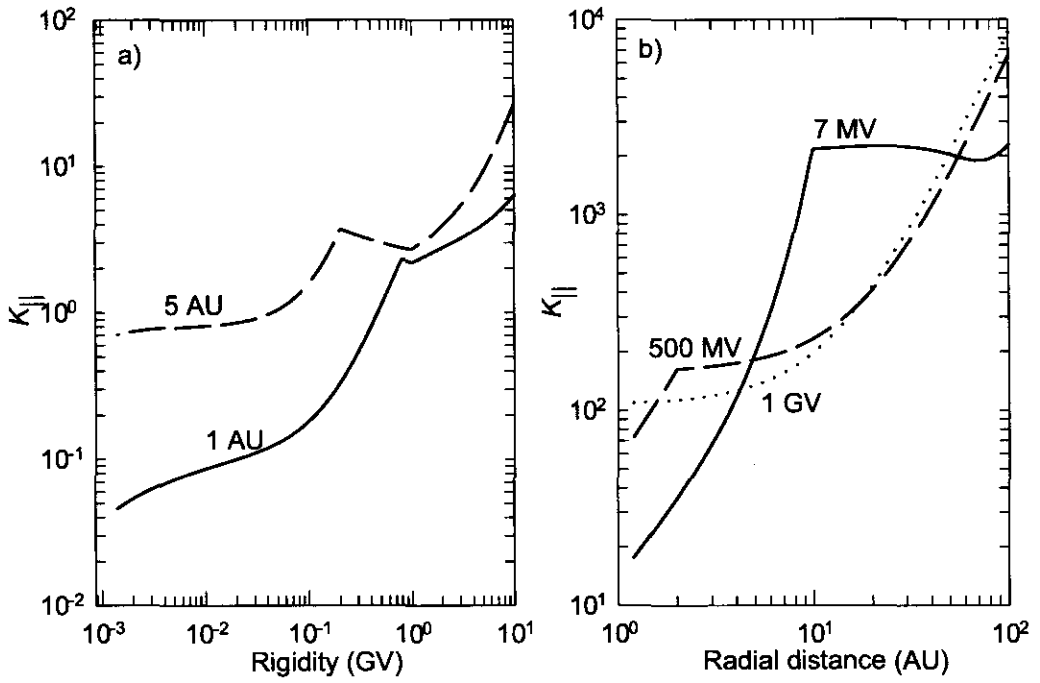

Figure 5-4: Panel (a): The rigidity dependence of $K_{\parallel}$ for electrons at 1 AU and 5 AU in the equatorial plane. Panel (b): The radial dependence of $K_{\parallel}$ in the equatorial plane at rigidities 7 MV (solid line), 500 MV (dashed line) and 1 GV (dotted line), respectively. $K_{\parallel}$ is in units of 6.0×10^{20} cm^2 s^{-1}.

5.3.2 The spatial dependence

Figure 5-4 (b) shows $K_{\parallel}$ as a function of radial distance in the equatorial plane for 7 MV (solid line), 500 MV (dashed line) and 1.0 GV (dotted line) respectively. It is evident that for low rigidity (7 MV) that $K_{\parallel}$ increases rapidly up to 10 AU and remains approximately constant in the outer heliosphere. For 500 MV $K_{\parallel}$ also increases rapidly up to $\sim$ 1 AU, then changes and remains moderate up to $\sim$ 10 AU, but increases significantly as a function of increasing radial distance in the outer heliosphere. This spatial dependence of $K_{\parallel}$ hinges on the radial dependence of the function $e\,(r\,)$ given by Equation (5.17). This function modifies the radial dependence of $K_{\parallel}$ for $r > 10$ AU mainly for $P < 500$ MV. However, for $P \geq 500$ MV, it is evident that $K_{\parallel}$ has a weak radial dependence up to $\sim$10 AU in the inner heliosphere but acquires a strong radial dependence for $r > 10$ AU due to the dominance of the radial dependence of the

function $h(r, P)$. Furthermore, $K_{\parallel}$ has no latitudinal or polar dependence because it depends on the function $f_1(r, P)$. This aspect might need to be investigated further for future studies.

5.4 The perpendicular diffusion coefficients

It is well known in the field of cosmic ray modulation studies that perpendicular diffusion occurs due to two important physical phenomenon: (i) the gyro-centres of particles are displaced transverse to the mean HMF due to scattering, and (ii) the field line random walk (e.g., Giacolone and Jokipii, 1999; Kóta and Jokipii, 1999). These important phenomena which CRs particles experience in the heliosphere are incorporated into the numerical modulation model via a perpendicular diffusion coefficient described by $K_{\perp}$. However, $K_{\perp}$ consists of two assumingly independent coefficients, $K_{\perp r}$ and $K_{\perp \theta}$, which give perpendicular diffusion in the radial and polar direction of the heliosphere as illustrated in Figure 5-1.

Because no rigorous theory has yet been developed to adequately account for $K_{\perp}$ in all respects (e.g., le Roux et al., 1999), it became standard in numerical modelling to assume that $K_{\perp}$ scales spatially as $K_{\parallel}$ (e.g., Jokipii and Kóta, 1995; Potgieter, 1996; Potgieter and Ferreira, 199a; Ferreira et al., 2000; Burger et al., 2000). Then by assuming $K_{\perp} \propto K_{\parallel}$, it follows that

$$K_{\perp r} = aK_{\parallel} \tag{5.18}$$

and

$$K_{\perp \theta} = bK_{\parallel} \tag{5.19}$$

where a and b are either constant or a function of rigidity. In this Chapter, $a = 0.010$ and $b = 0.015$ are assumed as in the studies of Ferreira et al. (2001a, b) to allow compatibility to the observations of low energy Jovian and galactic electrons in the equatorial regions during solar minimum conditions. For a detail discussion see Ferreira (2002).

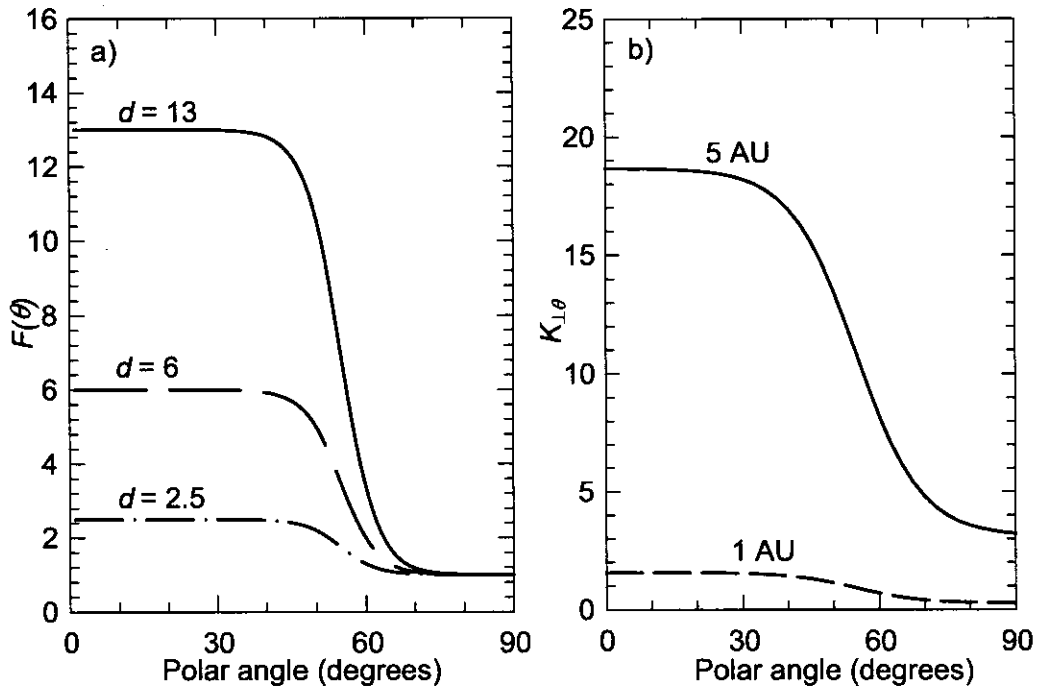

Figure 5-5: Panel (a): Illustration of $F(\theta)$ in Equation (5.21) as a function of polar angle θ for the scenarios d = 2.5; 6 and 13 repectively. Panel (b) shows $K_{\perp\theta}$ as a function of polar angle at 1 AU and 5 AU for 7 MeV electrons. $K_{\perp\theta}$ is in units of 6.0×10^{20} cm^2 s^{-1}.

5.4.1 The rigidity dependence

The $K_{\perp\theta}$ has the same rigidity dependence (not shown) as $K_{\parallel}$, the only difference is that it is ~15% of $K_{\parallel}$. The same treatment applies to the rigidity dependence of $K_{\perp r}$, since it is assumed to be ~5% of $K_{\parallel}$.

5.4.2 The spatial dependence

The spatial dependence of $K_{\perp\theta}$ (not shown) is determined by the spatial dependence of $K_{\parallel}$. The only difference is the value of b as assumed in Equation (5.19). The $K_{\perp r}$ has the same radial dependence as $K_{\parallel}$, according to Equation (5.18) and is shown in Section 5.5.

5.4.3 The latitudinal dependence

Burger et al. (2000) illustrated that in order to produce the correct magnitude and rigidity dependence of the observed latitudinal CR proton density gradient by Ulysses, an enhanced latitudinal transport is required (see also Kóta and Jokipii, 1995; Potgieter et al., 1997, Burger et al., 2000). This was followed by the inclusion of the function $F(\theta)$ on the right hand side of Equation (5.18) that increases $K_{\perp\theta}$ towards the poles with respect to the value in the equatorial region. That is:

$$K_{\perp\theta} = bK_{\parallel}F(\theta) \tag{5.20}$$

with

$$F(\theta) = A^{+} \pm A^{-} \tanh\left[\frac{1}{\triangle\theta}\left(\theta_A - 90^0 + \theta_F\right)\right] \tag{5.21}$$

where $A^{\pm} = \frac{1}{2}(d \pm 1)$, $\triangle\theta = 1/8, \theta_A = \theta$, and $\theta_F = 35^0$ for $\theta \leq 90^0$ while for $\theta > 90^0$, $\theta_A = 180 - \theta$ and $\theta_F = -35^0$. Shown in Figure 5.5 (a) is $F(\theta)$ as a function of polar angle for $\sim$ 7 MeV electrons with $d = 2.5$; 6 and 13, respectively. It is clearly illustrated how $F(\theta)$ in Equation (5.20) enhances $K_{\perp\theta}$ with respect to $K_{\parallel}$ by a factor d from the value in the equatorial regions towards the poles. The physical argument for increasing $K_{\perp\theta}$ is based on Ulysses measurements which indicate that the variance is increased more in the transverse and normal direction of the HMF than in the radial direction, resulting in effective diffusion in these directions (e.g., Jokipii and Kota, 1995; Burger et al., 2000; Ferreira et al., 2000).

Figure 5-5 (b) shows $K_{\perp\theta}$ as a function of polar angle at 1 AU and 5 AU for 7 MeV electrons with $d = 6$. The $K_{\perp\theta}$ is significantly enhanced at 5 AU towards high heliolatitude. This implies that heliospheric electrons produced by a source such as the Jovian magnetosphere located at 5 AU in the ecliptic plane, may be more effectively transported to high heliolatitude than electrons at 1 AU. The role of this enhanced latitudinal transport form an integral part of this study and will be thoughtfully discussed in the later Chapters.

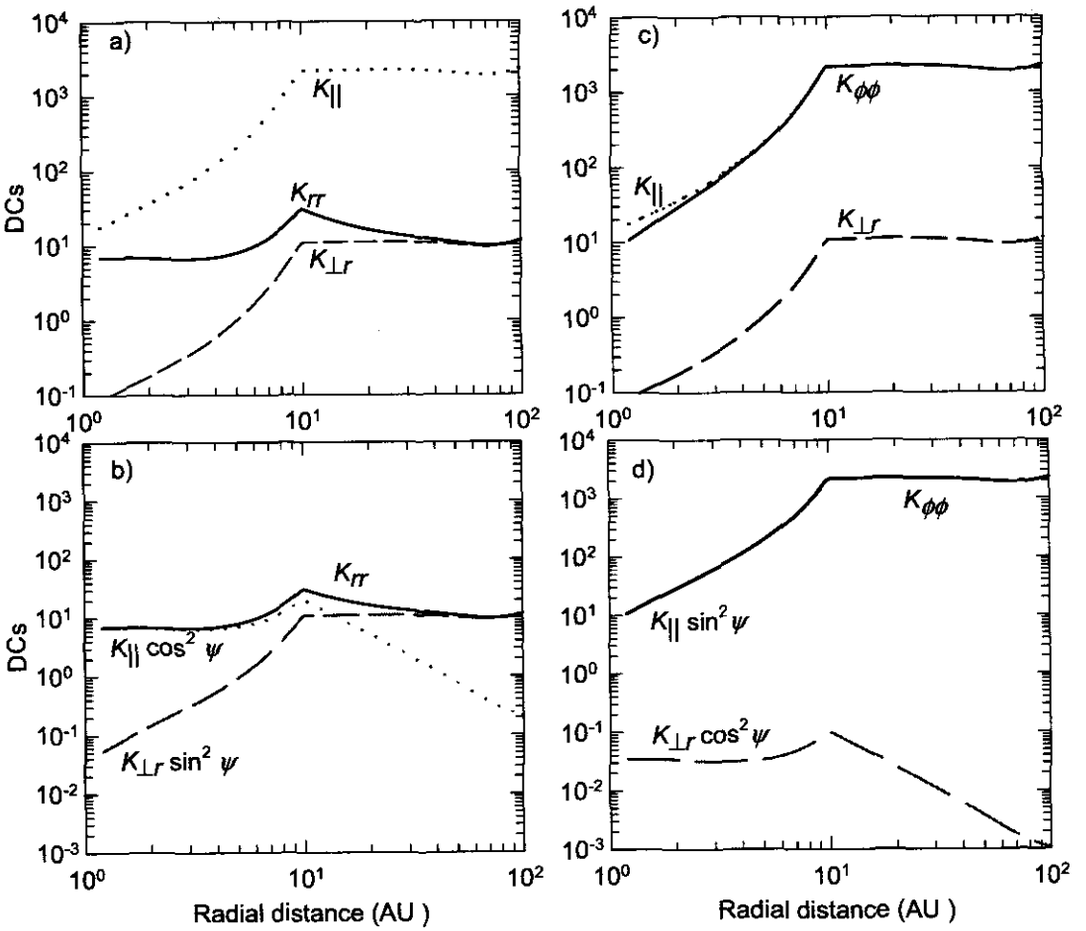

Figure 5-6: Panels (a), (b), (c) and (d) illustrate the radial dependence of K_{rr} and $K_{\phi\phi}$ (solid lines) in the equatorial plane for the 7 MeV electrons. Shown also in (a) and (b) is $K_{||}$ and $K_{\perp r}$ (dashed lines) as a function of radial distance. Modifications caused by $\cos^2\psi$ and $\sin^2\psi$ to the values of the diffusion coeffiecients (DCs) are shown in (c) and (d) respectively. The DCs are in units of 6.0×10^{20} cm^2 s^{-1}.

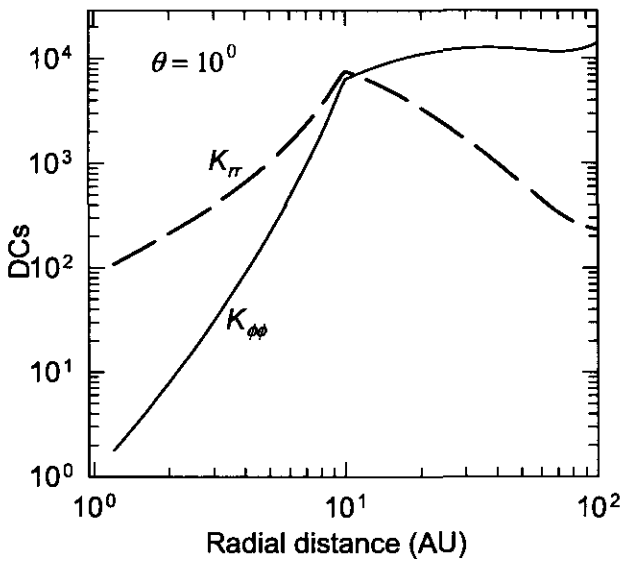

Figure 5-7: The radial dependence of K_{rr} (dashed line) and $K_{\phi\phi}$ (solid line) near the heliospheric poles ($\theta = 10^0$) for 7 MeV electrons. The DCs are in the units of 6.0×10^{20} cm^2 s^{-1}.

5.5 The effective diffusion coefficient in the radial and azimuthal direction

The effective radial diffusion coefficient K_{rr} is expressed as a linear combination of $K_{\parallel} \cos^2 \psi$ and $K_{\perp r} \sin^2 \psi$ as given by Equation (5.6) and describes the radial inward diffusion of CRs particles entering the heliosphere isotropically to become modulated due to heliospheric magnetic field and the solar wind. The effective diffusion coefficient in the azimuthal direction $K_{\phi\phi}$ is also expressed as a combination of the terms $K_{\parallel} \sin^2 \psi$ and $K_{\perp r} \cos^2 \psi$ given by Equation (5.8). These diffusion coefficients contributing to diffusion in the azimuthal direction were neglected in the 2D modulation studies and will be investigated in this study because of the essentiality of the azimuthal transport of low-energy electrons in the inner heliosphere.

5.5.1 The spatial dependence

Figure 5-6 (a), (b), (c) and (d) show the radial dependence of $K_{\phi\phi}$ and K_{rr} (solid lines) in the equatorial plane. Shown also in panels (a) and (c) is the value of $K_{\parallel}$ (dotted lines) and of $K_{\perp r}$ (dashed lines) in comparison to the radial dependence of K_{rr} and $K_{\phi\phi}$. Shown in panel (c) is that $K_{\parallel}$ has the same radial dependence as $K_{\phi\phi}$ where $r > 10$ AU but, in the inner heliosphere, small differences occur between the values. Shown in panels (b) and (d) are the modifications of $\cos^2\psi$ and $\sin^2\psi$ to $K_{\parallel}$ and $K_{\perp r}$ respectively. These modifications indicate that $K_{\parallel}$ dominates K_{rr} in the inner heliosphere where $r < 10$ AU while $K_{\perp r}$ dominates in the outer heliospheric equatorial region. It is also evident in panel (d) that $K_{\parallel}$ dominate $K_{\phi\phi}$ throughout the heliospheric equatorial region. Furthermore, Figure (b) and (d) indicate that $K_{\phi\phi}$ is significantly larger than K_{rr} in the equatorial plane throughout most of the heliosphere. It is also clear in panel (d) that $K_{\phi\phi} = K_{\parallel}\sin^2\psi$ determines azimuthal dependence in the equatorial plane. These results will be applied in the following Chapter to explain the distribution of 7 MeV Jovian electrons in the inner heliosphere from a point source such as the Jovian magnetosphere positioned at 5 AU in the ecliptic plane.

Shown in Figure 5-7 is the radial dependence of K_{rr} and $K_{\phi\phi}$ near the poles $\left(\theta = 10^0\right)$ for 7 MeV Jovian and galactic electrons. It is evident that K_{rr} dominates $K_{\phi\phi}$ where $r < 10$ AU, and is similar to $K_{\phi\phi}$ when $r = (10 \pm 2)$ AU while $K_{\phi\phi}$ dominates in the outer heliospheric polar regions.

5.5.2 The rigidity dependence

Figure 5-8 (a) and (b) illustrate the rigidity dependence of $K_{\phi\phi}$ and K_{rr} at 1 AU (solid lines) and 5 AU (dashed lines) respectively in the equatorial plane. The rigidity dependence of $K_{\phi\phi}$ is essentially determined by the rigidity dependence of $K_{\parallel}$ because $K_{\parallel}\sin^2\psi$ dominates $K_{\phi\phi}$ throughout the heliospheric equatorial region as discussed in the preceding section. The rigidity dependence of K_{rr} is also determined by the rigidity dependence of $K_{\parallel}$ because $K_{\parallel}\cos^2\psi$ dominates K_{rr} in the inner heliosphere where $r < 10$ AU. It is also evident that the rigidity dependence of $K_{\phi\phi}$ and K_{rr} is a function of radial distance, an important feature of how DCs are treated in current modulation models.

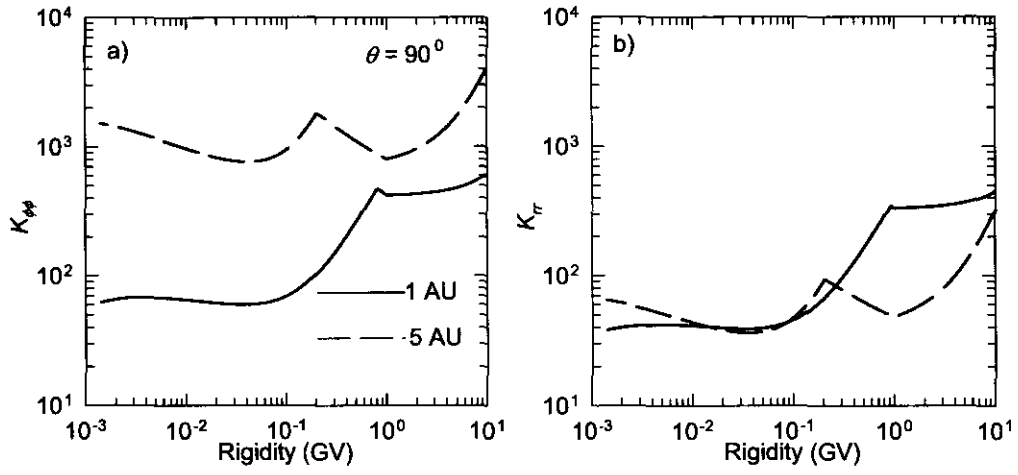

Figure 5-8: Panels (a) and (b) illustrate the rigidity dependence of K_{rr} and $K_{\phi\phi}$ at 1 AU (solid lines) and at 5 AU (dashed lines) in the equatorial plane ($\theta = 90^0$). The DCs are in the units of 6.0×10^{20} cm^2 s^{-1}.

5.5.3 The latitudinal dependence

Shown in Figure 5-9 (a) and (b) are the latitudinal dependence of $K_{\phi\phi}$ and K_{rr} at 1 AU (dashed lines) and 5 AU (solid lines). In (a) it is indicated that $K_{\phi\phi}$ is large in the equatorial plane and decreases towards the poles, even more rapidly at 1 AU, while K_{rr} shown in (b) becomes significantly larger towards the poles. The consequences of this effect on the modulation of Jovian and galactic electrons will be discussed in Chapter 6.

5.6 The drift coefficient

The large scale heliospheric magnetic field leads to gradient and curvature drifts of cosmic rays in the heliosphere. Drift effects were neglected until Jokipii et al. (1977) pointed out that particle drifts are an important mechanism of cosmic ray modulation. The inclusion of drifts into Equation (4.2) leads to important implications for CR modulation in the heliosphere (e.g., Jokipii and Thomas, 1981; Potgieter, 1984; Potgieter and Moraal, 1985; Burger, 1987; Hattingh, 1998; Ferreira and Potgieter, 2004a,b). See also Ferreira, (2002) for more elaboration on the implications.

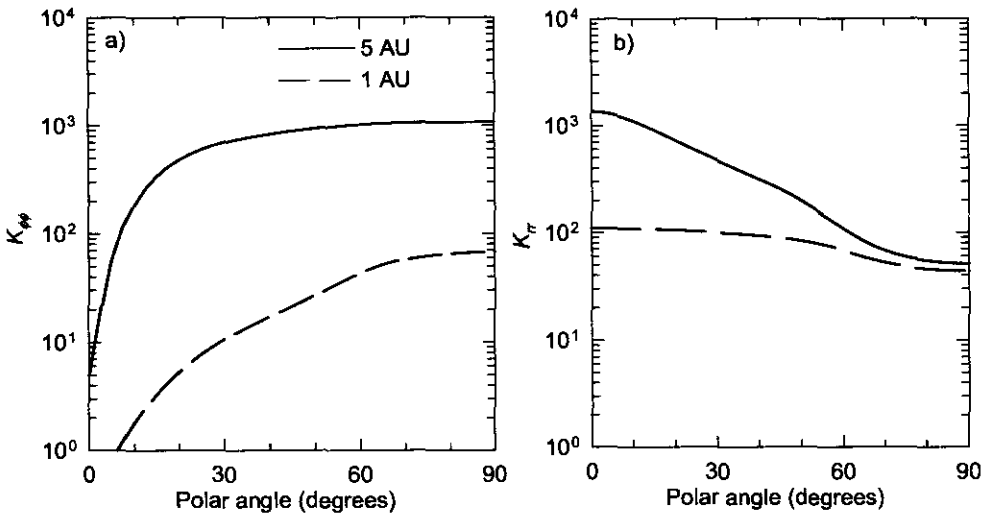

Figure 5-9: (a) K_{rr} and (b) $K_{\phi\phi}$ as a function polar angle at 1 AU (dashed line) and 5 AU (solid lines) for 7 MeV electrons. The DCs are in units of 6.0×10^{22} cm^2 s^{-1}.

The drift coefficient under the assumption of weak scattering is given by

$$(K_A)_{\text{standard}} = (K_A)_0 \frac{\beta P}{3B_m}. \tag{5.22}$$

The constant $(K_A)_0$ is dimensionless and may be chosen e.g. as 1.0, 0.5 and 0.2 which describe what Potgieter et al. (1989) termed 100%, 50% and 20% drifts. The drift coefficient used by Burger et al. (2000) and Ferreira et al. (2002) differs slightly from the standard form and is given by

$$K_A = \frac{(K_A)_0 \, K_{drift}\,(P)}{3B_m}, \tag{5.23}$$

with B_m the modified HMF and $K_{drift}\,(P)$ is given by

$$K_{drift}\,(P) = \beta P \left(\frac{D_{fak} P^2}{D_{fak} P^2 + 1} \right), \tag{5.24}$$

typically with $D_{fak} = 10.0$ and $(K_A)_0 = 1.0$.

Equation (5.23) is shown in Figure 5-10 as a function of rigidity at 1 AU in the equatorial

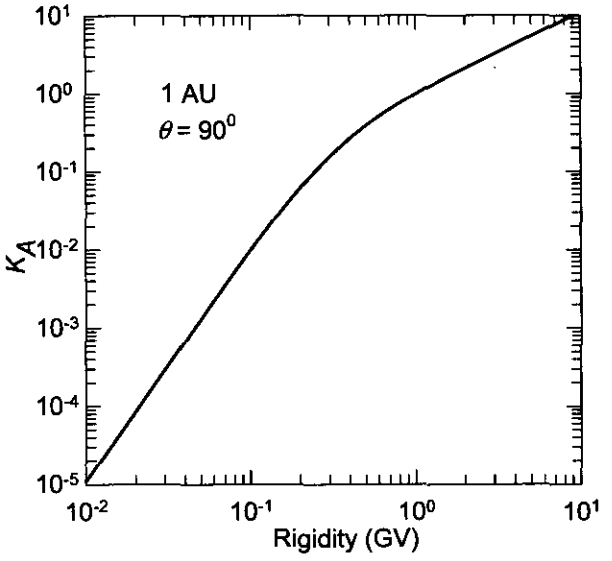

Figure 5-10: The rigidity dependence of K_A at Earth according to Equation (5.24) in units of 6.0×10^{20} cm^2 s^{-1}.

plane. It is evident that K_A decreases slightly stronger as a function of decreasing rigidity than Equation (5.22). This illustration is consistent with the conclusions from Potgieter (1996), Potgieter and Ferreira (1999b), and Ferreira (2002) that drifts become less important with decreasing rigidity, especially with decreasing electron energy to have almost no effect on electron modulation below $100 - 200$ MeV. (See also Chapter 7).

5.7 Summary and conclusions

Diffusion of cosmic ray particles in the heliosphere is one of four important modulation processes as described by the heliospheric diffusion tensor. In this Chapter, a theoretical background was given on certain aspects of this tensor, and further investigation on the spatial and rigidity dependence of important elements of the tensor applicable to low-energy electron modulation (e.g., Ferreira, 2002) as revealed by Ulysses spacecraft (e.g., Heber et al., 2001a) during solar minimum conditions. Some elements of the tensor such as the effective diffusion in the azimuthal direction ($K_{\phi\phi}$) and diffusion coefficient in $r\phi$ direction ($K_{r\phi}$), which were mostly neglected in

previous studies due to the limitations imposed by 2D modulation models, were also investigated in this Chapter.

Simulations revealed that the K_{rr}, which is dominated in the equatorial plane by $K_{\parallel}\cos^2\psi$ in the inner heliosphere and by $K_{\perp r}\sin^2\psi$ in the outer heliosphere, is an important modulation parameter in the heliospheric polar regions, while $K_{\phi\phi}$, which is also dominated by $K_{\parallel}\sin^2\psi$ throughout most of the heliosphere, is an essential modulation parameter in the heliospheric equatorial plane. It was also shown that the rigidity dependence of $K_{\phi\phi}$ and K_{rr} is a function of radial distance and is assumingly determined by the rigidity dependence of $K_{\parallel}$. The rigidity dependence has to be revised as progress on the theory of $K_{\perp}$is made (see Matthaeus et al., 2003; Minnie et al. (2003a,b); Schalchi et al., 2004; Bieber et al., 2004; Zank et al., 2004).

It is also evident that $K_{\phi\phi}$ should play an important role in the inner heliosphere concerning the modulation of Jovian electrons. This will be highlighted in Chapter 6. The DCs $K_{\phi r}$ and $K_{r\phi}$ are essentially 'correction' terms to the distribution of CRs as determined by K_{rr} and $K_{\phi\phi}$, together with $K_{\theta\theta}$ which is significantly modified by assuming it to be enhanced toward the poles.

In the next Chapter, effects of changing the solar wind speed on the propagation of low energy electrons is studied.

Chapter 6

Effects of changing solar wind speed profiles on the heliospheric transport of few-MeV electrons

6.1 Introduction

Observations made by the Pioneer 10 (e.g., Simpson et al., 1974; Teergarden, 1974; Chenette et al., 1974), Mariner 10 (e.g., Eraker and Simpson et al., 1979) and the most recent Jupiter fly-by by the Ulysses spacecraft (e.g., Heber et al., 2003a,b) confirmed that Jupiter 's magnetosphere located at ~5 AU in the ecliptic plane is a continuous source of few-MeV electrons in the inner heliosphere. It was also proposed that the release of these electrons from the Jovian magnetosphere is strongly controlled by variation of the solar wind speed (e.g., Morioka et al., 1997; Tsuchiya et al., 1999). Hence, this Chapter is devoted to modelling different solar wind speed V profiles which could be applicable during solar minimum conditions while using a typical solar maximum scenario as a reference for the study. A 3D steady-state modulation model (Ferreira, 2002) based on Parker's transport equation including the Jovian electron source (see also Chapter 4) is used to investigate the effects of the variability of V on the transport of few-MeV Jovian and galactic electrons in the inner heliosphere. In particular, the electron intensity time-profile along the Ulysses trajectory is calculated and compared to the 3 - 10 MeV

V (km s^{-1})	α^*	β^*
(a) 800 - 300	1.375	0.625
(b) 800 - 400	1.5	0.5
(c) 400	1.0	0.0
(d) 800 - 600	1.75	0.25

Table 6.1: Solar wind speed modulation parameters

electron flux observed by Ulysses from launch (1990) up to the end of the first out-of-ecliptic orbit (~2000). The content of this work was published in Ferreira et al. (2003a,b).

6.2 Solar wind speed parameters

The previous modulation studies (e.g., Hattingh, 1998; Ferreira, 1998; Minnie, 2002; Ferreira, 2002; Langner, 2004) assumed a V profile applicable to the solar minimum conditions to be highly latitude dependent, changing from a slow speed in the heliospheric equatorial regions with an average of 400 km s^{-1} to a fast speed of 800 km s^{-1} in the heliospheric polar regions. This assumption is consistent to Ulysses observations during the solar minimum conditions of a high solar wind speed $\sim$ 760 km s^{-1} towards the polar regions but a slow speed for the equatorial region as shown by the light shaded data band (e.g., Phillips et al., 1995; McComas et al., 2002b) in Figure 6-1. In this work, the latitudinal dependence of V given by Equation (2.3) (e.g., Hattingh, 1998) is now expressed in generic form as

$$V(\theta) = \alpha^* \mp \beta^* \tanh\left[\frac{2\pi}{\theta_s}(\theta - 90^0 \pm \varphi)\right], \tag{6.1}$$

where α^* and β^* are introduced as new solar wind speed parameters, with $\theta_s = 45^0$ and $\varphi = 35^0$. These parameters are required to model the different V profiles applicable to varying heliospheric conditions. The solar wind velocity given by Equation (2.1) takes the general form in terms of radial distance and polar angle:

$$\mathbf{V}(r,\theta) = \left\{V_0\left[1 - \exp\left(\frac{40}{3}(r_\odot - r)\right)\right]\right\} \cdot \left\{\alpha^* \mp \beta^* \tanh\left[\frac{2\pi}{\theta_s}(\theta - 90^0 \pm \varphi)\right]\right\} \mathbf{e}_r, \tag{6.2}$$

with $V_0 = 400$ km s^{-1} and $r_\odot$ the solar radius. Of central importance to this Chapter, is the selection of the paramaters α^* and β^*as in Table 6.1 to model the mentioned V scenarios.

The scenarios are illustrated in Figure 6-1 as follows: (a) corresponds to a slow V in the equatorial regions with an average of 300 km s^{-1} to a fast speed of 800 km s^{-1} in the heliospheric polar regions; (b) is similar to (a) but changes from 400 km s^{-1} in the equatorial regions to 800 km s^{-1} in the polar regions; (d) V changes from 600 km s^{-1} in the equatorial regions to 800 km s^{-1} in the polar regions. The preceding scenarios are for solar minimum conditions. Scenario (c) is used as a reference for the solar maximum conditions and corresponds to isotropic solar wind speed with an average speed of 400 km s^{-1} at all heliolatitude.

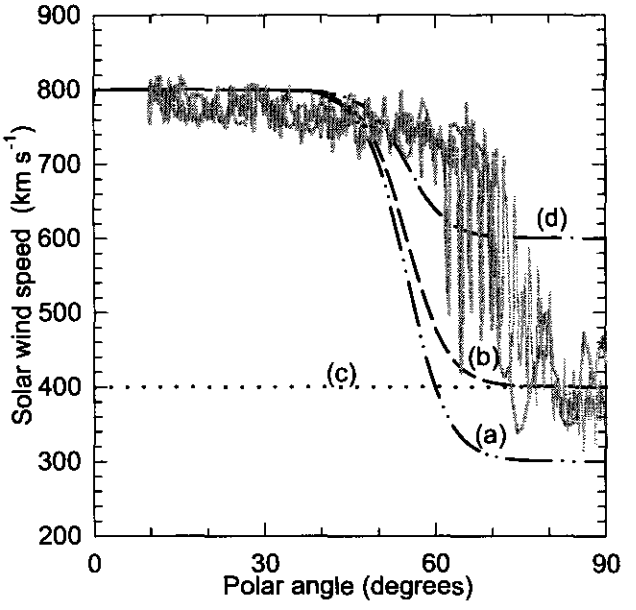

Figure 6-1: Computer simulations of four assumptions of the solar wind speed V as a function of polar angle θ for $r \geq 0.3$ AU. The scenarios are for V decreasing from (a) 800 km s^{-1} to 300 km s^{-1}, (b) 800 km s^{-1} to 400 km s^{-1}, (d) 800 km s^{-1} to 600 km s^{-1} and (c) for an average speed of 400 km s^{-1} at all heliolatitudes. Latitude dependence of V as observed by Ulysses (e.g., McComas et al., 2002b) for solar minimum activity conditions (light shaded data) is shown for comparison.

The effects of these assumptions of V on the computed Jovian and galactic electron intensities are investigated in the following sections using the modulation model discussed in Chapter 4. The scenarios given in Figure 6-1 will be revisited in Chapter 7.

6.3 Distribution of electrons in the inner heliosphere

Jupiter is a strongly magnetised rotating planet. Apart from the Sun, its magnetosphere is the largest object in the heliosphere. It has been evident from several space probes observations that this magnetosphere at ~ 5 AU in the ecliptic plane is a relatively strong source of electrons with energies up to ~ 30 MeV (e.g., Simpson et al., 1974; Teegarden et al., 1974; Chenette et al., 1974; Ferrando et al., 1996; Ferrando, 1997; and Heber et al., 2001a,b). These electrons were also observed at Earth, and outward in the equatorial plane (e.g., Eraker and Simpson, 1979; Eraker, 1982). In this section the model is used to compute the effects of changing *only* V profiles on the distribution of these low-energy electrons in the inner heliosphere.

Figures 6-2 a(i), b(i) and Figures 6-3 c(i) and d(i) show the model simulations of the three dimensional distribution of 7 MeV Jovian electron intensities in the inner heliosphere where Jupiter is positioned at coordinates (5,0) as a point source, and produces low energy electrons which propagate along and across the HMF spiral, away and towards the Sun positioned at the center (0,0). The electron intensities in the equatorial plane are computed for the different solar wind speed scenarios as simulated in Figure 6-2 respectively. The labels of the contour lines are in units of particles m^{-2} s^{-1} sr^{-1} MeV^{-1}. Shown also in Figure 6-2: a(i), b(i) and Figure 6-3: c(i) and d(i) are the corresponding HMF spiral superimposed on the intensity contours. The corresponding solar wind speed scenarios are repeated for convenience in Figures 6-2 a(ii), b(ii) and Figure 6-3 c(ii), d(ii) respectively.

It is evident from the contours plots that Jovian electrons largely follow the HMF spiral due to the dominance of $K_{\parallel} \sin^2 \psi$ in Equation (5.8) in the inner heliosphere but they are also transported across the HMF lines to some lesser extent due to $K_{\perp r}$. Since $K_{\phi\phi} > K_{rr}$ in the inner heliospheric equatorial regions as discussed in Chapter 5, these results indicate that Jovian electrons diffuse more effectively in the azimuthal direction than in the radial direction.

By comparing the scenarios a(i), b(i) and d(i) characterised to represent solar minimum periods, it is illustrated that when V increases from 300 km s^{-1} to 400 km s^{-1} and further to 600 km s^{-1} in the equatorial plane, the HMF spiral becomes less wound and the computed Jovian intensities follow the trend as expected. The scenario c(i) used as reference for the solar maximum period has the same features in the equatorial plane as scenario b(i) because both have an average speed of $V = 400$ km s^{-1} but one should expect differences at high latitudes.

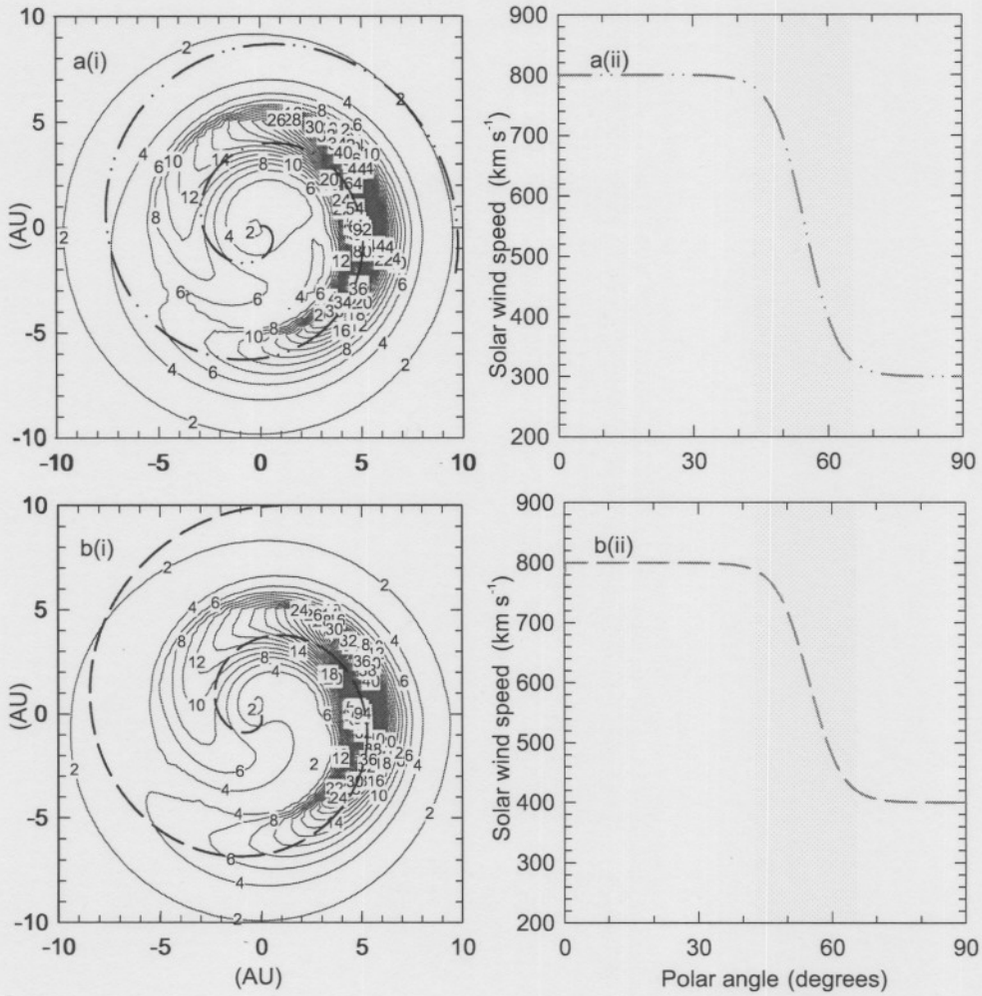

Figure 6-2: The computed 7 MeV Jovian electron intensities in the equatorial plane are shown in a(i) and b(i) as contour plots for the assumed solar wind speed scenarios in a(ii) and b(ii). The labels of the contour lines are in units of particles m^{-2} s^{-1} sr^{-1} MeV^{-1}. Shown also in a(i) and b(i) is the HMF spiral (dark lines) superimposed on the intensity contours where Jupiter is situated at (5,0) with the Sun at the center (0,0).

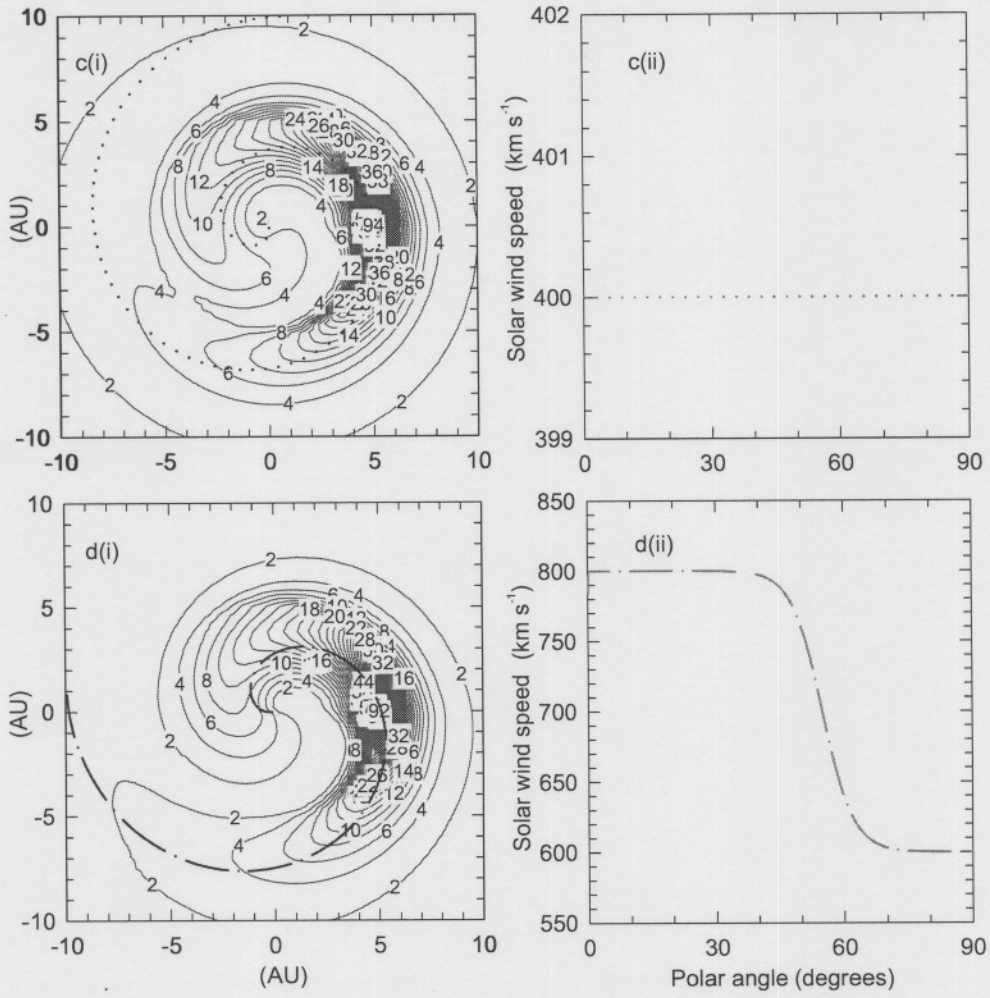

Figure 6-3: Similar to Figure 6-2 but with different solar wind speed scenarios as shown in c(ii) and d(ii).

It is also evident from the contours plots how the different V scenarios change the spiral angle ψ of HMF, given by Equation (2.5). These changes in ψ induce changes in $K_{\phi\phi}$ and K_{rr} which cause considerable changes in the Jovian electron intensity.

6.4 Latitudinal dependent effects of different V profiles

Figures 6-4 (a), (b), (c) and (d) from Ferreira (2002) illustrate the computed distribution of 7 MeV Jovian and galactic electrons along cones at $\theta = 90^0$, $\theta = 60^0$, $\theta = 30^0$ and $\theta = 15^0$ respectively. The computations are shown for the solar wind speed profiles in Figure 6.2 b(ii) with $d = 13$ and $b = 0.005$ in Equation (5.21), respectively. It is clear that the Jovian contribution to the total intensity is much higher than the galactic contribution up to $\theta \geq 60^0$ as illustrated by the spiral contours in (a) and (b) respectively. For $\theta = 30^0$ and $\theta = 15^0$ shown in (c) and (d), the galactic contribution dominates the electron intensity as illustrated by the circles. These results indicate that the azimuthal transport of Jovian electrons diminishes towards the poles and is consistent with results obtained in Chapter 4 that $K_{rr} > K_{\phi\phi}$ near the poles. Since the geometry of HMF near the poles is nearly radial as shown in Chapter 5, the galactic electrons from an isotropic astrophysical source get easy access into the inner heliosphere through K_{rr} which is dominated by $K_{\|}$ in this region. How and where the galactic contribution dominates will be illustrated in more detail in the next section.

Figure 6-5 shows computed 7 MeV electron intensities as a function of polar angle at 1 AU and 5 AU for the assumed V profiles shown in Figure 6.3 a(ii), b(ii), c(ii) and d(ii) respectively. Panels (a) and (b) show computed Jovian electron intensities only, while (c) and (d) show computed galactic electron intensities only. Obviously, Jovian electrons have a much stronger latitudinal dependence at the 5 AU than at 1 AU, whereas for the galactic electrons the latitudinal dependence is much less, with less difference between 1 AU and 5 AU. Also note that the signs of the latitudinal gradients for the Jovian electrons are opposite to those for the galactic electrons.

The most appreciable result is that when V changes from a scenario applicable to solar minimum (e.g. b(ii)) to one for solar maximum activity (e.g. c(ii)), a considerable increase of Jovian electrons towards the poles is evident but galactic electron intensities (isotropic source)

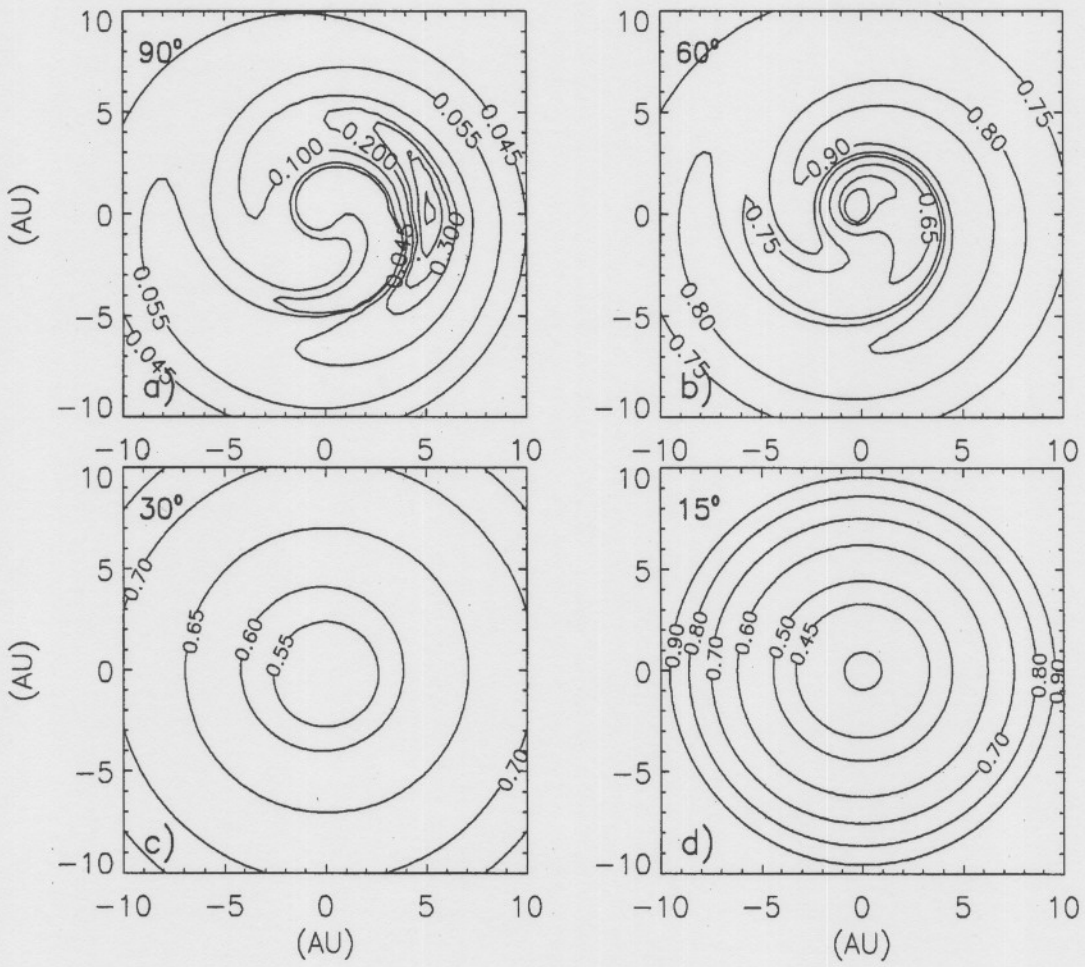

Figure 6-4: Parallel-mapping (of a 3D intensity distribution on a 2D surface) of computed 7 MeV Jovian and galactic electrons at four polar angles for V scenario shown in Figure 6.2 b(i) and b(ii). Values are normalised to the source value at 5 AU. The intensities are shown for: (a) $\theta = 90^0$, (b) $\theta = 60^0$, (c) $\theta = 30^0$ and (d) $\theta = 15^0$ respectively (from Ferreira, 2002).

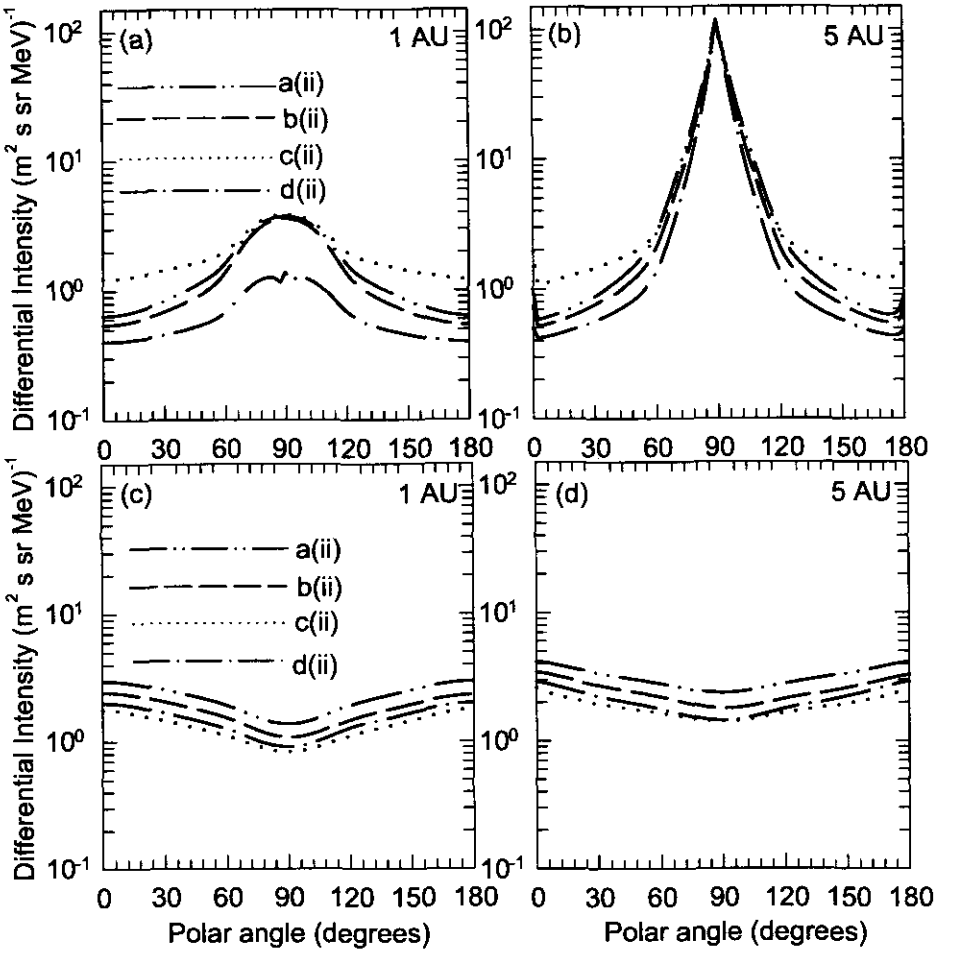

Figure 6-5: Computed 7 MeV electron intensities as a function of polar angle θ for the assumed V scenarios shown in Figure 6.3. Panels (a) and (b) show the Jovian electron intensities only, while panels (c) and (d) show the galactic electron intensities only.

decrease for all latitudes. This occurs as a result of a smaller K_{rr} near the poles during solar maximum conditions, while $K_{\perp\theta}$ remains unchanged by changes in V. This produces a larger value for $K_{\perp\theta}/K_{rr}$, implying that the latitudinal transport with respect to radial transport becomes more effective, resulting in relatively more particles being transported towards the poles from a point source such as the Jovian magnetosphere.

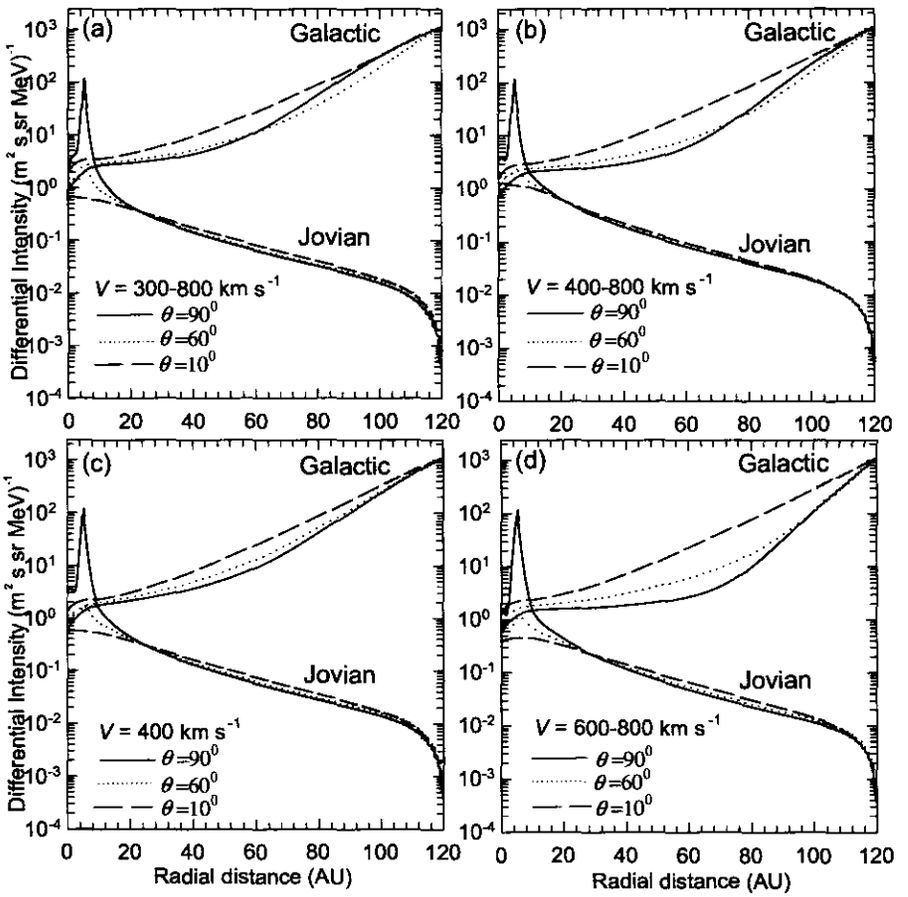

Figure 6-6: Comparison of computed 7 MeV Jovian and galactic electron intensities as a function of radial distance for the assumed V profiles shown in Figures 6.1 to 6.3. The intensities are shown in the equatorial plane $\theta = 90^0$ (solid line), near the poles $\theta = 10^0$ (dashed lines) and at $\theta = 60^0$ (dotted lines). The Jovian electron source is prominent at 5 AU. The local interstellar spectrum for galactic electrons is specified at 120 AU.

6.5 Radial dependent effects of different V profiles

In this section the model is used to compute the effects of the different V profiles on the radial dependence of a few-MeV electrons in the heliosphere. However, it is important to emphasize that this work is mainly focused on modelling of galactic and Jovian electrons in the inner heliosphere ($r \leq 10$ AU) where *in situ* measurements of low energy electrons are made continuously with space probes.

Shown in Figure 6-6 (a), (b), (c) and (d) are the comparisons of model simulations of 7 MeV Jovian and galactic electron's intensities as a function of radial distance for the V profiles illustrated in Figures 6-1 to 6-3. The solutions are shown at $\theta = 10^0$, $\theta = 60^0$ and $\theta = 90^0$ respectively. It is evident from all panels that the Jovian electron population dominates its galactic counterpart in the equatorial plane with $r \leq 10$ AU while the galactic population dominates for $r \geq 10$ AU and at all radial distances near the heliospheric poles. For $r > 15$ AU the Jovian electrons decrease significantly to be completely dominated by the galactic component. The effects of the different V profiles on the galactic electron intensities are clearly illustrated in the outer heliosphere in all panels, quite significantly at $\theta = 90^0$, due to $K_{\perp r}\ \sin^2\psi$ which dominates K_{rr} in this region.

6.6 Effects of different V profiles on electron intensities along the Ulysses trajectory

In this section the model is used to study the 3D transport of 7 MeV Jovian and galactic electrons in the inner heliosphere for the assumed V profiles shown in Figure 6.1. The solutions are compared to the 3 - 10 MeV observed (e.g., Heber et al., 2003a,b) from launch in 1990 up to 2000 as shown in Figure 6-7.

The third panel shows the computed combined Jovian and galactic electron intensities, the fourth panel the Jovian electron intensities only, and the bottom panel the galactic electron intensities only. The trajectory of the Ulysses spacecraft in radial and latitudinal coordinates is shown in the top two panels respectively (data from http: /SWOOPS.lanl.gov/recentvu.html) as discussed qualitatively in Chapter 2. The model computations along the Ulysses trajectory in Figure 6-1 for the V scenario (b) which correspond to solar minimum conditions and (c) which

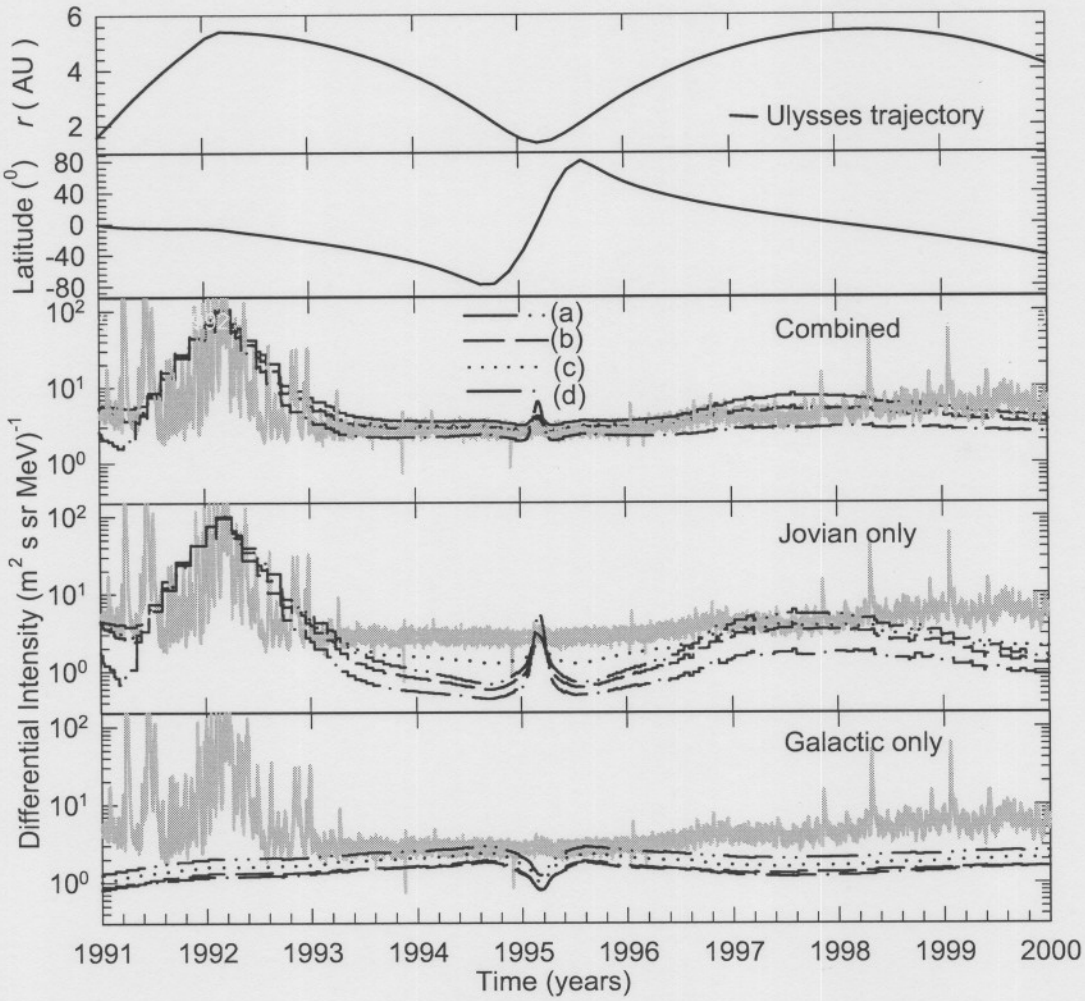

Figure 6-7: The top panels show the Ulysses trajectory in radial and heliographic coordinates (data from http: /SWOOPS.lanl.gov/recentvu.html). In the third panel the computed combined 7 MeV Jovian and galactic electron intensities are shown; fourth panel: Jovian electron intensities only and bottom panel the galactic electron intensities only. The computations are shown for the four different assumptions of V in comparison with the observed $3-10$ MeV (gray band) Ulysses/KET electron data (e.g., Heber et al., 2003a,b).

correspond to solar maximum are not much different and provide good compatibility with the data up to 1998 when Ulysses completed the first solar orbit, but when Jupiter was on the other side of the Sun $\sim$ 10 AU away from the spacecraft. Scenario (d) produces intensities less than observed while scenario (a) results in intensities slightly higher than the observations, which are not preferable solutions. The computed electron intensities for the period after 1998 are all significantly less than the observations, indicating that the solar wind speed related changes *alone* for the changing heliospheric conditions cannot produce realistic low-energy electron modulation. This incompatibility between model solutions and the observed electron intensities is associated with the increase in the solar activity towards solar maximum and obviously cannot be explained by model parameters used for solar minimum conditions (before 1998). It is essential also to note as argued by Heber (2002) that these observed intensities cannot be attributed to either solar particle events or locally accelerated electrons based on their different spectral shapes, and must be of Jovian or galactic origin. However, in order to produce realistic modulation for these electron's intensities, Ferreira et al. (2003a,b) argued that there is a need for realistic time-dependent diffusion coefficients, especially for the latitudinal transport. These aspects will be studied further in the next Chapter.

6.7 Summary and conclusions

In this Chapter solar wind speed parameters α^* and β^* were introduced to generalise the solar wind speed model to simulate different solar wind scenarios applicable to changing heliospheric conditions shown in Figure 6-1 (a), (b), (c) and (d). Effects of the four assumed V profiles on the distribution of 7 MeV Jovian and galactic electrons in the inner heliosphere were computed using the 3D steady-state modulation model (Ferreira, 2002) and were illustrated as surface contour plots in the equatorial plane. It was found that the changes in V from a scenario applicable to a solar minimum (e.g. Figure 5-1(b)) to one for solar maximum (e.g. Figure 5-1(c)) induce changes in the ψ spiral angle of the HMF which lead to considerable changes in Jovian electron intensities in the inner heliosphere as illustrated by Figure 6-2 and 6-3. The solar minimum V scenario causes Jovian electrons not to reach the high latitudes (see also Ferreira, 2002; Ferreira et al., 2003a, 2003b).

The effects of the assumed V profiles on the radial dependence of Jovian and galactic electron intensities were also computed at different latitudes. Referring also to the work of Ferreira (2002), it was found that Jovian electron intensity dominates the galactic contribution in the equatorial plane up to $\sim$ 10 AU while the galactic contribution dominates for $r \geq 10$ AU, in the equatorial plane and near the heliospheric poles for all the assumed V profiles.

The combined Jovian and galactic electron intensities were computed along the Ulysses trajectory for the different assumptions of V and compared to the observed 3 - 10 MeV electrons. It was found that the model solutions for solar minimum scenarios shown in Figure 6-2 (b) and for solar maximum conditions shown in Figure 6-2 (c) were not much different and provide a good compatibility with the observations up to 1998 while solutions with scenarios shown in Figure 6-2 (a) and (d) are not preferable. All model solutions after 1998 are significantly less than the KET observations which indicate that the solar wind speed changes *alone* related to changing heliospheric conditions, cannot produce realistic compatibility with observations towards solar maximum conditions, although it did rather well for solar minimum conditions. There is obviously a need for time-dependent diffusion coefficients, especially for latitudinal transport as argued by Ferreira et al. (2003a,b,c). These aspects will be further investigated in the following Chapter.

Chapter 7

Modulation of electrons from solar minimum to solar maximum

7.1 Introduction

The solar activity transition from solar minimum to solar maximum conditions that started in 1998 led to a incompatibility between the 3 -10 MeV KET observations on board the Ulysses spacecraft and the model predictions which were successfully used to fit observations made during solar minimum conditions as discussed in Chapter 6. Considerable improvements were made by Ferreira et al. (2003c,d) by emphasizing the necessity of reducing of enhancement of $K_{\perp\theta}$ towards solar maximum periods, and Henize et al. (2003) by varying the strength of the Jovian source function in attempts to produce model solutions compatible with observations. In this Chapter, as a further attempt to model the KET observations more realistically, a new relation is established between the heliospheric polar diffusion and the latitudinal dependence of the solar wind speed. Based on this new connection between the transport parameters, a transition from solar minimum to intermediate and then to maximum activity conditions is modelled from a heliospheric polar diffusion perspective correlated with changes in the solar wind speed as observed by the SWOOPS instrument (e.g., McComas et al., 2002b) aboard the Ulysses spacecraft. Effects of these scenarios of heliospheric polar diffusion are computed using the steady-state 3D modulation model as described in Chapter 4 and presented as a series of solutions in comparison with the electron flux observed by the KET instrument along the

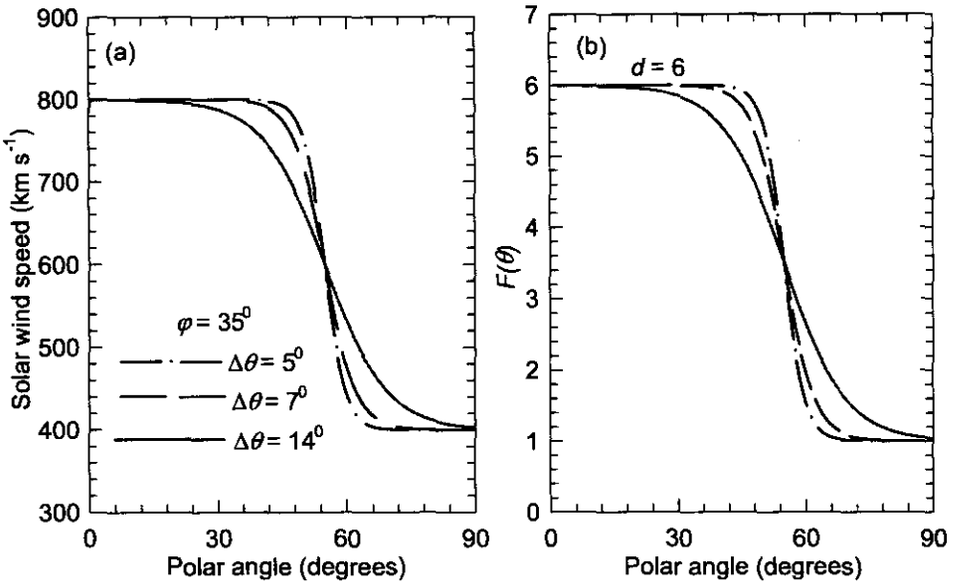

Figure 7-1: (a) Solar wind speed V and (b) $F(\theta)$ as a function of polar angle for $\Delta\theta = 5^0, 7^0$ and 14^0 respectively. Values are shown for a typical solar minimum V scenario, with $d = 6$ in Equation (5.21).

Ulysses trajectory from 1998 to the end of 2003. Subsequent effects of these different scenarios are also illustrated on electron modulation.

7.2 New relation between the solar wind speed and the heliospheric polar diffusion coefficient

The 3 - 10 MeV electron observations made by the KET instrument after the period 1998 are incompatible with the model predictions as discussed in Chapter 6. A reason may be that the changes in the solar wind parameters and the diffusion coefficients, in particular the heliospheric polar diffusion, have not been taken into account as solar activity picks up from solar minimum towards solar maximum periods. In an attempt to explain this, Ferreira et al. (2003c,d) showed that a reduction in the enhancement of $K_{\perp\theta}$ towards the poles from its solar minimum value is necessary. In addition, Henize et al. (2003) also varied the Jovian source strength, increasing with solar activity as an improvement to fit the KET observations, but this will be discussed

briefly in section 7.4.

Here is argued that the reduction in the enhancement of $K_{\perp\theta}$ with increasing solar activity alone is not adequate to account for these observations. It should also be correlated with changes in the latitudinal dependence of V observed by the SWOOPS instrument (Phillips et al., 1995; McComas et al., 2002b) while assuming a steady-state Jovian source function given in Equation (4.10). To treat this problem, consider the latitudinal dependence of V, given by Equation (6.1), and the $F(\theta)$ in the expression for heliospheric polar diffusion $K_{\perp\theta}$, given by Equation (5.20). By comparison, it becomes clear that both have the same hyperbolic function (tanh) with arguments containing $\theta_A = \theta$ the polar angle and $\theta_F = \varphi$ the critical angle respectively.

To establish a relation between these functions, the term $1/\Delta\theta$ in $F(\theta)$ given by Equation (5.21) and the term $2\pi/\theta_s$ given in Equation (6.1) are equated so that:

$$\frac{1}{\Delta\theta} = \frac{2\pi}{\theta_s}, \tag{7.1}$$

where

$$\theta_s = 2\pi\Delta\theta. \tag{7.2}$$

Substituting Equation (7.2) into (6.1) yields

$$V(\theta) = \alpha^* \mp \beta^* \tanh\left[\frac{1}{\Delta\theta}\left(\theta - 90^0 \pm \varphi\right)\right], \tag{7.3}$$

which has the same functional behavior as $F(\theta)$. The parameter $\Delta\theta$ determines the rate of change of V from a slow solar wind speed in the equatorial regions to a high speed towards heliospheric polar regions. Figures 7-1 (a) and (b) show the connection between V and $F(\theta)$ as a function of polar angle for possible values of $\Delta\theta$, that is $\Delta\theta = 5^0$, $\Delta\theta = 7^0$ and $\Delta\theta = 14^0$ with an enhancement factor $d = 6$ for heliospheric polar diffusion. It is evident that for a larger value of $\Delta\theta$, the changes in V from the equatorial plane to high latitude become much steeper than for the case of a smaller value, e.g. $\Delta\theta = 5^0$.

The critical angle φ is defined as the "angular width" where the solar wind speed increases from the equatorial minimum value to the high latitude maximum value, e.g. a critical angle of $\varphi = 35^0$ means that at $(90^0 - 35^0)$ and $(90^0 + 35^0)$, $V = \frac{1}{2}\left(V_{\text{maximum}} + V_{\text{minimum}}\right)$. The selection

of this angle and other solar wind speed parameters such as α^*, β^* and $\Delta\theta$ to fit observations form a crucial part of this Chapter and are the subject of interest for the study in the following section.

7.3 Modelling V from solar minimum to solar maximum conditions

The transition from solar minimum to solar maximum is the restructuring of the entire heliosphere from the solar wind perspective. The average solar magnetic field strengthens, the solar surface fields becomes more chaotic, the tilt angle of HMF increases and transient events such as coronal mass ejections (CMEs) become more frequent (e.g., Richardson et al., 2001). The highly latitude-dependent, uniformly-fast solar wind speed emanating from huge polar coronal hole observed by the SWOOPS experiment during the solar minimum diminishes gradually towards solar maximum as the polar coronal hole shrinks and the width of the slow V region in the equatorial region increases towards high latitudes (e.g., Phillips et al., 1995 ; McComas et al., 2002b). The critical angle also increases from its typical value assumed for solar minimum conditions to a maximum value during intermediate solar activity and has no physical significance at solar maximum conditions. The reduction of the enhancement of $K_{\perp\theta}$ becomes important in relation to realistic changes of the solar wind speed profiles.

Model solutions for the solar wind speed used previously for the solar minimum conditions assumed a larger $\varphi = 35^0$, shown in the upper panel of Figure 7-2 (solid line) than the one apparently observed (light shaded data) by the SWOOPS instrument. To improve this aspect of the model, the set $\varphi = 20^0$, $\alpha^* = 1.45$, and $\beta^* = 0.45$ were selected to produce values compatible with observations as shown in Figure 7-2 (dashed line) by using a polar diffusion coefficient with parameters $d = 6$ and $b = K_{\perp\theta}/K_{\parallel} = 0.015$ in the equatorial region (e.g., Ferreira et al., 2002) as shown in the bottom panel of Figure 7-2 (dashed line).

With the aid of the new connection between the latitudinal dependence of V and $K_{\perp\theta}$, an ideal intermediate V scenario is modelled simulating the transition from solar minimum to solar maximum by selecting $\varphi = 55^0$, $\alpha^* = 1.25$, and $\beta^* = 0.25$. This is assumed to correlate with the selection of $b = K_{\perp\theta}/K_{\parallel} = 0.015$ in the equatorial plane in Equation (5.20), with the

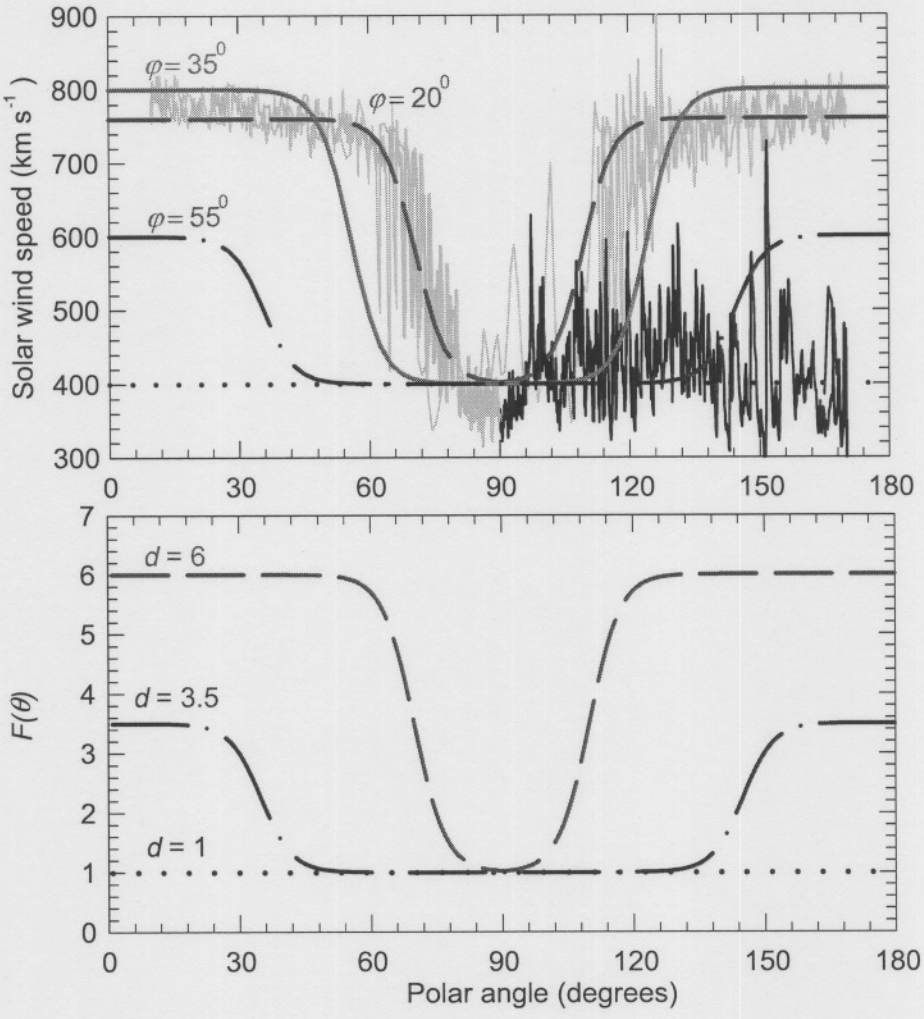

Figure 7-2: The solar wind speed V and $F(\theta)$ as a function of polar angle. Simulations are for $\varphi = 20^0$ corresponding to $d = 6$, a scenario assumed for solar minimum, $\varphi = 55^0$ corresponding to $d = 3.5$, a scenario assumed for intermediate solar activity conditions and for $d = 1$, a scenario assumed to correspond to solar maximum conditions. Latitudinal dependence of V observed by the SWOOPS instrument (e.g., McComas et al., 2002b) for solar minimum (light data curve) and solar maximum conditions (light data curve) is shown in the upper panel for comparison.

enhancement factor in $F(\theta)$ reduced from its value assumed for the solar minimum conditions $d = 6$ to $d = 3.5$ as shown in Figure 7-2 (dash-dot-dash lines). This scenario corresponds to V with an average speed of 400 km s^{-1} from the equatorial plane to mid-latitude and an average speed of 600 km s^{-1} near the heliospheric polar regions. In this study it is proposed to be related to the transition made by the evolution of a large polar coronal hole from its maximum size during solar minimum to an intermediate size as it retreats toward solar maximum conditions.

During solar maximum periods, no well-defined high solar wind speed is observed (e.g., Richardson, 2001) as shown by the black shaded data curve in the upper panel of Figure 7-2 (McComas et al., 2002b). These observations are consistent with the concept that the large polar coronal holes in the northern and southern hemispheres of the Sun observed during the solar minimum first shrink as the solar activity picks up and disappear entirely at solar maximum (See Bravo and Gruz-Abreyro, 1996). As a result, the fast solar wind speed disappears and the concept of a critical angle vanishes naturally when an average $V = 400$ km s^{-1} is observed at all heliolatitudes. To simulate this scenario in the model, the parameters $\alpha^* = 1.0$, and $\beta^* = 0$ are selected in Equation (7-3) to produce compatibility with observations as shown in Figure 7-2 (dotted line) respectively. This scenario assumingly correlates with the selection of $d = 1$ and $b = K_{\perp\theta}/K_{\parallel} = 0.015$ in the equatorial plane for heliospheric polar diffusion as shown in the bottom panel of Figure 7-2 (dotted line).

Implications of these new scenarios of heliospheric polar diffusion with its respective ambient solar wind profiles on KET observations after 1998 will be further investigated in the following section.

7.4 Application of a series of steady-state solutions to 3-10 MeV KET observations during solar maximum

In this section, the 3D steady-state modulation model discussed in Chapter 3 is employed with the new scenarios of heliospheric polar diffusion and solar wind speed discussed in the preceding section. It is used to compute 7 MeV electron intensities along the Ulysses trajectory from the end of the first out-of-ecliptic orbit (1998) to the end of 2003 as shown in Figure 7-3. Also discussed in this section is how Henize et al. (2003) varied the strength Jovian source Q given

by Equation (4.10) as an improvement to fit observations.

The Ulysses trajectory in radial and latitudinal coordinates is again displayed in the top panels (Data from http: /SWOOPS.lanl.gov/recentvu.html) for the second solar orbit. The third panel displays the computed combined Jovian and galactic intensities, the fourth panel the Jovian electrons only and the bottom panel only the galactic electron intensities. It is evident for the period after 1998 that the model solution with the $d = 6$ scenario (applicable to solar minimum) is significantly below the KET observations for almost all of the solar maximum period, except the short time when the Sun was relatively inactive just after 2002. This transient period of decreased solar activity is also confirmed by the tilt angle data shown in Chapter 2. During this period, the KET observations dropped significantly to be comparable to solar minimum conditions.

Solutions with $d = 1$ assumed for solar maximum conditions show incompatibility with the KET observations, particularly from mid-2000 throughout the second fast latitude scan to the end of 2002. The solution with $d = 3.5$ assumed for intermediate solar activity provides an improved compatibility to the observations for the period after mid-1998 to mid-2000. It is evident that the series of time-independent solutions are not sufficient to account for observations made throughout the entire solar maximum periods, but yield an indication as to changes in the transport parameters during the solar maximum such as a reduction in the enhancement of heliospheric polar diffusion, the change in solar wind speed parameters α^*, β^* and the critical angle φ . In order to fit the KET observations for the entire solar maximum period, these results suggest the need for a time-dependent model with time-dependent heliospheric diffusion, the corresponding solar wind speed profiles and most likely also for other modulation parameters like CIR's.

All the solutions converge towards the end of 2003 as expected, because it was the time when the spacecraft was approaching Jupiter from higher northern latitudes for the second close encounter. This had occurred already in February 2004 when the spacecraft was within 1 AU of the giant planet and is not shown.

What will also be of interest to investigate is how the Jovian source function evolves with time as the solar activity increases from solar minimum to solar maximum conditions. This was done earlier by Henize et al. (2003) by fitting a gaussian curve (with maximum enhancement

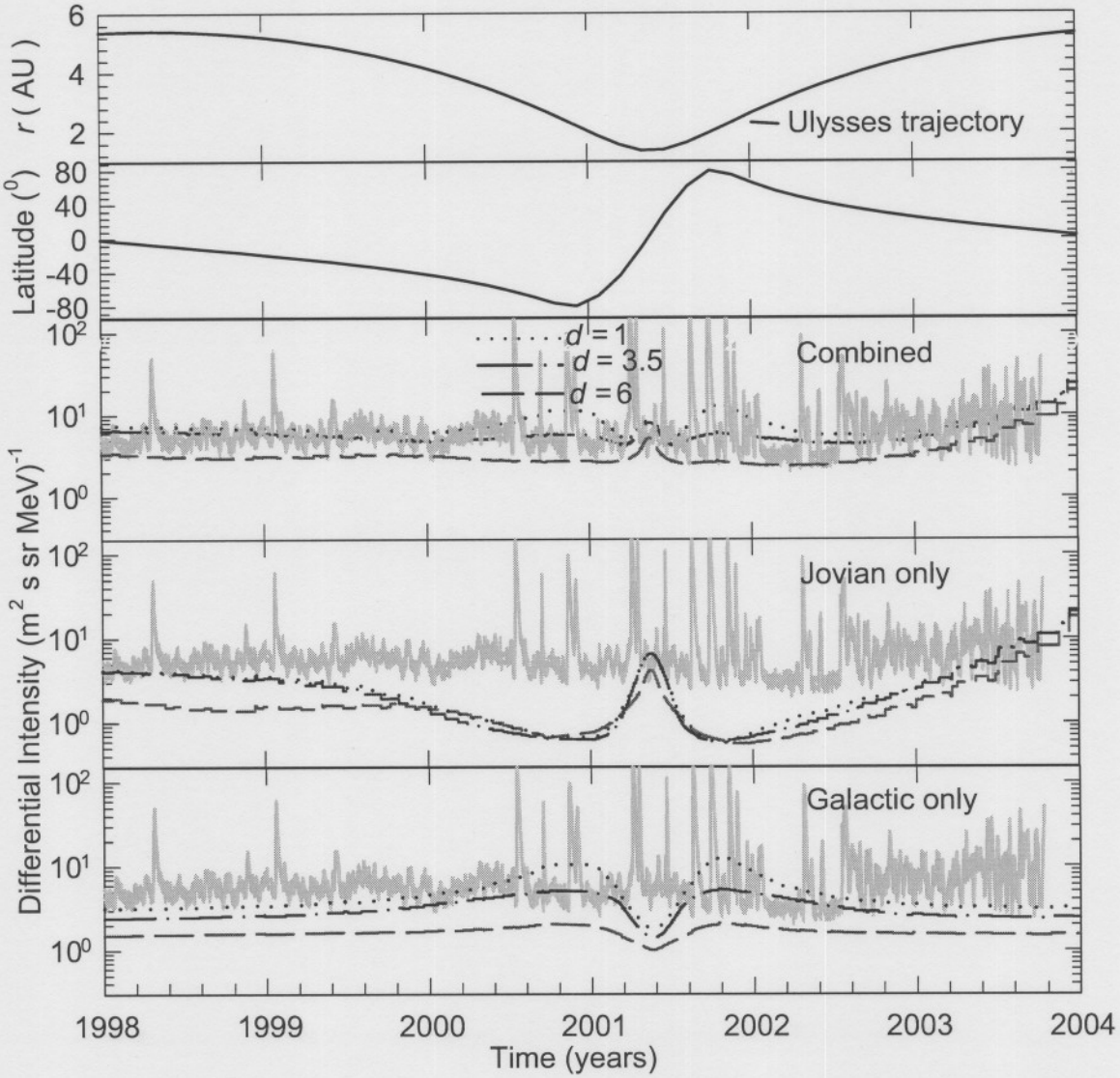

Figure 7-3: Similar to Figure 6-7 in Chapter 6, but the computed solutions are shown for three different d scenarios correlated to different solar wind profiles shown in Figure 7.2 in comparison with the observed $3 - 10$ MeV Ulysses/KET electron data (Heber et al., 2003a,b).

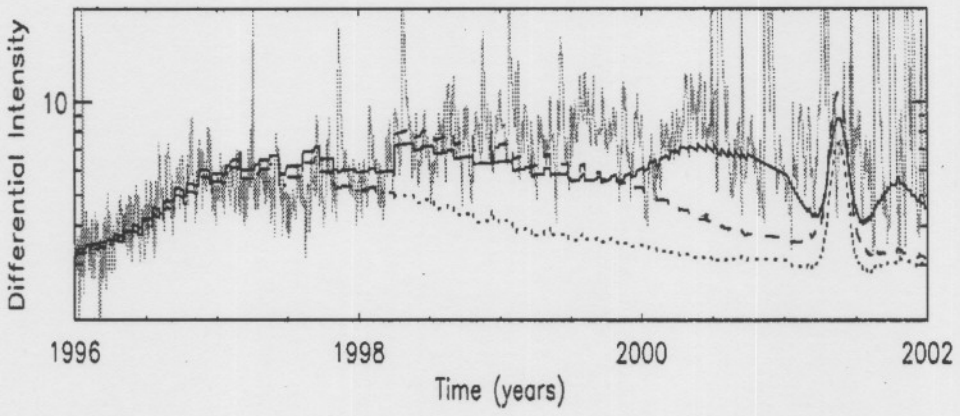

Figure 7-4: Three computed 7 MeV scenarios are shown along the Ulysses trajectory (from Henize et al., 2003). The dotted line denotes the model solution for typical solar minimum conditions (e.g., Ferreira et al., 2002). The dashed line shows the source function Q increased as per electron intensity enhancement observed at 1 AU by the SOHO spacecraft starting in mid-1998. The variation of the d parameter with the electron source increase is plotted as a solid line. The 3-10 MeV Ulysses observations (Heber et al., 2003a,b) are illustrated in gray. The differential intensity is in units of particles $(\mathrm{m}^2\ \mathrm{s\ sr\ MeV})^{-1}$.

of a factor of 2.5) centered about mid-1999 to the Jovian source Q enhancement revealed by analysis of SOHO/CST data. The Jovian source was varied accordingly in the model and the result is shown in Figure 7-4 by a dashed line in comparison to the model solution applicable to solar minimum conditions (dotted line). This has only improved model compatibility with KET observations for the period of mid-1998 to mid-1999. After this, much greater increases in Q would be required to fit observations, which is a condition not favoured by SOHO/CST and IMP8/GME electron observations. For this work, such further enhancements of Q are considered to be unrealistic.

However, as a further attempt to fit the KET observations after mid-1999, Henize et al. (2003) also considered a reduction in the enhancement parameter d of $K_{\perp\theta}$ from a value applicable to solar minimum ($d = 6$) to a value assumed to be applicable to solar maximum conditions ($d = 1$) (e.g., Ferreira et al., 2003a,b) and again fitted an inverse gaussian curve centered about mid-2000. This, and the inclusion of the Q enhancement has made a considerable improvement in the model's compatibility to the KET observations as shown by the solid line

in Figure 7-4, but could not fit the period from 1999 to mid-2000. Again it is evident that the combination of several parameters can improve compatibility of the model to observations.

The Ulysses electron observations represent a picture of a very complicated interplay of several modulation parameters for solar maximum activity. The complexity of solar modulation at solar maximum, especially for these low energies where a solar contribution is likely, has made the applicability of a steady-state approach unsatisfactory. It is therefore beyond the scope of this work to further improve the model's compatibility with observations and must be left for time-dependent models with a more sophisticated handling of the various parameters.

In the following section the effect of the assumed d scenarios of heliospheric polar diffusion on electron modulation in the inner heliosphere with their corresponding solar wind speed profiles are investigated.

7.5 Effects on electron modulation at all energies

7.5.1 Spectra

In this section, effects of the assumed scenarios of heliospheric polar diffusion and their corresponding solar wind speed profiles are illustrated on electron spectra.

Shown in Figure 7-5 are electron spectra at 1 AU computed with $\theta = 10^0$, $\theta = 60^0$ and $\theta = 90^0$ respectively for the $A > 0$ magnetic polarity epoch with tilt angle $\alpha = 5^0$. The solar cycle-related changes due to drifts were not considered for this study because the focus was on low energy ($\sim$ 7 MeV) electrons, although for high energy ($>$ 300 MeV) studies, drifts are crucial (e.g., Potgieter, 1996). Of particular interest to the study low-energy electron modulation is that they respond directly to the energy dependence of the diffusion coefficients, in contrast to protons which experience large adiabatic energy losses at these energies. At higher energies, drifts begin to dominate so that this effect gets hidden. Panels (a), (c) and (e) show galactic spectra with the electron LIS given by Equation (4.12) from Langner et al. (2001) while (b), (d) and (f) show Jovian electron spectra. The computations are for different d scenarios assumed to correspond to different V profiles shown in Figure 7-2. The effects of these d scenarios on galactic spectra are more pronounced near the heliospheric poles than at $\theta = 60^0$ and $\theta = 90^0$, while for Jovian electrons it is noticeable in the low energy region ($<$ 30 MeV) of the

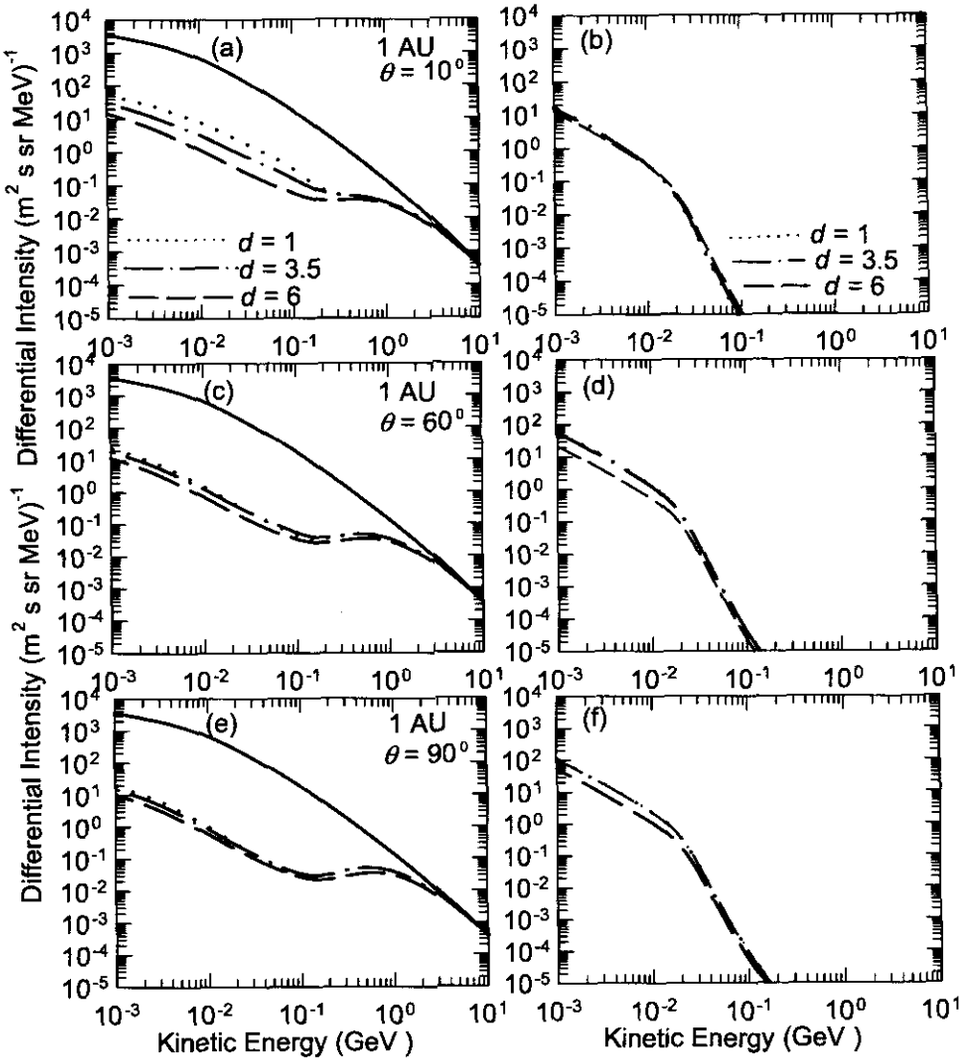

Figure 7-5: Computed electron spectra at 1 AU and shown at $\theta = 10^0$ (upper panels), $\theta = 60^0$ (middle panels) and $\theta = 90^0$ (bottom panels) for $A > 0$ magnetic polarity epoch. Figures (a), (c), and (e) are galactic spectra only while (b), (d) and (f) are Jovian spectra. The computations are for different d scenarios shown in Figure 7.2, without considering any changes in drifts. The tilt angle was kept at $\alpha = 5^0$.

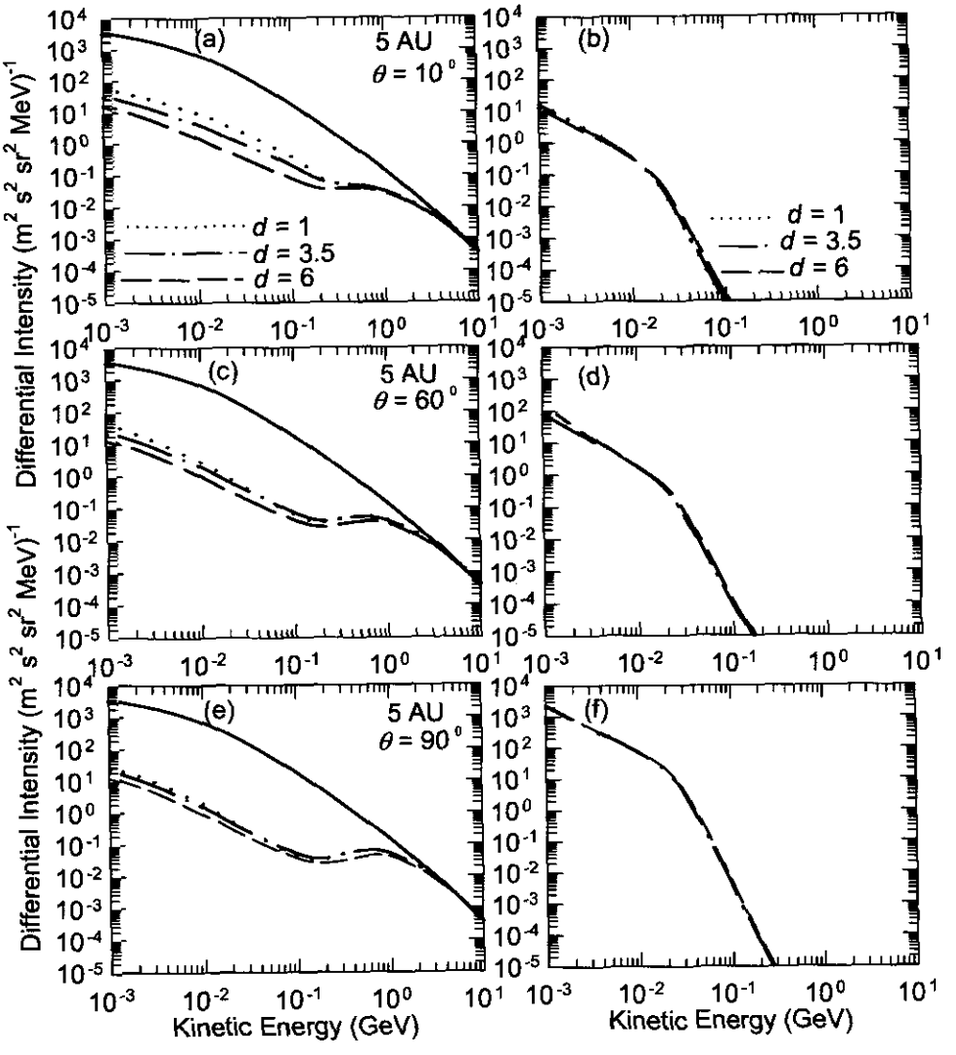

Figure 7-6: Similar to Figure 7-5, but the computed spectra are shown at 5 AU. As expected the Jovian electron spectra remain almost unaltered, which serves as a check on the reliability of the model.

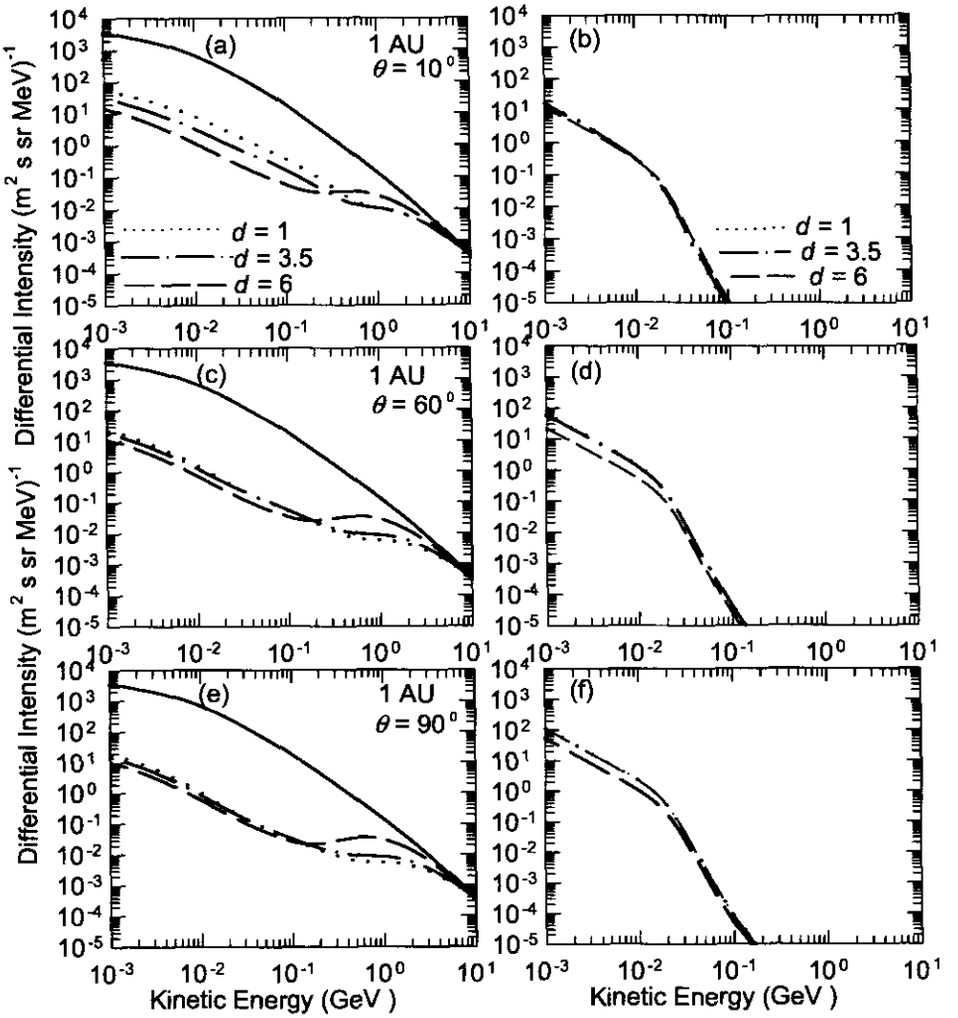

Figure 7-7: Similar to Figure 7-4, but spectra are computed with tilt angle $\alpha = 5^0$ and $(K_A)_0 = 1.0$ for $d = 6$, $\alpha = 30^0$ and $(K_A)_0 = 0.5$ for $d = 3.5$, and $\alpha = 55^0$ and $(K_A)_0 = 0.2$ for $d = 1$ respectively- see Equation (5.24).

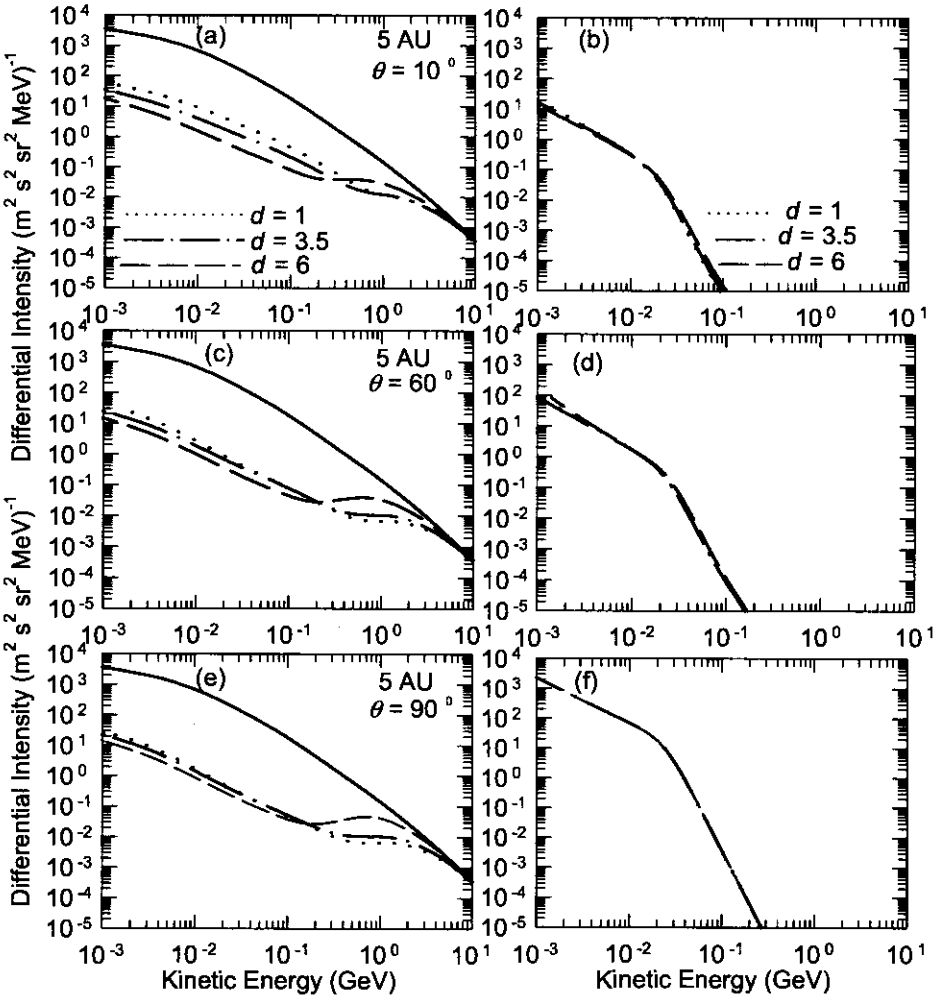

Figure 7-8: Similar to Figure 7-6, but the computed spectra are shown at 5 AU.

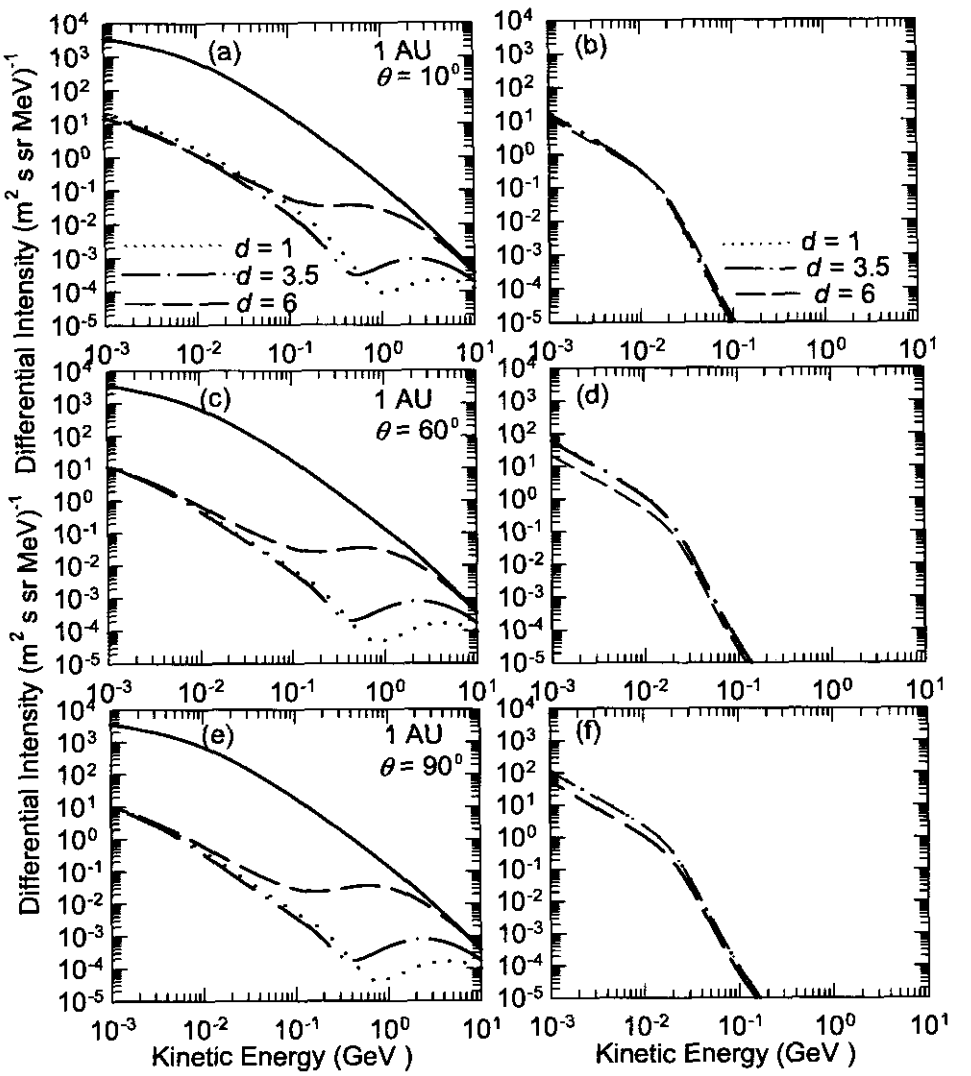

Figure 7-9: Similar to Figure 7-7, but the galactic spectra for the $A > 0$ polarity cycle are computed at $\theta = 10^0$ with $K_{\perp\theta}/K_{\parallel} = 0.025$ and $K_{\perp r}/K_{\parallel} = 0.001$; $\theta = 60^0$ with $K_{\perp\theta}/K_{\parallel} = 0.02$ and $K_{\perp r}/K_{\parallel} = 0.001$; $\theta = 90^0$ with $K_{\perp\theta}/K_{\parallel} = 0.03$ and $K_{\perp r}/K_{\parallel} = 0.001$ all for $d = 1$; then at $\theta = 10^0$ with $K_{\perp\theta}/K_{\parallel} = 0.015$ and $K_{\perp r}/K_{\parallel} = 0.002$; $\theta = 60^0$ with $K_{\perp\theta}/K_{\parallel} = 0.015$ and $K_{\perp r}/K_{\parallel} = 0.002$; $\theta = 90^0$ with $K_{\perp\theta}/K_{\parallel} = 0.015$ and $K_{\perp r}/K_{\parallel} = 0.002$ for $d = 3.5$. For $d = 6$ the galactic electron spectra are computed with $K_{\perp\theta}/K_{\parallel} = 0.015$ and $K_{\perp r}/K_{\parallel} = 0.010$ as used in the study of Ferreira et al. (2002).

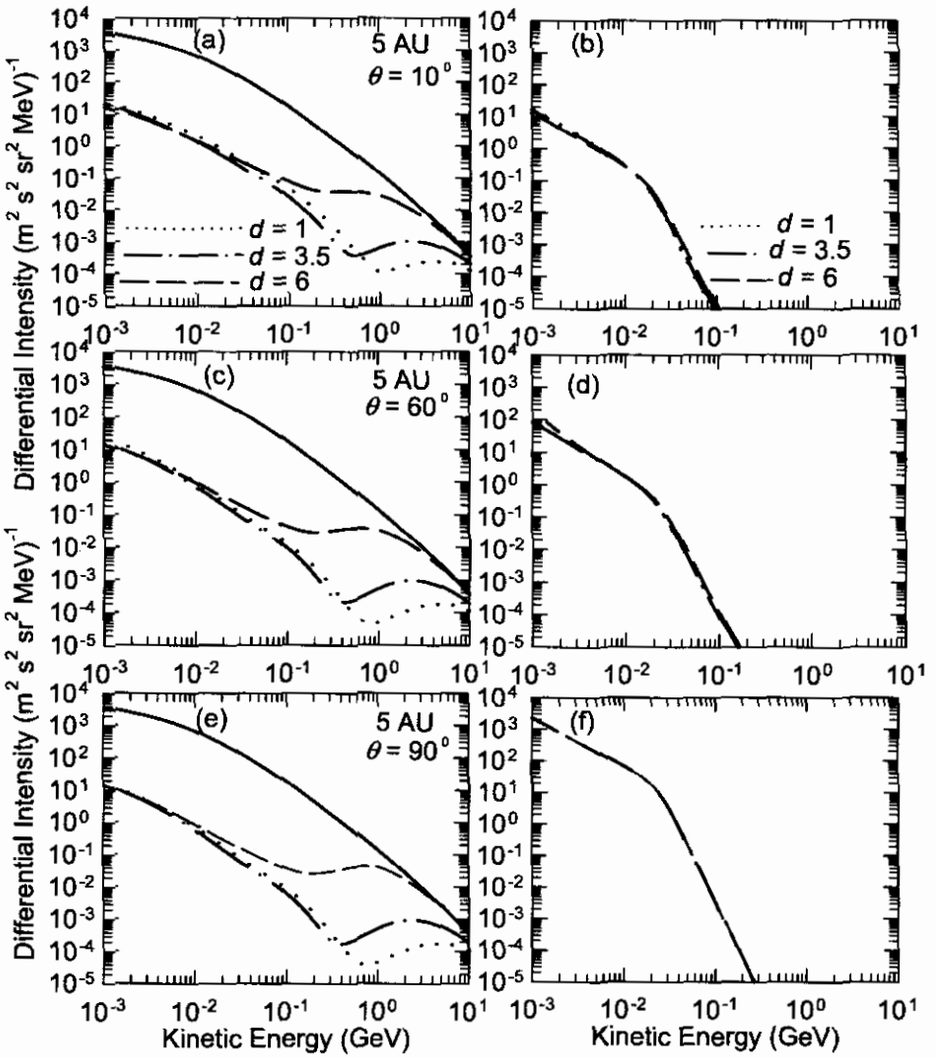

Figure 7-10: Similar to Figure 7-9, but with spectra shown at 5 AU.

spectra at $\theta = 60^0$ and $\theta = 90^0$ rather than near the poles. The $d = 1$ scenario assumed to correspond to solar maximum conditions has higher intensities at all energies than for $d = 3.5$ which assumingly corresponds to intermediate solar activity and $d = 6$ which corresponds to solar minimum conditions. In fact, the difference in the computed galactic electron intensities between the $d = 6$ and the $d = 1$ scenario at $\theta = 10^0$, $\theta = 60^0$ and $\theta = 90^0$ as energies below 100 MeV is in contrast to what is observed (Heber 2003a,b) for these electrons. An attempt to resolve this aspect is done later in this section.

Figure 7-6 is similar to Figure 7-5 but shown at 5 AU. Panels (a), (c) and (e) are galactic spectra only while (b), (d) and (f) are Jovian spectra. As before, effects of the d scenarios on galactic electron spectra are more pronounced in the low energy region (< 200 MeV) near the polar regions than at $\theta = 60^0$ and $\theta = 90^0$, while for Jovian electrons there are no significant changes at all energies, as expected at 5 AU. By comparing Figure 7-5 and Figure 7-6, not much difference is noted between the galactic spectra computed at $\theta = 10^0$, $\theta = 60^0$ and $\theta = 90^0$ respectively. For the Jovian spectra, a significant differences are noticeable at $\theta = 60^0$ and $\theta = 90^0$ but not at $\theta = 10^0$. It is evident that Jovian electron intensities are mainly modulated in the ecliptic plane, while galactic electrons may experience considerable modulation differences in the inner heliospheric polar regions.

At high energies (> 300 MeV), the effects of changing *only* the d scenarios which were correlated with different solar wind speed profiles could not produce realistic electron modulation as shown in Figure 7-5 and 7-6 respectively. It is expected that electron intensities computed for the $d = 1$ scenario would decrease at these energies with respect to electron intensities computed with $d = 6$. This implies that certain transport parameters such as the tilt angle α and drifts have to be consistently changed in the model with increasing solar activity. To treat this problem accordingly, it is well established in the field of cosmic ray modulation studies that when solar activity increases from solar minimum conditions to solar maximum conditions, the tilt angle α should increase while drifts gradually vanish (e.g., Potgieter, 1996; Ferreira and Potgieter, 2004a,b). This aspect is incorporated in the model by changing $\alpha = 5^0$ assumed for solar minimum conditions with constant $(K_A)_0 = 1.0$ (100% drift) for the $d = 6$ scenario to $\alpha = 30^0$ for intermediate solar activity with $(K_A)_0 = 0.5$ (50% drift) for the $d = 3.5$ scenario and to $\alpha = 55^0$ assumed for solar maximum conditions with $(K_A)_0 = 0.2$ (20% drift) for

$d = 1$ respectively, where $(K_A)_0$ is given by Equation (5.24). (See also Ferreira and Potgieter, 2004a,b). This yields more realistic electron modulation as shown in Figure 7-7 (a), (c), (e) and Figure 7-8 (a), (c) and (e) respectively. It is evident that electron intensity computed for $d = 6$ with 100% drift increases significantly at higher energies (> 300 MeV) while electron intensity computed for $d = 1$ with 20% drift decreases more rapidly than the electron intensities computed for $d = 3.5$ with 50% drift. It is also evident that at lower energies (< 200 MeV) drift has no effect on both Jovian and galactic electron modulation. It is now well established that these low-energy electrons are mainly modulated by diffusion and convection..

Finally, a case study is conducted as an attempt to find a set of perpendicular diffusion coefficients ($K_{\perp r}$ and $K_{\perp\theta}$) for low energy galactic electrons to reduce the difference in the computed spectra between $d = 1$ and $d = 6$ in the heliospheric polar regions ($\theta = 10^0$) and in the equatorial plane ($\theta = 90^0$) mentioned earlier in this section. This is done in two-fold a case study as follows.

CASE A:

Firstly, the ratio $K_{\perp\theta}/K_{\parallel} = b = 0.015$ is kept constant in the equatorial plane while varying $K_{\perp r}/K_{\parallel} = a$ for the assumed d scenarios in the model. The following were used: $a = 0.010$ for $d = 6$ applicable to solar minimum conditions (Ferreira et al., 2003), $a = 0.002$ for $d = 3.5$ which assumingly corresponds to intermediate solar activity conditions and $a = 0.001$ for the $d = 1$ which may be considered as solar maximum conditions in this study.

CASE B:

Secondly, the a values obtained in the CASE A for the assumed d scenarios are kept unchanged while varying the parameter b. For $d = 1$, it is found that $b = 0.03$ is a suitable value in the equatorial plane but this changes to $b = 0.025$ in the heliospheric polar region. For the $d = 3.5$ and $d = 6$ the value of $b = 0.015$.

By using the values of $K_{\perp\theta}/K_{\parallel}$ and $K_{\perp r}/K_{\parallel}$ found in the preceding case studies in the model, the computed galactic spectra are shown in the equatorial plane ($\theta = 90^0$), mid-latitude ($\theta = 60^0$), and in the heliospheric polar region ($\theta = 10^0$) at 1 AU and 5 AU for the d scenarios in Figure 7-9 (a), (c), (e) and 7-10 (a), (c), (e), respectively. It is evident for the galactic electron spectra in the equatorial plane, that the intensities are now similar in the lower energy region (< 100 MeV) for the assumed d scenarios.

In the heliospheric polar regions $(\theta = 10^0)$, the low energy galactic electron intensities computed for $d = 1$ are about a factor of ~ 2 larger than for the $d = 6$, while there is no significant difference between the $d = 3.5$ and the $d = 6$ scenarios. This is not the case at high energies (≥ 1 GeV), where the galactic electron intensities computed for $d = 6$ are significantly larger than for the $d = 1$. The latter is consistent with the current knowledge of cosmic ray modulation. For low energies, one can argue that if the factor of ~ 2 increase in the electron intensities observed in the heliospheric polar regions by the 3 - 10 MeV KET instrument (e.g., Heber et al., 2003a,b) as solar activity picks up from solar minimum to solar maximum condition could be interpreted as a contribution from galactic electrons, then this study will have important implications to the transport and modulation of these low-energy electrons in the inner heliosphere. The plausible alternative is that this increase could be attributed to solar electrons, which was ruled out by Heber et al. (2002b) based on the spectral shapes of these electron spectra.

7.5.2 The polar dependence of electron intensities

Figure 7-11 shows the computed electron intensities as a function of polar angle at 1 AU and 5 AU for the assumed d scenarios shown in Figure 7-2 respectively. Panels (a) and (b) show computed Jovian electron intensities only while panels (c) and (d) display the galactic electron intensities. The diffusion coefficients resulted from the previous CASE studies corresponding to Figures 7-9 and 7-10 are used to compute these electron intensities.

For the Jovian electron intensities, the solution with $d = 3.5$ at 1 AU is indistinguishable from the solution with $d = 1$ from $\theta \geq 60^0$, that is towards the equatorial regions, but they differ significantly towards the polar regions. The difference between the $d = 3.5$ and $d = 6$ solutions is maximum in the equatorial regions diminishing towards the poles. There is a remarkable difference in Jovian electron intensities at 1 AU for all polar angles between the solutions with $d = 6$ applicable to solar minimum and with $d = 1$ assumed to correspond to solar maximum. Panel (b) illustrates that the Jovian electron intensities have a very strong latitudinal dependence towards and away from the source and this latitudinal dependence is not really influenced by changing the parameter d.

For galactic electron intensities, in contrast to the Jovian electron intensities, the latitudinal gradients are small and negative between 0^0 and 90^0 at 1 AU and at 5 AU, which is consistent

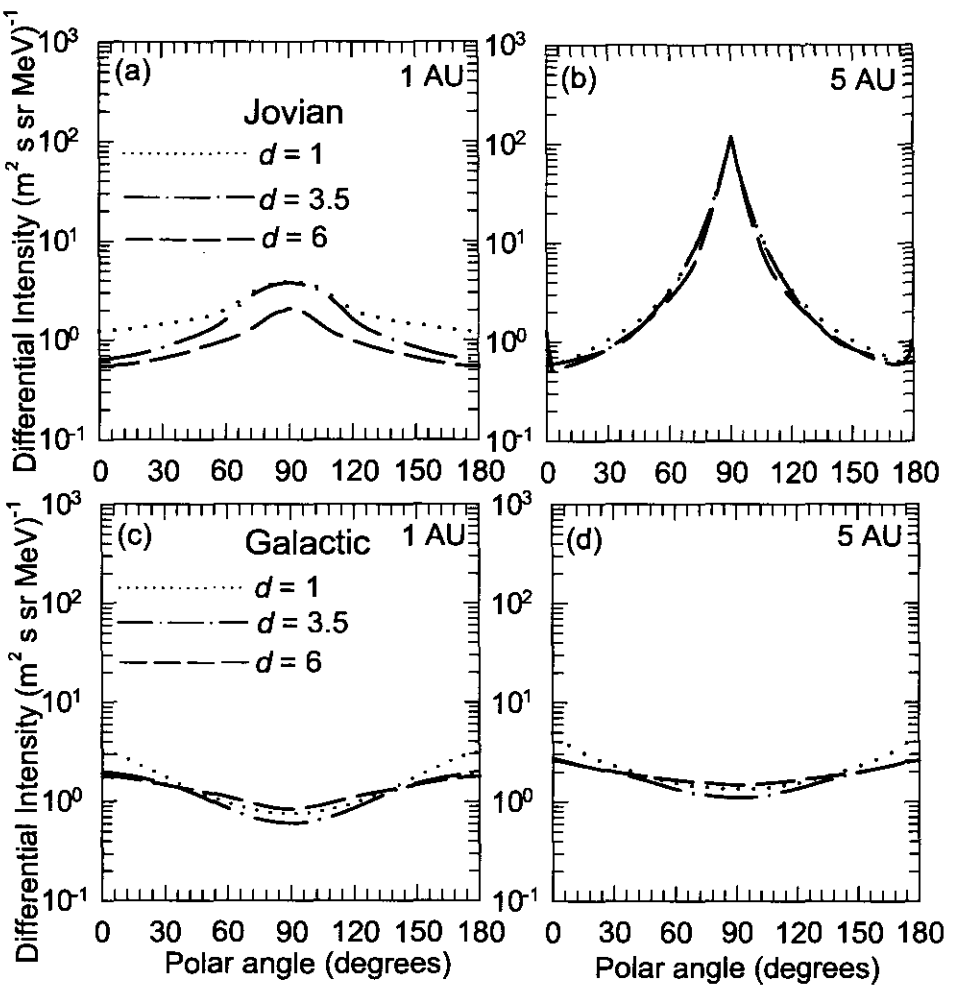

Figure 7-11: Computed 7 MeV electron intensities at 1 AU and 5 AU as a function of polar angle for the assumed d scenario displayed in Figure 7.2. Panels (a) and (b) show computed Jovian electron intensities only, while panels (c) and (d) show the galactic electron intensities.

with what Potgieter et al. (1997) concluded. In the polar regions, there is a factor ~ 2 difference between solutions for $d = 6$ and $d = 1$ at 1 AU and at 5 AU, with the differences decreasing with increasing radial distance. The differences between the $d = 1$, $d = 3.5$ and the $d = 6$ solutions are almost negligible in the equatorial plane at 1 AU and 5 AU.

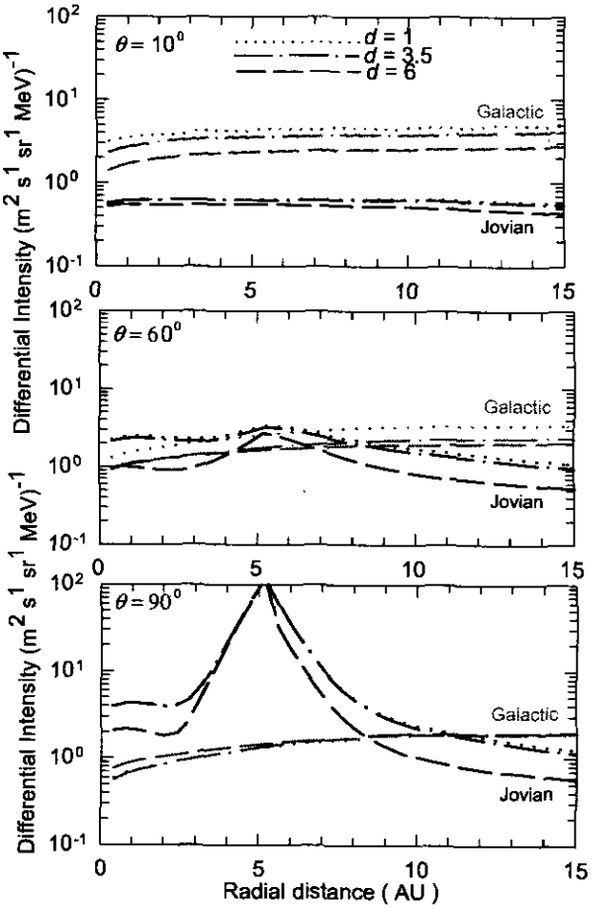

Figure 7-12: Radial dependence of the computed 7 MeV Jovian (black lines) and galactic (gray line) intensities for the different d scenarios correlated to different solar wind speed profiles shown in Figure 7.2, with the rest of the modulation parameters for galactic electrons as in Figure 7.9. The computations are shown at $\theta = 10^0$, $\theta = 60^0$ and $\theta = 90^0$ respectively.

7.5.3 Radial dependence of electron intensities

Figure 7-12 shows the radial dependence of the computed 7 MeV Jovian and galactic electron intensities for the assumed d scenarios shown in Figure 7-2. Again the diffusion coefficients resulting from the CASE studies are used to compute galactic electron intensities and may not necessarily produce compatibility with the Pioneer 10 data (e.g., Eraker et al., 1982). The computations are shown at $\theta = 10^0$ in the upper panel, at $\theta = 60^0$ in the middle panel and at $\theta = 90^0$ in the bottom panel, respectively.

At $\theta = 10^0$ galactic intensities dominate overall and the effects of the assumed scenarios of d are clearly more pronounced on the radial dependence of galactic intensities than for Jovian intensities. There is about a factor of ~ 2 change in the galactic intensities at this energy from the $d = 6$ to the $d = 3.5$, to the $d = 1$ scenario.

At mid-heliolatitude ($\theta = 60^0$), the Jovian intensities already show a radial dependence caused by the source at 5 AU, especially for the $d = 6$. Obviously, the change in the sign of the radial gradients for Jovian electrons does not occur for galactic electrons. There are, however, almost no differences in the radial dependence of Jovian electrons for the $d = 1$ and the $d = 3.5$ scenarios, and similarly for the radial dependence of galactic electrons.

In the inner-heliospheric equatorial regions ($\theta = 90^0$) Jovian electron intensities have a strong positive radial dependence towards the source and completely dominate galactic electron intensities. There is factor ~ 2 increase in the Jovian electron intensities at Earth for $d = 6$ to $d = 1$, with almost no difference between $d = 3.5$ and $d = 1$. No significant effects of different d scenarios on galactic electron intensities are noticeable in the equatorial plane, but this depends on the set of diffusion coefficients used, in particular $K_{\perp r}/K_{\parallel}$ and $K_{\perp \theta}/K_{\parallel}$.

7.6 Summary and conclusions

In this Chapter a new relation was established between the latitudinal dependence of the solar wind speed V and heliospheric polar diffusion to enable improved modelling of these parameters with changing heliospheric conditions. The transition from solar minimum to solar maximum of the heliospheric polar diffusion and the solar wind speed were modelled based on the concept of the time evolution of large polar coronal holes and compared to the solar wind speed

observations (e.g., McComas et al., 2002b) made by the SWOOPS instrument. The concept of a critical angle in the latitudinal dependence of the solar wind speed was introduced together with other important V related parameters.

The 3D electron modulation model (e.g., Ferreira, 2002), together with invoking different d scenarios assumed to correlate to different V profiles was used to compute a series of steady state solutions for the electron intensities along the Ulysses trajectory and compared to the 3 - 10 MeV KET observations (e.g., Heber et al., 2003a,b) after 1998. It was found that these steady-state solutions are not adequate to account for the entire solar maximum observations, but only give an indication as to how the heliospheric polar diffusion and the V profiles are changing during solar maximum conditions. Also discussed is how Henize et al. (2003) varied the strength of the Jovian electron source Q by fitting a gaussian curve (with maximum enhancement of a factor of 2.5 revealed by analysis of SOHO/CST data) coupled with changes of $K_{\perp\theta}$ with increasing solar activity in an attempt to fit the 3 -10 MeV observations. This has improved model compatibility with the observations for the period mid-1998 to mid-1999. A much greater increases in Q was required to fit the observations after this period, a condition considered not realistic according to the SOHO/CST electron observations. This led to the conclusion that the Ulysses electron observations represent a picture of a very complicated interplay of several modulation parameters for solar maximum activity. The complexity of solar modulation at maximum activity, especially for these low energies electrons where a solar contribution is likely, has made the applicability of a steady-state approach unsatisfactory. It is therefore beyond the scope of this work to further improve the model's compatibility with observations and must be left for time-dependent models with a more sophisticated handling of the various modulation parameters.

The effects of the assumed d scenarios were also illustrated on low energy electron modulation at 1 AU and 5 AU respectively. It was found that for galactic electrons the effects of different d scenarios are significant in the polar regions and in the equatorial plane at both radial distances, while for Jovian electrons the effects are about a factor of ~ 2 between the $d = 6$ scenario and $d = 1$ scenario at 1 AU in the equatorial plane. Although drifts effects are not important for low energy (< 200 MeV) electrons, it was shown that for high energy drifts effects are essential to compute realistic electron modulation. This was done only for the $A > 0$

magnetic polarity cycle.

A case study was conducted to find suitable diffusion coefficients for modulation of low-energy galactic electrons for the assumed different d scenarios especially at the heliospheric equatorial region. It was found that electron intensities computed in the polar regions with $d = 1$ are about a factor of ~ 2 larger than for the $d = 6$ scenario. There were almost no differences in the intensities computed for all d scenarios in the equatorial region. It was also argued that if the factor of ~ 2 increase in the electron intensities (3 - 10 MeV) observed in the heliospheric polar regions as solar activity picks up, could be interpreted as a contribution from galactic electrons, then this study will have important consequences to the transport and modulation of these low-energy electrons in the inner heliosphere. Alternatively, this increase could be caused by a contribution from solar electrons, which was ruled out by Heber et al. (2003b) based on the spectral forms of these electrons.

Effects of different d scenarios were also illustrated on the latitudinal dependence of both Jovian and galactic electron intensities at 1 AU and 5 AU. It was found that Jovian electron intensities are about a factor of $\sim$2 larger at 1 AU in the equatorial plane for $d = 1$ scenario than for $d = 6$ scenario. It was also evident that the Jovian electron intensities have a strong latitudinal dependence near the source. For galactic electron intensities, it was found that there is a factor of (1.5 ± 0.5) difference between $d = 6$ and $d = 1$ near the poles, both at 1 AU and 5 AU. It was also shown that these electrons have a small and negative latitudinal gradients from $\theta = 10^0$ to $\theta = 90^0$ in the inner heliosphere as found by Potgieter et al. (1997).

Effects of different d scenarios were also illustrated on the radial dependence of both Jovian and galactic electron intensities in the inner heliosphere at $\theta = 10^0$, $\theta = 60^0$, $\theta = 90^0$, respectively. For galactic electron intensities these effects were significant in heliospheric polar regions where galactic intensities dominate Jovian electrons intensities. Effects on Jovian electrons at ~ 1 AU are found to be more pronounced between the $d = 1$ and the $d = 6$ scenarios.

Out of the results of this study, it is concluded that these low-energy electrons are mainly modulated by diffusion and convection, with adiabatic energy losses less important and drifts insignificant.

The next Chapter gives a brief summary of the thesis and the main conclusions of this work.

Chapter 8

Summary and conclusions

After introducing the study of modelling of galactic and Jovian electrons in the heliosphere in **Chapter 1**, a brief overview was given in **Chapter 2** of the cosmic rays and the heliosphere. This covered short discussions about the Sun and the solar wind plasma, the heliosphere, the heliospheric magnetic field and the current sheet and the solar cycle variations. Discussion was also given about the successes of the Ulysses space mission together with the KET and SWOOPS instruments which provided the electron and solar wind speed data used in this study.

In **Chapter 3**, a short overview of the propagation and modulation of low energy electrons (3 - 10 MeV) in the inner heliosphere was given, with the main emphasis on Jovian electrons. This included the sources contributing to the few-MeV electron intensities in the inner heliosphere, an overview of Jovian electron propagation and modulation models, and a brief discussion on the observed modulation and spectra of Jovian electrons.

A brief discussion was given in **Chapter 4** on the well known Parker transport equation and the transport processes applicable to the modulation of cosmic rays. The 3D Jovian electron modulation model and the numerical implementation thereof were also discussed including the Jovian source function, and the electron LIS.

In **Chapter 5**, a theoretical background was given on certain aspects of the heliospheric diffusion tensor, and further investigation on the spatial and rigidity dependence of the important elements of the tensor applicable to low-energy electron modulation (e.g., Ferreira 2002) as revealed by the Ulysses spacecraft (e.g., Heber et al., 2001a,b) during solar minimum conditions. Some elements of the tensor such as the effective diffusion in the azimuthal direction ($K_{\phi\phi}$)

and the diffusion coefficient in the $r\phi$ direction ($K_{r\phi}$), which were mostly neglected in previous studies due to the limitations imposed by 2D modulation models, were also investigated in this Chapter. In particular, it was emphasized that:

- K_{rr} which is dominated in the equatorial plane by $K_{\parallel}\cos^2\psi$ in the inner heliosphere and by $K_{\perp r}\sin^2\psi$ in the outer heliosphere is also an important modulation parameter in the heliospheric polar regions, while $K_{\phi\phi}$, which is dominated by $K_{\parallel}\sin^2\psi$ throughout most of the heliosphere, is an essential modulation parameter in the heliospheric equatorial plane.

- The rigidity dependence of $K_{\phi\phi}$ and K_{rr} is a function of radial distance and is assumingly determined by the rigidity dependence of $K_{\parallel}$. It was also suggested that the rigidity dependence has to be revised as progress on the theory of $K_{\perp}$ is made (see Matthaeus et al., 2003; Minnie et al., 2003a,b; Schalchi et al., 2004; Bieber et al., 2004).

- $K_{\phi\phi}$ should play an important role in the inner heliosphere concerning the modulation of Jovian electrons. The DCs $K_{\phi r}$ and $K_{r\phi}$ are essentially "correction" terms to the distribution of CRs as determined by K_{rr} and $K_{\phi\phi}$, together with $K_{\theta\theta}$ which is usually significantly modified by assuming it to be enhanced toward the poles.

The solar wind plasma speed modulation parameters α^* and β^* (see Equation (6.1)) were introduced in **Chapter 6** to generalise the solar wind speed model to simulate different solar wind profiles applicable to changing heliospheric conditions. Four profiles were used and classified as shown in Figure 6-1. Effects of these four assumed V profiles on the distribution of 7 MeV Jovian and galactic electrons in the inner heliosphere were computed using a 3D steady-state modulation model (Ferreira, 2002) and were illustrated as surface contour plots in the equatorial plane. It was found that:

- Jovian electron modulation mainly follows the HMF spiral, due to the $K_{\parallel}\sin^2\psi$ which dominates $K_{\phi\phi}$ in the inner heliospheric equatorial plane, but they are also transported across the HMF field lines to some lesser extent due to $K_{\perp r}$.

- If V changes from a profile applicable to a solar minimum to one for solar maximum, the

spiral angle ψ of the HMF becomes tightly wound and the distribution of Jovian electrons follows the same trend.

The effects of the assumed V profiles on the radial and latitudinal dependence of Jovian and galactic electron intensities were also computed at different latitudes. Referring also to Ferreira et al. (2002), it was found that:

- Jovian electron intensity dominates the galactic contribution in the equatorial plane up to $\sim$ 10 AU, while the galactic contribution dominates for $r \geq 10$ AU in the equatorial plane and in the heliospheric polar regions for all the assumed V profiles.
- When V changes from a scenario applicable to the solar minimum to the one for solar maximum, it produces a larger value for $K_{\perp\theta}/K_{rr}$, implying that the latitudinal transport with respect to radial transport becomes more effective, resulting in relatively more particles transported towards the poles from a point source such as the Jovian magnetosphere.
- The azimuthal transport of Jovian electrons diminishes toward the heliospheric polar regions, when the value of $K_{rr}/K_{\phi\phi} > 1$, resulting in the dominance of galactic electron intensities (isotropic source).
- The transport and distribution of Jovian electrons in the inner heliosphere is truly three-dimensional and cannot be adequately be described by 2D models.

The combined Jovian and galactic electron intensities were computed along the Ulysses trajectory for the different assumptions of V and compared to the $3-10$ MeV electrons observed by the KET aboard the spacecraft during solar minimum activity. It was found that:

- The model solutions obtained for a typical solar minimum and for a typical solar maximum profile were not much different and provide a good compatibility with the observations up to 1998 while other solutions are not preferable.
- The solar minimum V profile inhibits Jovian electrons from reaching high latitudes (Ferreira et al., 2003a,b) so that galactic electrons dominate.

- All model intensities after 1998 are significantly less than the KET observations, which led to the conclusion that the solar wind speed changes relating to changing heliospheric conditions *alone*, could not produce realistic compatibility with data towards solar maximum conditions, although it did rather well for solar minimum conditions. This emphasized a need for time-dependent diffusion coefficients, especially for the latitudinal transport as argued by Ferreira et al. (2003a,b).

In **Chapter 7**, a new relation was established between the latitudinal dependence of the solar wind speed and heliospheric polar diffusion to enable improved modelling of these parameters with changing heliospheric conditions. The transition from solar minimum to solar maximum of the heliospheric polar diffusion and the solar wind speed were modelled based on the assumption of the time evolution of polar coronal holes and compared to the solar wind speed observations (e.g., McComas et al., 2002b) made by the SWOOPS instrument aboard the Ulysses spacecraft. The concept of a critical angle φ in the latitudinal dependence of V (see Figure 7-2) was also introduced together with other important solar wind speed related parameters. The 3D electron modulation model, together with invoking different d scenarios for the enhancement of $K_{\perp\theta}$ in the polar direction assumed to correlate to different V profiles as shown in Figure 7-2 were used to compute a series of steady-state solutions for the electron intensities along the Ulysses trajectory and compared to the 3 - 10 MeV KET observations (e.g., Heber et al., 2003a,b) after 1998. It was found that:

- The solution for the d scenario assumed for solar minimum could produce compatibility with the KET observations during the short period just after 2002 when the Sun was relatively inactive. This confirmed the suitability of the model for periods of minimum to moderate solar activity.

- The solution for the d scenario assumed for intermediate solar activity produced an improved compatibility to the observations for the period from mid-1998 to mid-2000.

- All solutions converge and increase uniformly towards the end of 2003 as expected because it was the time when Ulysses was again approaching the Jovian electron source.

- These steady-state solutions are not adequate to account for the entire solar maximum

period of KET observations, but give an indication as to how the heliospheric polar diffusion and the solar wind speed profiles could be changing during solar maximum conditions.

Also discussed is how Henize et al. (2003) varied the strength of the Jovian electron source Q by fitting a gaussian curve (with maximum enhancement of a factor of 2.5 revealed by an analysis of SOHO/CST data) coupled with changes of $K_{\perp\theta}$ with increasing solar activity in an attempt to represent the $3 - 10$ MeV observations. This has improved model compatibility with the observations for the period from mid-1998 to mid-1999. A much greater increasing Q would be required to fit the observations after this period, a condition considered not realistic according to SOHO/CST electron observations. This led to the important conclusion that:

- The Ulysses electron observations represent a picture of a very complicated interplay of several modulation parameters for solar maximum activity. The complexity of solar modulation at maximum activity, especially for these low energy electrons where a solar contribution is likely, has made the applicability of a steady-state approach unsatisfactory. It is therefore beyond the scope of this work to further improve the model's compatibility with observations and must be left for time-dependent models with a more sophisticated handling of the various parameters.

The effects of the assumed d scenarios for the enhancement of $K_{\perp\theta}$ were also illustrated on low-energy electron spectra at 1 AU and 5 AU respectively. It was found that:

- When d changes from a scenario assumed for solar minimum to one for solar maximum there is an improbably large increase in the galactic electron intensities in the heliospheric polar regions, while for Jovian electrons there is a realistic factor of ~ 2 increase for this situation, in line with KET observations.

- Although drifts are not important for low energy (< 200 MeV) electrons, it was shown that at high energies, drifts are essential to compute realistic electron modulation. This was done only for the $A > 0$ magnetic polarity cycle. In order to establish compatibility with observations at high energies, drifts effects had to be reduced with increasing solar activity. (See also Ferreira and Potgieter, 2004a,b).

Because of the above-mentioned large increase in galactic electron intensities in the polar regions as a result of changes in the d scenarios towards solar maximum conditions, a case study was conducted to find suitable diffusion coefficients for modulation of low-energy galactic electrons. This was done as a modelling exercise by selecting a set of diffusion coefficients, particularly the ratios $K_{\perp\theta}/K_{\parallel}$ and $K_{\perp r}/K_{\parallel}$ for the respective d scenarios (see Figure (7-9) and (7-10)). It was found that:

- The galactic electron intensities computed in the polar regions with a d scenario assumed for solar maximum reduced to be a factor of ~ 2 larger than for the d scenario assumed for solar minimum conditions. There was almost no difference in the galactic electron intensities computed for all d scenarios in the equatorial plane.

It was also argued that if the factor of ~ 2 increase in the electron intensities (3 - 10 MeV) observed in the heliospheric polar regions by the KET instrument (Heber et al., 2003) as solar activity picked up from solar minimum to solar maximum conditions, could be interpreted as a contribution from galactic electrons, then this study will have important consequences to the transport and modulation of these low energy electrons in the inner heliosphere. Alternatively, this increase could be caused by a contribution from solar electrons, however, this was ruled out by Heber et al. (2002b) based on the spectral forms of these electrons.

Effects of different d scenarios were also illustrated on the latitudinal dependence of both Jovian and galactic electron intensities at 1 AU and 5 AU. It was found that:

- Jovian electron intensities are a factor of $\sim$2 higher at 1 AU in the polar regions for the d scenario assumed for solar maximum than for the d scenario assumed to represent solar minimum conditions.

- The Jovian electron intensities have a strong latitudinal dependence towards and away from the source.

- For galactic electron intensities, there is a factor of (1.5 ± 0.5) difference between d assumed for solar minimum and d assumed for solar maximum near the heliospheric poles at 1 AU and 5 AU.

- Galactic electrons have small and negative latitudinal gradients from $\theta = 10^0$ to $\theta = 90^0$ in the inner heliosphere as found by Potgieter et al. (1997).

Effects of different d scenarios were also illustrated on the radial dependence of both Jovian and galactic electron intensities in the inner heliosphere at $\theta = 10^0$, $\theta = 60^0$, and $\theta = 90^0$ respectively. For galactic electron intensities these effects were significant in the heliospheric polar regions where they dominate the Jovian electron intensities. Effects on Jovian electrons intensities at ~ 1 AU are found to be more pronounced between the d scenario assumed for solar maximum and the d scenario assumed for solar minimum conditions. Out of these results, it is concluded that:

- The study of diffusion coefficients such as $K_{r\phi}$ and $K_{\phi\phi}$, which were neglected in the previous 2D modulation studies, has improved our understanding of diffusive propagation of low-energy electrons in the inner heliosphere, in particular related to the ratio $K_{\perp\theta}/K_{rr}$.

- The concept of the time evolution of polar coronal holes for modelling the latitudinal dependence of the average solar wind speed with varying heliospheric conditions has improved our understanding of the role of this parameter in the modulation models and it seems to be a good approximation.

- Establishment of a relation between the latitudinal dependence of the solar wind speed and the heliospheric polar diffusion has improved modelling of the post-1998 discrepancy between the modulation model and KET observations.

- The low-energy electrons (< 200 MeV) are mainly modulated by diffusion and convection, with adiabatic energy losses less important and drifts insignificant.

- There is a need for the application of a true time-dependent 3D electron modulation model.

For future studies the following can be mentioned:

- A 3D time-dependent electron model is required to realistically fit the observed 3 - 10 MeV electron observations by KET for solar maximum modulation conditions.

- Jovian magnetospheric studies are required to fully understand the solar cycle variation of the electron source and to account for the Jovian bursts or jets observed during the two different fly-by periods of Jupiter by the Ulysses spacecraft.
- Effects of CIRs on low-energy electron modulation. These aspects have in fact been recently investigated (Kissmann et al., 2004).
- Adiabatic deceleration of electrons in the inner heliosphere (Moses, 1987)

References

1) Baker, D. N., and J. A. Van Allen, Energetic electrons in the Jovian magnetosphere, *J. Geophys. Res.*, **81**, 617, 1976.

2) Balogh, A., E. J. Smith, B. T. Tsurutani, D. J. Southwood, R. J. Forsyth, and T. S. Horbury, The heliospheric magnetic field over the south polar region of the Sun, *Science*, **268(5213)**, 1007, 1995.

3) Bieber, J. W., and W. H. Matthaeus, Cosmic ray pitch angle scattering in dynamical magnetic turbulence, *Proc. 22nd Inter. Cosmic Ray Conf., Dublin*, **3**, 248,1991.

4) Bieber, J. W., W. H. Matthaeus, and A. Schalchi, Nonlinear guiding center theory of perpendicular diffusion: General properties and comparison with observation, *Geophys. Res. Lett.*, **31(L10805)**, 2004.

5) Bieber, J. W., W. H. Matthaeus, C. W. Smith, W. Wanner, M-B. Kallenrode, and G. Wibberenz, Proton and electron mean free paths: The Palmer consensus revisited, *Astrophys. J.*, **420(1)**, 294, 1994.

6) Biermann, L., Kometenschwiefe und solare korpuskularstrahlung, *Zeit. Astrophys.*,**29**, 274, 1951.

7) Biermann, L., The solar wind and the interplanetary media, *In Space Astrophys.*, edited by W. Liller, McGraw-Hill, *New York*, 150, 1961.

8) Bravo, S., J. A. L. Cruz-Abeyro, The 22-yr modulation of galactic cosmic rays and its relation to coronal holes, *Geophys. Res. Lett.*, **23(6)**, 613, 1996.

9) Burger, R. A., On the theory and application of drift motion of charged particles in inhomogeneous magnetic fields, *Ph.D. thesis, Potchefstroom University for CHE, South Africa*, 1987.

10) Burger, R. A., and M. Hattingh, Effect of Fisk-type heliospheric magnetic fields on the latitudinal transport of cosmic rays, *Proc. 27th Inter. Cosmic Ray Conf., Hamburg*, **9**, 3698, 2001.

11) Burger, R. A., M. S. Potgieter, and B. Heber, Rigidity dependence of cosmic-ray proton latitudinal gradients measured by the Ulysses spacecraft: Implications for the diffusion tensor, *J. Geophys. Res.*, **105(A12)**, 27447, 2000.

12) Chenette, D. L., T. F. Conlon, K. R. Pyle, and J. A. Simpson, Observations of Jovian electrons at 1 AU throughout the 13 month Jovian synodic, *Astrophys. J.*, **215**, L95, 1977.

13) Chenette, D. L., T. F. Conlon, K. R. Pyle, and J. A. Simpson, Jupiter's magnetosphere as a point source for electrons propagating from 1AU to 12AU, *Proc. of 15th Inter. Cosmic Ray Conf.., Plovdiv, Bulgaria*, 1978.

14) Chenette, D. L., T. F. Conlon, and J. A. Simpson, Bursts of relativistic electrons from Jupiter observed in interplanetary space with the time variation of the planetary rotation period, *J. Geophys. Res.*, **79**, 3551, 1974.

15) Gleeson, L. J., and Axford, The modulation of galactic cosmic rays, *Astrophys. J. Lett.*, **149**, L115, 1967.

16) Gleeson, L. J., and W. I. Axford, The compton-getting effect, *Astrophys. and Space Science*, **2**, 431, 1968.

17) Conlon, T. F., The interplanetary modulation and transport of Jovian electrons, *J. Geophys. Res.*, **83**, 541, 1978.

18) Conlon, T. F., and J. A. Simpson, Modulation of Jovian electron intensity in interplanetary space by co rotating interaction regions, *Astrophys. J.*, **211**, L45, 1977.

19) del Peral, L., R. Gómez-Herrero, M. D. Rodríguez-Frías, J. Gutiérrez, Müller-mellin, H. Kunow, Jovian electrons in the heliosphere: new insights from EPHIN on board SOHO, *Astroparticle Physics.*, **20**, 235, 2003.

20) Douglas, J., On the numerical integration of $((\partial^2 u)/(\partial x^2))+((\partial^2 u)/(\partial y^2))=((\partial u)/(\partial t))$ by implicit methods, *J. Soc. Indust. Appl. Math.*, **3**, 42, 1955.

21) Douglas, J., Alternating direction implicit methods for three space variables, *Numerische Mathematik*, **4**, 417, 1962.

22) Dröge, W., Particle scattering by magnetic fields, *Space Science Reviews*, **93(1/2)**, 121, 2000.

23) Eraker, J. H., Origins of the low-energy relativistic interplanetary electrons, *Astrophys. J.*, **257(1)**, 862, 1982.

24) Eraker, J. H., and J. A. Simpson, Jovian electron propagation close to the Sun (< 0.5 AU), *Astrophys. J.*, **232(2)**, L131, 1979.

25) Fahr, H. J., A 5-fluid hydrodynamic approach to model the solar system interstellar medium interaction, *Astron. Astrophys.*, **357**, 268, 2000.

26) Ferrando, P., MeV to GeV electron propagation and modulation: Results of the KET-telescope onboard Ulysses, *Adv. Space Res.*, **19(6)**, 905, 1997.

27) Ferrando, P., R. Ducros, C. Rastoin, and A. Raviart, Jovian electron jets in interplanetary space, *Plan. and Space Science*, **41**, 839, 1993a.

28) Ferrando, P., R. Ducros, C. Rastoin, A. Raviart, H. Kunow, R. Müeller-Mellin, H. Sierks, and G. Wibberenz, Propagation of Jovian electrons in and out of the ecliptic, *Adv. Space Res.*, **13(6)**, 107, 1993b.

29) Ferrando, P., R. Müller-Mellin, H. Sierks, G. Wibberenz, A. Raviart, R. Ducros, and L. Treguer, The Kiel electron telescope onboard Ulysses, *Proc. of the 22nd Inter. Cosmic Ray Conf., Dublin*, **3**, 366, 1991.

30) Ferrando, P., A. Raviart, L. J. Haasbroek, M. S. Potgieter, W. Dröge, B. Heber, H. Kunow, R. Müeller-Mellin, H. Sierks, G. Wibberenz, and C. Paizis, Latitude variations of ~ 7 MeV and >300 MeV cosmic ray electron fluxes in the heliosphere: Ulysses COSPIN/KET results and implications, *Astron. and Astrophys.*, **316**, 528, 1996.

31) Ferrando, P., A. Raviart, B. Heber, V. Bothmer, H. Kunow, R. Müeller-Mellin, and C. Paizis, Observation of a ~ 7 MeV electron super-flux at 5 AU by Ulysses, *Proc. 26th Inter. Cosmic Ray Conf., Salt Lake City,* 7, 135, 1999.

32) Ferreira, S. E. S., A study of the modulation of cosmic ray electrons in the heliosphere, *M.Sc. dissertation., Potchefstroom University for CHE, South Africa*, 1998.

33) Ferreira. S. E. S., The heliospheric transport of galactic cosmic rays and Jovian electrons, *Ph.D. thesis., Potchefstroom University for CHE, South Africa*, 2002.

34) Ferreira, S. E. S., and M. S. Potgieter, Effects of anisotropic perpendicular diffusion on the energy and spatial dependence of galactic electron intensities in the heliosphere, *Proc. of the 26th Inter. Cosmic Ray Conf., Salt lake*, 7, 25, 1999a.

35) Ferreira, S. E. S., and M. S. Potgieter, The modulation of 4- to 16-MeV electrons in the outer heliosphere: Implications of different local interstellar spectra, *J. Geophys. Res.*, **107(A8)**, SSH12-1, 2002.

36) Ferreira, S. E. S., and M. S. Potgieter, Galactic cosmic rays in the heliosphere, *Adv. Space Res.*, **34**, 115, 2004a.

37) Ferreira, S. E. S., and M. S. Potgieter, Long-term cosmic ray modulation in the heliosphere, *Astrophys. J.*, 603, 744, 2004b.

38) Ferreira, S. E. S., M. S. Potgieter, R. A. Burger, and B. Heber, Modulation effects of anisotropic perpendicular diffusion on cosmic ray electron intensities in the heliosphere, *J. Geophys. Res.*, **105(A8)**, 18305, 2000.

39) Ferreira, S. E. S., M. S. Potgieter, R. A. Burger, B. Heber, and H. Fichtner, Modulation of Jovian and galactic electrons in the heliosphere 1. Latitudinal transport of a few MeV electrons, *J. Geophys. Res.*, **106(A11)**, 24979, 2001a.

40) Ferreira, S. E. S., M. S. Potgieter, R. A. Burger, B. Heber, H. Fichtner, and C. Lopate, Modulation of Jovian and galactic electrons in the heliosphere: 2. Radial transport of a few MeV electrons, *J. Geophys. Res.*, **106(A12)**, 29313, 2001b.

41) Ferreira, S. E. S., M. S. Potgieter, B. Heber, H. Fichtner, and R. A. Burger, Latitudinal transport of 7 MeV Jovian and galactic electrons, *Proc. 27th Inter. Cosmic Ray Conf.*, Hamburg, **8**, 3702, 2001c.

42) Ferreira, S. E. S., M. S. Potgieter, B. Heber, H. Fichtner, R. A. Burger, and P. Ferrando, A study of the compatibility between observations and model simulations for Jovian and galactic electrons, *Adv. Space Res.*, **27(3)**, 553, 2001d.

43) Ferreira, S. E. S., M. S. Potgieter, B. Heber, H. Fichtner, and R. Kissmann, Transport of few MeV Jovian and galactic electrons at solar maximum, *Adv. Space Res.*, **32**, 669, 2003c.

44) Ferreira, S. E. S., M. S. Potgieter, B. Heber, H. Fichtner, and G. Wibberenz, Latitudinal transport effects on the modulation of a few MeV cosmic ray electrons from solar minimum to solar maximum, *J. Geophys. Res.*, **109**, A02115, 2004c.

45) Ferreira, S. E. S., M. S. Potgieter, and D. M. Moeketsi, Modulation effects of changing solar wind speed on low-energy electrons, *Adv. Space Res.*, **32(4)**, 645, 2003a.

46) Ferreira, S. E. S., M. S. Potgieter, D. M. Moeketsi, B. Heber, and H. Fichtner, Solar wind effects on the transport of 3 –10 MeV cosmic ray electrons from solar minimum to solar maximum, *Astrophys. J.*, **594**, 552, 2003b.

47) Fichtner, H., Anomalous cosmic rays: Messengers from the outer heliosphere, *Space Science Reviews*, **95(3/4)**, 639, 2001a.

48) Fichtner, H., M. S. Potgieter, S. E. S. Ferreira, and R. A. Burger, On the propagation of Jovian electrons in the heliosphere: transport modelling in 4-D phase space, *Geophys. Res. Lett.*, **27(11)**, 1611, 2000b.

49) Fichtner, H., M. S. Potgieter, S. E. S. Ferreira, and B. Heber, Time-dependent 3D modelling of the heliospheric propagation of few-MeV electrons, *Proc. 27th Inter. Cosmic Ray Conf., Hamburg*, **8**, 3666, 2001b.

50) Fichtner, H., and K. Scherer, The heliosphere: A brief overview, in the outer heliosphere: Beyond the planets, edited by K. Scherer, H. Fichtner, and E. Marsch, *Copernicus Gesellschaft, Katlenburg-Lindau*, **1**, 2000a.

51) Fisk, L. A., Motion of the footpoints of heliospheric magnetic field lines at the Sun: Implications for recurrent energetic particle events at high heliographic latitudes, *J. Geophys. Res.*, **101(A7)**, 15547, 1996.

52) Fisk, L. A., B. Koslovsky, and R. Ramaty, An interpretation of the observed oxygen and nitrogen enhancements in low energy cosmic rays, *Astrophys. J. Letters*, **190**, L35, 1974.

53) Forbush, E., Three unusual cosmic ray increases probably due to charged particles from the Sun, *Physical Review*, **70**, 771, 1946.

54) Gazis, P. R., A. Barnes, J. D. Mihalov, and A. J. Lazarus, The structure of the inner heliosphere from Pioneer, Venus and IMP observations, in solar wind, edited by E. Marsch and R. Schwenn, *Pergamon Press., New-York*, 183, 1991.

55) Gazis, P. R., A. Barnes, J. D. Mihalov, and A. J. Lazarus, Solar wind velocity and temperature in the outer heliosphere, *J. Geophys. Res.*, **99**, 6561, 1994.

56) Garcia-Munoz, M., G. M. Mason, and J. A. Simpson, The abundance of galactic cosmic ray carbon, nitrogen, and oxygen and their astrophysical implications, *Astrophys. J.*, **184**, 967, 1973.

57) Giacalone, J., and J. R. Jokipii, The transport of cosmic rays across a turbulent magnetic field, *Astrophys. J.*, **520(1)**, 204, 1999.

58) Haasbroek, L. J., Modulation of cosmic rays in the heliosphere: A model study for the Ulysses mission (in Afrikaans), *M.Sc. dissertation, Potchefstroom University for CHE, South Africa,* 1993.

59) Haasbroek, L. J., The transport and acceleration of charged particles in the heliosphere, *Ph.D thesis, Potchefstroom University for CHE, South Africa,* 1997.

60) Haasbroek, L. J., M. S. Potgieter, and J. A. le Roux, Acceleration of galactic and Jovian electrons at the heliospheric solar wind termination shock, *Adv. Space Res.*, **19(6)**, 953, 1997a.

61) Haasbroek, L. J., M. S. Potgieter, and J. A. le Roux, Some modulation effects of termination shock accelerated galactic and Jovian electrons, *Proc. 25th Inter. Cosmic Ray Conf., Durban,* **2**, 29, 1997b.

62) Hamilton, D. C., and J. A. Simpson, Jovian electron propagation out of the solar equatorial plane - Pioneer 11 observations, *Astrophys. J.*, **228(2)**, L123, 1979.

63) Hattingh, M., Drift of cosmic rays at a wavy neutral sheet in the heliosphere (in Afrikaans), *M.Sc. dissertation, Potchefstroom University for CHE, South Africa,* 1993.

64) Hattingh, M., The modulation of galactic cosmic rays in a three-dimensional heliosphere, *Ph.D thesis, Potchefstroom University for CHE, South Africa,* 1998.

65) Heber, B., Modulation and propagation of cosmic rays in the inner three-dimensional heliosphere: Ulysses observations, *habilitation study, Universität Osnabrück, Germany,* 2002.

66) Heber, B., J. M. Clem, R. Müller-Mellon, H. Kunow, S. E. S. Ferreira, and M. S. Potgieter, Evolution of the galactic cosmic ray electron to proton ratio: Ulysses COSPIN/KET observations, *Geophys. Res. Lett.*, **30(19)**, 2003c.

67) Heber B., P. Ferrando, A. Raviart, C. Paizis, R. Müller-Mellin, and H. Kunow, Propagation of 3 - 10 MeV electrons in the inner heliosphere: Ulysses observations, *Adv. Space Res.*, **27(3)**, 547, 2001a.

68) Heber B., P. Ferrando, A. Raviart, C. Paizis, G. Sarri, A. Posner, G. Wibberenz, R. Müller-Mellin, H. Kunow, M. S. Potgieter, S. E. S. Ferreira, R. A. Burger, and H. Fichtner, Quite-time MeV electron increases at solar maximum: Ulysses COSPIN/KET observations, *Adv. Space Res.*, **32**, 663, 2003a.

69) Heber, B., S. E. S. Ferreira, H. Fichtner, M. S. Potgieter, V. K. Henize, R. Kissmann, and D. M. Moeketsi, Out-of-ecliptic quiet time MeV electron increases: Ulysses COSPIN/KET observations, *American Institute of Physics Conference Series,* **703**, 157, 2004.

70) Heber B., H. Fichtner, R. Kissmann, M. S. Potgieter, S. E. S. Ferreira, Quiet-time MeV electron increases at solar maximum: Ulysses COSPIN/KET observations, *Astronomosche Nacherichten,* **324**, 87, 2003b.

71) Heber, B., and R. G. Marsden, Cosmic Ray Modulation over the poles at solar maximum: Observations, *Space Science Reviews,* **97**, 309, 2001b.

72) Heber, B., M. S. Potgieter, and P. Ferrando, Solar modulation of galactic cosmic rays: The 3D heliosphere, *Adv. Space Res.,* **19(5)**, 795, 1997.

73) Heber, B., G. Wibberenz, M. S. Potgieter, R. A. Burger, S. E. S. Ferreira, R. Müller-Mellon, H. Kunow, P.Ferrando, A. Raviart, C. Paizis, C. Lopate, F. B. McDonald, and H. V. Cane, Ulysses Cosmic Ray and Solar Particle Investigation/Kiel Electron Telescope observations: Charge sign dependence and spatial gradients during the 1990-2000 A > 0 solar magnetic cycle, *J. Geophys. Res.,* **107(A10)**, 2002.

74) Henize, V. K., M. S. Potgieter, and S. E. S. Ferreira, Modeling a few – MeV Jovian and galactic spectra in the inner heliosphere, *Proc. 28th Inter. Cosmic Ray Conf., Tsubuka,* 3819, 2003.

75) Hess, V. F., *Physikal. Zeits.,* **13**, 1084, 1912.

76) Hoeksema, J. T., Large scale structure of the heliospheric magnetic field: 1976 – 1991, In Marsh, E. and R. Schwenn eds. Solar wind seven. *Pergamon press, New York,*191, 1992.

77) Hu, Y. Q., S. R. Habbal, Y, Chen, and X. Li, Are coronal holes the only source of fast solar wind at solar maximum? *J. Geophys. Res.,* **108(A10)**, SSH8-1, 2003

78) Hundhausen, A. J., An interplanetary view of coronal holes, in coronal holes and high speed streams, edited by J. B. Zirker, *Colorado Associated Univ. Press, Colorado,* 114, 1977.

79) Jokipii, J. R., and J. Kóta, The polar heliospheric magnetic field, *Geophys. Res. Lett.,* **16**, 1, 1989.

80) Jokipii, J. R., and J. Kóta, On the interpretation of the high cosmic-ray electron fluxes observed in 1986, *Proc. 22nd Inter. Cosmic Ray Conf., Dublin,* **3**, 569, 1991.

81) Jokipii, J. R., and J. Kóta, The maximum energy of anomalous cosmic rays, *Proc. of the 24th Inter. Cosmic Ray Conf., Rome,* **4**, 718, 1995.

82) Jokipii, J. R., E. H. Levy, and W. B. Hubbard, Effects of particle drift on cosmic ray transport. I - General properties, application to solar modulation, *Astrophys. J.,* **213**, 861, 1977.

83) Jokipii, J. R., and E. N. Parker, On the convection, diffusion and adiabatic deceleration of cosmic rays in the solar wind, *Astrophys. J.,* **160**, 735, 1970.

84) Jokipii, J. R., and B. Thomas, Effects of drift on the transport of cosmic rays. IV - Modulation by a wavy interplanetary current sheet, *Astrophys. J.,* **243**, 1115, 1981.

85) Jones, F. C., and D. C. Ellison, The plasma physics of shock acceleration, *Space Science Reviews,* **58(3-4)**, 259, 1991.

86) Kanekal, S. G., D. N. Baker, J. B. Blake, M. D. Looper, R. A. Mewaldt, and C. A. Lopate, Modulation of Jovian electrons at 1 AU during solar cycles 22 – 23, *Geophys. Res. Lett.,* **30**, SSC1, 2003.

87) Kissmann, R., H. Fichtner, and Ferreira, The influence of CIRs on the energetic electron flux at 1 AU, *Astron. and Astrophys.*, **419**, 357, 2004.

88) Kojima, M., H. Washmimi, H. Misawa, and K. Hakamada, Solar wind observed within 0.3 AU with interplanetary scintillation, in solar wind, edited by E. Marsch, and R. Schwenn, *Pergamon Press, New York*, 201, 1991.

89) Kóta, J., and J. R. Jokipii, Effects of drift on the transport of cosmic rays. VI - A three-dimensional model including diffusion, *Astrophys. J.*, **265**, 573, 1983.

90) Kóta, J., and J. R. Jokipii, 3-D simulation of heliospheric transport: A comparison of models, *Proc. 25th Inter. Cosmic Ray Conf., Durban*, **2**, 25, 1997.

91) Kóta, J., and J. R. Jokipii, Cosmic ray modulation and the structure of the heliospheric magnetic field, *Proc. 26th Inter. Cosmic Ray Conf., Salt Lake City*, **7**, 9, 1999.

92) Koyama, K., R. Petre, E. V. Gotthelf, U. Hwang, M. Matsuura, M. Ozaki, and S. S. Holt, Evidence for shock acceleration of high-energy electrons in the supernova remnant SN: 1006, *Nature*, **378(6554/NOV16)**, 255, 1995.

93) Krieger, A. S., A. F. Timothy, and E. C. Roelof, A coronal hole and its identification as the source of a high velocity solar wind stream, *Solar Physics*, **29**, 505, 1973.

94) Krimigis, S. M., R. B. Decker, E. C. Roelof, and D. Lario, Energetic particle intensity increases at Voyagers 1 and 2 during 2002-03, *Proc. 28th Inter. Cosmic Ray Conf., Tsukuba*, 3769, 2003.

95) Langner, U. W., Effects of different local interstellar spectra on the heliospheric modulation of cosmic rays, *M.Sc. dissertation, Potchefstroom University for CHE, South Africa*, 2000.

96) Langner, U. W., Effects of termination shock acceleration on cosmic rays in the heliosphere, *PH.D Thesis, Potchefstroom University for CHE, South Africa*, 2004.

97) Langner, U. W., O. C. de Jager, and M. S. Potgieter, Proposed local interstellar spectra for cosmic ray electrons, *Proc. 27th Inter. Cosmic Ray Conf., Hamburg*, **4**, 3992, 2001a.

98) Langner, U. W., O. C. de Jager, and M. S. Potgieter, On the local interstellar spectrum for cosmic ray electrons, *Adv. Space Res.*, **27(3)**, 517, 2001b.

99) Langner, U. W., and M. S. Potgieter, Heliospheric modulation of cosmic rays computed with new local interstellar spectra, *Proc. 27th Inter. Cosmic Ray Conf., Hamburg*, **4**, 3686, 2001c.

100) Lapidus, L., and G. F. Pinder, Numerical solution of partial differential equations in science and engineering, *Wiley, New York*, 1982.

101) Le Roux, J. A., G. P. Zank, and V. S. Ptuskin, An evaluation of perpendicular diffusion models regarding cosmic ray modulation on the basis of a hydromagnetic description for solar wind turbulence, *J. Geophys. Res.*, **104**, 14845, 1999.

102) L'Heureux, J., and P. Meyer, Quite-time increases of low-energy electrons: The Jovian origin, *Astrophys. J.*, **209**, 995, 1976.

103) Longair, M. S., Cosmic rays and the Galactic radio background emission, in Low Frequency Astrophysics from Space, *Springer-Verlag,* 227, 1990.

104) Lopate, C., Jovian and galactic electrons (2-30 GeV) in the heliosphere from 1 to 50 AU, Proc. 23rd Inter. *Cosmic Ray Conf., Calgary,* **3**, 415, 1991.

105) Marsch, E., Kinetic physics of the solar wind plasma, in Physics of the Inner Heliosphere, edited by R. Schwenn and E. Marsch, *Springer-Verlag, Berlin,* **45**, 1991.

106) Marsch, E., W. I. Axford, and J. F. McKenzie, Solar wind, in dynamic Sun, edited by B. N. Dwivedi, *Cambridge University Press, Cambridge,* 374, 2003.

107) Marsden, R. G., The intrepid heliospheric explorer, *Physics World,* **6(11)**, 36, 1993.

108) Marsden, R.G. (Ed.), The high latitude heliosphere, *Space Science Reviews,* **72(1/2)**, 1995.

109) Marsden, R.G. (Ed.), The 3-D heliosphere at solar maximum, *Space Science Reviews,* **97(1-4)**, 2001.

110) Matthaeus, W. H., G. Qin, J. W. Bieber, and G. P. Zank, Nonlinear collisionless perpendicular diffusion of charged particles, *Astrophys. J.,* **590**, L53, 2003.

111) McComas, D.J., S. J. Bame, B. L. Barraclough, W. C. Feldman, H. O. Funsten, J. T. Gosling, P. Riley, R. Skoug, A. Balogh, R. Forsyth, B. E. Goldstein, and M. Neugebauer, Ulysses return to the slow solar wind, *Geophys. Res. Lett.*, **25**, 1, 1998.

112) McComas, D. J., H. A. Elliot, J. T. Gosling, D. B. Reisenfield, R. M. Skoug, B. E. Goldstein, M. Neugebauer, and A. Balogh, Ulysses 's second fast-latitude scan: Complexity near solar maximum and the reformation of polar coronal holes, *Geophys. Res. Letters,* **29(9),** 4-1, 2002b.

113) McComas, D. J., A. Elliot, and R. Von Steiger, Solar wind from high–latitude coronal holes at solar maximum, *Geophys. Res. Lett.,* **29 (9)**, 28(1-4), 2002a.

114) McDonald, F. B., T. L. Cline, and G. M. Simnett, Multifarious temporal variations of low-energy relativistic cosmic ray electrons, *J. Geophys. Res.,* **77**, 2213, 1972.

115) Mewaldt, R. A., E. C. Stone, and R. E. Vogt, Observations of Jovian electrons at 1 AU, *J. Geophys. Res.,* **81**, 2397, 1976.

116) Minnie, J., Observational constraints on the heliospheric diffusion tensor for galactic cosmic rays, *M.Sc. dissertation, Potchefstroom University for CHE, South Africa,* 2002.

117) Minnie, J., R. A. Burger, S. Parhi, J. W. Bieber, and W. H. Matthaeus, The solar cycle dependent heliospheric turbulence on cosmic ray modulation, *Adv. Space Res.,* **32**, 567, 2003a.

118) Minnie, J., R. A. Burger, S. Parhi, W. H. Matthaeus, J. W. Bieber, and S. Pahri, Ab Initio modulation modeling: The effects of a nonlinear description of perpendicular diffusion, *American Geophys. Union,* 2003b.

119) Moraal, H., J. R. Jokipii, and R. A. Mewaldt, Heliospheric effects on cosmic-ray electrons, *Astrophys. J.,* **367**, 191, 1991.

120) Morioka, A., F. Tsuchiya, and H. Misawa, Modulation of Jovian electrons by the solar wind, *Adv. Space Res.*, **20**, 209, 1997.

121) Moses, D., Jovian electrons at 1 AU - 1978-1984, *Astrophys. J.*, **313**, 471, 1987.

122) Neugebauer, M., and P. C. Liewer, Creation and destruction of transitory coronal holes and their fast solar wind streams, *J. Geophys. Res.*, **108**, SHH3-1, 2003.

123) Neugebauer, M., P. C. Liewer, E. J. Smith, R. M. Skoug, and T. H. Zurbuchen, Sources of the solar wind at solar activity maximum, *J. Geophys. Res.*, **107**, SSH13-1, 2002.

124) Nolte, J. T., Coronal holes as source of solar wind, *Solar Physics*, **46**, 303, 1976.

125) Odstrcil, D., Modeling 3-D solar wind structure, *Adv. Space Res.*, **32(4)**, 497, 2003.

126) Parker, E. N., Cosmic ray modulation by the solar wind, *Physical Reviews*, **110**, 1445, 1958.

127) Parker, E. N., Sudden expansion of the corona following a large solar flare and the attendant magnetic field and cosmic-ray effects, *Astrophys. J.*, **133**, 1014, 1961.

128) Parker, E. N., Interplanetary dynamical processes, *Interscience, New York*, 1963.

129) Parker, E. N., The passage of energetic charged particles through interplanetary space, *Planetary and Space Science*, **13**, 9, 1965.

130) Phillips, J. L., A. Balogh, S. J. Bame, B. E. Goldstein, J. T. Gosling, J. T. Hoeksema, D. J. McComas, M. Neugebauer, N. R. Sheeley, and Y. M. Wang, Ulysses at 50° south: constant immersion in the high-speed solar wind, *Geophys. Res. Lett.*, **21(12)**, 1105, 1994.

131) Phillips, J. L., S. J. Bame, A. Barnes, B. L. Barraclough, W. C. Feldman, B. E. Goldstein, J. T. Gosling, G. W. Hoogeveen, D. J. McComas, M. Neugebauer, and S. T. Suess, Ulysses solar wind plasma observations from pole to pole, *Geophys. Res. Lett.*, **22(23)**, 3301, 1995.

132) Potgieter, M. S., The modulation of galactic cosmic rays as described by a three-dimensional drift model, *Ph.D thesis, Potchefstroom University for CHE, South Africa*, 1984.

133) Potgieter, M. S., Heliospheric modulation of galactic electrons: Consequences of new calculations for the mean free path of electrons between 1 MeV and ~10 GeV, *J. Geophys. Res.*, **101(A11)**, 24411, 1996.

134) Potgieter, M. S., Implications of enhanced perpendicular diffusion in the heliosphereric modulation of cosmic rays, *Proc. 25th Inter. Cosmic Ray Conf., Durban*, **2**, 1, 1997.

135) Potgieter, M. S., and S. E. S. Ferreira, The importance of perpendicular diffusion in the heliospheric modulation of cosmic ray electrons, *Adv. Space Res.*, **23(3)**, 463, 1999a.

136) Potgieter, M. S., and S. E. S. Ferreira, Implications of cosmic ray electron observations on the modeling of electron modulation in the heliosphere, *Proc. 26th Inter. Cosmic Ray Conf., Salt Lake City*, 7, 21, 1999b.

137) Potgieter, M. S., and S. E. S. Ferreira, Effects of the solar wind termination shock on the modulation of Jovian and galactic electrons in the heliosphere, *J. Geophys. Res.*, **107**, SSH1-1, 2002.

138) Potgieter, M. S., L. J. Haasbroek, P. Ferrando, and B. Heber, The modeling of the latitude dependence of cosmic rays protons and electrons in the inner heliosphere, *Adv. Space Res.*, **19(6)**, 917, 1997.

139) Potgieter, M. S., J. A. le Roux, and R. A. Burger, Interplanetary cosmic ray radial gradients with steady state modulation models, *J. Geophys. Res.*, **94**, 2323, 1989.

140) Potgieter, M. S., and H. Moraal, A drift model for the modulation of galactic cosmic rays, *Astrophys. J.*, **294**, 425, 1985.

141) Rastoin, C., Jovian and galactic electrons in the heliosphere: Observations of the KET experiment on board the Ulysses spacecraft, *Ph.D. Thesis, University of Paris VII, France,* 1995.

142) Richardson, J. D., C. Wang, and K. I. Paularena, The solar wind: From solar minimum to solar maximum, *Adv. Space Res.*, **27(3)**, 471, 2001.

143) Scherer, K., H. Fichtner, H. J. Fahr, and E. March, The outer heliosphere: The next frontiers, edited by K. Scherer, H. Fichtner, H. J. Fahr, and E. March, *COSPAR colloquiua series,* 11, *Elsevier Science,* 2001.

144) Schwenn, R., The average solar wind in the inner heliosphere: Structures and slow variations, in Solar Wind Five, edited by M. Neugebauer, *NASA CP-2280,* 489, 1983.

145) Shalchi, A., J. W. Bieber, and W. H. Mathaeus, Analytical forms of the perpendicular diffusion coefficient in magnetostatic turbulence, *Astrophys. J.*, **604**, 675, 2004.

146) Shalchi, A., and R. Schlickeiser, The parallel mean free path of heliospheric cosmic rays in the composite slab/two-dimensional geometry. I. The damping model of dynamical turbulence, *Astrophys. J.*, **604**, 861, 2004.

147) Sheeley, N. R., Y. M. Wang, S. H. Hawley, G. E. Brueckner, K. P. Dere, R. A. Howard, M. J. Koomen, C. M. Korendyke, D. J. Michels, S. E. Paswaters, D. G. Socker, O. C. St. Cyr, D. Wang, P. L. Lamy, A. Llebaria, R. Schwenn, G. M. Simnett, S. Plunkett, and D. A. Biesecker, Measurements of low speeds in the corona between 2 and 30 R sub Sun, *Astrophys. J.*, **484**, 4728, 1997.

148) Simpson, J. A., Cosmic radiation: Particle astrophysics in the heliosphere, in frontiers in cosmic physics: Symposium in memory of Serge Korff, edited by R. B. Mendell, and A. J. Mincer, *New York Academy of Sciences, New York,* 97, 1992.

149) Simpson, J. A., The cosmic radiation: Reviewing the present and future, *Proc. 25th of the Inter. Cosmic Ray Conf., Durban:* Invited, Rapporteur & Highlighted Papers, 4, 1997.

150) Simpson, J. A., J. D. Anglin, A. Balogh, M. Bercovitch, J. M. Bouman, E. E. Budzinski, J. R. Burrows, R. Carvell, J. J. Connell, R. Ducros, P. Ferrando, J. Firth, M. Garcia-Munoz, J. Henrion, R. J. Hynds, B. Iwers, R. Jacquet, H. Kunow, G. Lentz, R. G. Marsden, R. B. Mckibben, R. Meuller-Mellin, D. E. Page, M. Perkins, A. Raviart, T. R. Sanderson, H. Sierks,

L. Treguer, A. J. Tuzzolino, K. P. Wenzel, and G. Wibberenz, The Ulysses cosmic ray and solar particle investigation, *Astron. Astrophys. Supp. Series,* **92(2)**, 365, 1992b.

151) Simpson, J. A., J. D. Anglin, A. Balogh, J. R. Burrows, S. W. H. Cowley, P. Ferrando, B. Heber, R. J. Hynds, H. Kunow, and R. G. Marsden, Energetic charged-particle phenomena in the Jovian magnetosphere - First results from the ULYSSES COSPIN collaboration, *Science,* **257(5076)**, 1543, 1992a.

152) Simpson, J. A., D. Hamilton, G. Lentz, R. B. McKibben, A. Mogro-Campero, M. Perkins, K. R. Pyle, A. J. Tuzzolino, and J. J. O'Gallagher, Protons and electrons in Jupiter's magnetic field: Results from the university of Chigago experiment on Pioneer 10, *Science,* **183(4122)**, 306, 1974.

153) Simpson, J. A., D. Hamilton, G. Lentz, R. B. McKibben, M. Perkins, K. R. Pyle, A. J. Tuzzolino, and J. J. O'Gallagher, Jupiter revisited - First results from the University of Chicago charged particle experiment on Pioneer 11, *Science,* **188**, 455, 1975.

154) Smith, E. J., The Sun, solar wind and magnetic field. I, in Proceedings of the International School of Physics "Enrico Fermi" Course CXLII, edited by B. Coppi, A. Ferrari, and E. Sindoni, *IOS Press., Amsterdam,* 179, 2000.

155) Smith, E. J., The heliospheric current sheet, *J. Geophys. Res.,* **106(A8)**, 15819, 2001.

156) Smith, E. J., and R. G. Marsden, Ulysses observations at solar maximum: Introduction, *Geophys. Res. Lett.,* **30(19)**, 1, 2003.

157) Smith, E. J., R. G. Marsden, A. Balogh, G. Gloeckler, J. Geiss, D. J. McComas, R. B. McKibben, R. J. MacDowall, L. J. Lanzerotti, N. Krupp, H. Krueger, and M. Landgraf, The Sun and heliosphere at solar maximum: *Review, Science,* **302**, 1165, 2003.

158) Snodgrass, H. B., Magnetic rotation of the solar photosphere, *Astrophys. J.,* **270**, 288, 1983.

159) Stone, E. C., and A. C. Cummings, Estimate of the location of the solar wind termination shock, *Proc. 27th Inter. Cosmic Ray Conf., Hamburg,* **10**, 4263, 2001.

160) Stone, E. C., and A. C. Cummings, The approach of Voyager 1 to the termination shock, *Proc. 28th Inter. Cosmic Ray Conf., Tsukuba,* 3889, 2003.

161) Stone, E. C., A. C. Cummings, and W. R. Webber, The distance to the solar wind termination shock in 1993 and 1994 from observations of anomalous cosmic rays, *J. Geophys. Res.,* **101(A5)**, 11017, 1996.

162) Suess, S. T., J. L. Phillips, B. E. Goldstein, M. Neugebauer, and Nerney, The solar wind – Inner heliosphere, *Space Science Rev.,* **83**, 75, 1998.

163) Tanimori, T., Y. Hayami, S. Kamei, S. A. Dazeley, P. G. Edwards, S. Gunji, S. Hara, T. Hara, J. Holder, A. Kawachi, T. Kifune, R. Kita, T. Konishi, A. Masaike, Y. Matsubara, T. Matsuoka, Y. Mizumoto, M. Mori, M. Moriya, H. Muraishi, Y. Muraki, T. Naito, K. Nishijima, S. Oda, S. Ogio, J. R. Patterson, M. D. Roberts, G. P. Rowell, K. Sakurazawa, T.

Sako, Y. Sato, R. Susukita, A. Suzuki, R. Suzuki, T. Tamura, G. J. Thornton, S. Yanagita, T. Yoshida, and T. Yoshikoshi, Discovery of TeV Gamma Rays from SN 1006: Further evidence for the supernova remnant origin of cosmic rays, *Astrophys. J.*, **497**, L25, 1998.

164) Teegarden, B. J., F. B. McDonald, J. H. Trainor, W. R. Webber, and E. C. Roelof, Interplanetary MeV electrons of Jovian origin, *J. Geophys. Res.*, **79**, 3615-3622, 1974.

165) Teufel, A., and R. Schlickeiser, Analytic calculation of the parallel mean free path of interplanetary cosmic rays I. Dynamical magnetic slab turbulence and random sweeping model, *Astron. Astrophys.*, **393**, 703, 2002.

166) Teufel, A., and R. Schlickeiser, Analytic calculation of the parallel mean free path of heliospheric cosmic rays II. Dynamical magnetic slab turbulence and random sweeping slab turbulence with finite wave power at small wave numbers, *Astron. and Astrophys.*, **397**, 15, 2003.

167) Tsuchiya, F., A. Moroika, and H. Misawa, Jovian electron modulations by the solar wind interaction with the magnetosphere, *Earth Planets Space,* **51**, 987, 1999

168) Thomas, B. T., and E. J. Smith, The structure and dynamics of the heliospheric current sheet, *J. Geophys. Res.*, **86**, 11105, 1981.

169) Van Niekerk, Y., An investigation into the causes and consequences of north-south asymmetries in the heliosphere, *M.Sc. dissertation, Potchefstroom University for CHE, South Africa,* 2000.

170) Wenzel, K. P., Ulysses - it's status and prospects, *Adv. Space Res.*, **13(6)**, 275, 1993.

171) Whang, Y. C., and L. F. Burlaga, Anticipated Voyager crossing of the termination shock, *Geophys. Res. Lett.*, **27(11)**, 1607, 2000.

172) Wilcox, J. M., and N. F. Ness, Quasi-stationary co rotating structure in the interplanetary medium, *J. Geophys. Res.*, **70**, 5793, 1965.

173) Williams, T., The influence of the wavy heliospheric neutral sheet on the modulation of cosmic rays (in Afrikaans), *M.Sc. dissertation, Potchefstroom University for CHE, South Africa,* 1990.

174) Zank, G. P., Li Gang, V. Florinski, W. H. Matthaeus, G. M. Webb, and A. Le Roux, Perpendicular diffusion coefficient for charged particles of arbitrary energy, *J. Geophys. Res.*, **109(A04107)**, 2004.

175) Zirker, J. B., Coronal holes: An overview, in coronal holes and high speed wind streams, edited by J. B. Zirker, *Colorado Associated Univ. Press., Colorado,* 1, 1977.

Acknowledgements

I would like to acknowledge my gratitude to the following, in no particular order:

- Prof. Marius Potgieter, my supervisor, with whom I worked for over a period of my undergraduate studies, I would like to thank him once again for his extra-ordinary leadership, excellent guidance, motivation and assistance with this work. I would also like to thank him for the stimulating lectures he has offered to me throughout my studies.
- Dr. Stefan Ferreira, my assistant supervisor, for his insight, useful discussions and assistance on various occasions.
- The organizers of the International Cosmic Ray Workshop in Potchefstroom (2002) and in Bochum, Germany (2003).
- Dr. V. Henize, Dr. H. Fichtner, Dr. B. Heber, Dr. A. Posner and Dr. U. Langner for discussions and their assistance on various occasions. A special thinks to Dr. Heber for providing me with the Ulysses data used in this work.
- Mrs. Anne Mans for her assistance to enable me to use the IBM RS/6000 Scalable POWERparallel Systems (SP) computer.
- Mr. Matthew Holleran for his assistance on various occasions with computer related problems and queries.
- Miss. Christina Eddington for editing the grammar and spelling of this thesis.
- The Unit for Space Physics at the North-West University (Potchefstroom Campus), the South African National Research Foundation and the Department of Labour of South Africa for financial support.
- Mr. G. G. Nyambuya, Mr. Kenneth Gaarogwe, Mr. Benjamin Moeketsi, Mr. Eddy Edward and Mr. D. Rambane for their friendship, motivation and discussions.
- Mrs. Petro Sieberhagen and Mrs. Lizelle le Roux for all their flexible administrative assistance.

A special thanks to:

- My parents, Elias and Dipuo Moeketsi, for their love, support, encouragement, and countless prayers and who have made many sacrifices to allow me to be where I am today.
- Mrs. H. F. Reinecke and Dr. E. Kotze for their support and motivation throughout the study.
- My girl friend, Cleopatra, for her love, support, understanding, and sacrifice.
- God, for letting me study a small portion of his magnificent creation.

I dedicate this thesis to my late sister and brother, Caroline Moeketsi (1970-2003) and Hendrick Moeketsi (1978-2000) who were always wishing me success with my studies.